UNCLASSIFIED

AD **429250**

DEFENSE DOCUMENTATION CENTER

FOR

SCIENTIFIC AND TECHNICAL INFORMATION

CAMERON STATION, ALEXANDRIA, VIRGINIA

UNCLASSIFIED

429250

S-237-R

ENERGY- AND RATE-DEPENDENCE STUDIES

FINAL REPORT

FEB 1 0 1964

EDGERTON,
GERMESHAUSEN &
GRIER, INC.

SANTA BARBARA LABORATORY

ENERGY- AND RATE-DEPENDENCE STUDIES
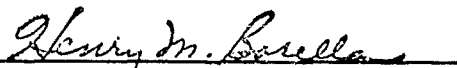
FINAL REPORT

R. K. Durkee
A. C. Lucas
N. B. York
T. S. Dahlstrom
G. E. Blair

Submitted to: U. S. Army Materiel Command
                Harry Diamond Laboratories
                Washington 25, D. C.

Delivered by EG&G, Santa Barbara Laboratory
pursuant to Contract No. DA-49-186-ORD-1059.
Government's use controlled by "data" article
of this contract which is ASPR 9-203.

Approved by: _H. M. Borella_

             H. M. Borella
             Programs

EDGERTON, GERMESHAUSEN & GRIER, INC.
Las Vegas, Nevada   Boston, Massachusetts
        Santa Barbara, California

CONTENTS

ILLUSTRATIONS

vi

TABLES

ENERGY- AND RATE-DEPENDENCE STUDIES

R. K. Durkee
A. C Lucas
N. B. York
T. S. Dahlstrom
G. E. Blair

ABSTRACT

Dosimeter systems of silver-activated phosphate glass rods, cobalt glass plates, and manganese-activated calcium fluoride were evaluated for their response to gamma rays, electrons, and neutrons. Response to gamma rays in the energy region from .022 to 15 Mev, rate dependence from 10 r/sec to 10^7 r/sec (in excess of 10^8 r/sec using 10 Mev electrons), and neutron sensitivity for fast and thermal neutrons were measured. Energy discriminatory shields and thermal neutron attenuation shields were designed, fabricated and evaluated for each dosimetry system.

I. INTRODUCTION

In this study, three types of radiation dosimetry systems have been considered: silver-activated phosphate glass rods, cobalt glass plates, and manganese-activated calcium fluoride thermoluminescent dosimeters. It was necessary to determine the rate and energy response of these systems to x-rays and gamma rays and their response to fast and thermal neutrons. Shields were designed and fabricated for uniform energy response to 10 Mev and thermal neutron attenuation for satisfactory use in mixed neutron and gamma-ray fields. A photodiode-fluor detector was constructed and calibrated for rate and energy dependence.

A previous study under contract DA-49-186-ORD-1011 for Harry Diamond Laboratories (formerly Diamond Ordnance Fuze Laboratory) was completed in 1961 by EG&G. This contract was for the development of an energy discrimination shield for a composite system of one- and two-phase chemical dosimeters and glass-rod microdosimeters, and for the determination of gamma-ray response and the thermal neutron attenuation of the shield. A shield was designed and fabricated which satisfied the contract requirements. The large over-response of the glass rods necessitated the use of a supplementary inner shield in the system which resulted in a loss of low-energy response for the glass rod microdosimeters. A shield utilizing the low-energy capability and small size of the glass rods alone was not realized in this contract.

The investigation of the energy response for the systems required several sources of x-rays and gamma radiation. A description of sources, methods used in determining beam characteristics, and exposure techniques employed is presented.

Accurate dose monitoring is a basic requirement. Various ionization chambers were constructed and calibrated to fulfill this requirement. Since precise and convenient evaluation of the dosimeters is required, the readout methods and apparatus were evaluated and improved where possible. Calibration studies were made for the three dosimeter systems. Response was determined for the range of energies and rates considered, as well as for thermal and fast neutrons. The effects of various shielding materials were studied with respect to the various dosimeter response characteristics. Prototype energy discriminatory shields were designed and constructed as a result of these evaluations.

II. RADIATION SOURCES

Various machines and radioactive sources were required throughout this study to provide x-rays, gamma rays, and neutrons. To cover the low-energy photon range, a conventional 250-kv constant potential x-ray machine was used with appropriate filters to provide effective energy points from 22.5 to 210 kev. This range was extended in one instance to 400 kev with a 1-Mev x-ray machine. For energy points above this region, radioactive sources were employed. Cesium-137 provides an effective energy at 662 kev and cobalt-60 at 1.25 Mev. To attain the 10-Mev requirement of the contract, it was necessary to use bremsstrahlen radiation from an electron linear accelerator (LINAC). Although monoenergetic radiation is available through positron conversion, the dose rate (10^6 photons/sec) is too low to be utilized here. For this reason, bremsstrahlen of 5, 10, and 15 Mev were used to more or less bracket the 10-Mev effective energy requirement. It is realized these are peak energies and the effective energies are well below these values. Also, the terminology of dose becomes difficult to define at these energies. The roentgen has been the accepted term for exposure dose in the low energies, however, this term is unsuitable for energies above 2 to 3 Mev. Therefore, a 5-cm Lucite wall cube in which an air-equivalent ionization chamber is placed to measure ion current has been utilized. This technique is described in the literature.[1] To provide a uniform presentation, the peak LINAC energies have been plotted as well as accepting an equivalence of 1 esu/r for the ion current collected at the center of the Lucite cube.

A convenient method of obtaining a wide range of dose rates for the rate study was found by using the LINAC electrons

3

directly. The assumption was made that the mechanism for dosimeter effect was identical to that caused from photon irradiation.

Two sources of fast neutrons were used: A 10-curie plutonium-beryllium (Pu-Be) source and a deuterium-tritium reaction from a 400-kv van de Graaff. Sulfur threshold detectors were used to monitor these sources. Thermal neutrons were made available from a paraffin geometry in which the Pu-Be source was placed and from the graphite thermal column at the General Dynamics/General Atomic TRIGA reactor facility in La Jolla, California. The monitoring system for these neutrons consisted of gold and cadmium-covered gold foils, with the 0.5-ev cadmium cutoff for thermal neutron definition.

A Field Emission flash x-ray machine was also used in determining the rate dependence of the silver-activated glass rods. This machine was also used in early investigations of the collection characteristics of the air-equivalent and aluminum thimble ionization chambers in a pulsed beam of gamma radiation.

A. X-RAY SOURCES

1. Constant Potential X-Ray Machine

A Westinghouse 250-kv constant potential industrial unit was used for determining the low- and medium-energy response of the dosimeters. This machine is cable connected and has a maximum operating current of 20 ma.

The x-ray machine was operated from an electromechanical line voltage stabilizer to ensure good reproducibility of data. The inherent filtration of the industrial x-ray tube was approximately equivalent to 0.25 mm copper. Lead diaphragms were used to define the fields in these experiments and to minimize the effects of scattering.

4

The operating voltages and filters for the x-ray machine were chosen to be consistent with those used by Villforth, Birkhoff, and Hubbell[2] in their study of x-ray spectra. The effective energy was taken as that of a mono-energetic beam of gamma radiation which results in the same first half-value layer as the heterogeneous beam. The kilovoltage-filter combinations and the resultant effective energies are shown in Table 1.

TABLE 1. X-Ray Filters and Effective Energies for 250-kv X-Ray Machine

Kilo-Voltage Set	Filter No.	Filter Materials (mg/cm^2)				Effective Energy (kev)
		Pb	Sn	Cu	Al	
30	1	-	-	-	133	22.4
50	2	-	-	233	133	37.5
75	-*	-	-	441	279	46.5
100	3	548	-	-	279	70
150	4	-	913	2790	279	123
200	5	716	1863	929	279	165
250	6	2363	861	959	279	211

*This filter was empirically determined later in the study to provide a better definition of the energy dependence of the shielded dosimeters.

A description of the measurements is presented in Appendix A and includes a re-evaluation of the effective energies after several x-ray machine component failures. A maximum of 7% error in some effective energy was noted. In addition, several filter-energy combinations for developing a nominal 50-kev energy point are listed.

5

2. 1-Mev X-Ray Machine

A General Electric Company 1-Mev x-ray machine was used for one energy point on the cobalt glass dosimeter. This was a therapy unit at Cottage Hospital in Santa Barbara, California. The machine was run at 1 Mev for the particular exposure and its effective energy determined by lead attenuation to be 425 kev (Appendix A).

3. Field Emission Pulsed X-Ray Machine

This flash x-ray machine produces a single pulse of 600-kvp x-rays for a duration of 200 nanoseconds. The dose output is a 5 r/pulse at the point of closest approach. This machine was used to advantage in the rate study of the more sensitive dosimeters where rates of the order of 10^7 r/sec are attainable.

The pulse is developed by discharging a capacitor into a specially designed tube with discharge currents as large as 1000 amp. This transfer of current and spark gap switching of several small capacitors into a series circuit generates strong rf signals. Active dosimetry, and specifically ionization chambers, must be well shielded against these undesirable signals.

B. RADIOACTIVE ISOTOPE SOURCES

Isotope sources were used to obtain effective gamma energies of 0.662 and 1.25 Mev. The containment of these isotopes presents a possibility of beam contamination from scatter which results in low-energy gamma rays and energetic electrons. A thin-window detector was constructed and buildup studies made of the sources used to determine the degree of contamination. In certain cases, corrective measures were taken by constructing appropriate collimators. Appendix B contains a more detailed description of these measurements.

6

1. Cesium-137 Sources

    a. EG&G 24-Curie Source

       The EG&G 24-curie source used for the 662-kev response of the dosimeters was located in a cylindrical lead shield containing a large segment notch. The source was mounted on a rod which could be raised to the notch position for sample exposures. A collimator was added during the study. It consisted of a 2-inch-diameter hole in a 2-inch-thick lead brick with an 0.83-mm copper filter. The exposure geometry is shown in Figure 1.
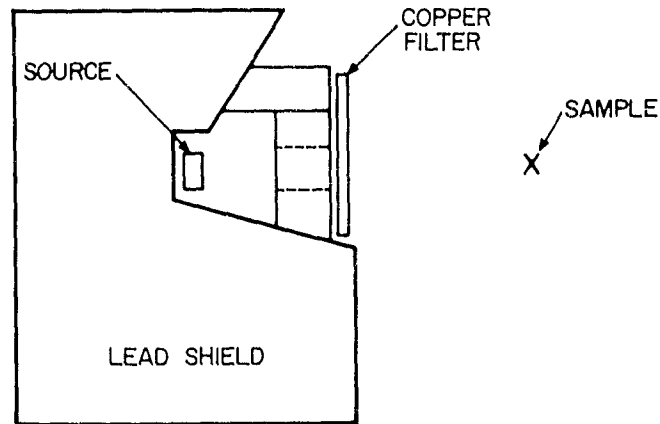
FIGURE 1. Cs^{137} EXPOSURE GEOMETRY

    b. Santa Barbara Cottage Hospital 1300-Curie Source

       The Santa Barbara Cottage Hospital 1300-Curie Source is a Picker teletherapy unit with several fixed field collimators. Exposures were made with a 4-by 4-cm collimator at a distance of 20 cm. The dose rate at this position was 171 r/min.

2. Cobalt-60 Sources

a. EG&G 50-Curie Source

The EG&G 50-curie source is a U.S. Nuclear Corporation
Model 57-1 pop-up device. Exposures were made with the source
and the samples 2 inches above a horizontal, 1-inch Plexiglas
surface. The distance of closest approach to the center of
the source was approximately 1-1/2 inches. Exposures were made
at distances of 4 to 30 inches as required by the particular
dosimeter being used, with due regard for exposure time and
the possible effects of positional error.

b. Santa Barbara Cottage Hospital 2000-Curie Source

The 2000-curie source at Santa Barbara Hospital is
a Picker Model C-1000 unit and is equipped with a Johns-Mackay
multivane collimator. Exposures were made at a distance of
32 cm in a 5- by 5-cm field. The dose rate at this position
was 252 r/min.

C. LINEAR ELECTRON ACCELERATOR

The General Dynamics/General Atomic 45-Mev L-Band
Electron Linear Accelerator (LINAC) was used to produce
5-, 10-, and 15-Mev bremsstrahlung radiation from a Fansteel
target.

All LINAC energy-dependence studies were made at a
distance of 1 meter from the target. Aluminum plates were
utilized to minimize the high-energy electrons from the exit
face of the target. A 1/2-inch plate was used for the 5-Mev
energy and a 1-inch plate was used for the 10- and 15-Mev
energies. The aluminum ionization chamber was interposed
as a monitor at a distance of 50 cm from the target. The
monitor was standardized at each energy by exposing the
monitor chamber at 50 cm and the air equivalent ionization

8

chamber in an 11.5-cm cube of Lucite at 1 meter simultaneously. Test dosimeter systems were exposed in place of the air-equivalent ionization chamber; the monitor was then used to normalize the ensuing exposure.

The response of the dosimeter systems was eventually determined in terms of the absorbed dose in the air-equivalent ionization chamber. The response of this chamber in the 11.5-cm Lucite cube is well documented[1] and may be interpreted in terms of absorbed dose or radiation intensity as desired. In addition, 10-Mev electrons were also obtained for rate-dependence studies. Effective dose rates of 10^4 to 10^9 r/sec were realized. The advantages of the LINAC were in evaluating the response of the dosimeter systems to higher energies and rates than those obtained from more conventional x-ray machines and radioactive sources.

D. NEUTRON SOURCES

1. General Atomic TRIGA Reactor

The General Atomic TRIGA Mark-F Reactor with its associated thermal column provided thermal neutrons. The reactor was operated in its normal pulsed mode with a large graphite-filled tank adjacent to the core. Exposures were made in the furthest access port from the core where the cadmium ratio was determined to be 520 and the thermal flux was approximately 1.3×10^{12} nvt/pulse.

Evaluation of the sintered Lithium-6-enriched lithium fluoride thermal neutron attenuation shields as well as the thermal neutron response of the various dosimeter systems were made at this position.

2. High Voltage Engineering Van de Graaff

A High Voltage Engineering 400-kv Van de Graaff using the reaction of deuterium on tritium (d,t) provided 14-Mev neutrons. Beam current was 100 μa and the average neutron output was 10^7 neutrons/second for a typical exposure.

3. 10-Curie Plutonium-Beryllium Source

A 10-curie NUMEC plutonium-beryllium source was also used as a source of fast neutrons. This device is contained in a stainless steel cylinder 1.5 inches diameter by 4 inches long and produced 10^7 neutrons/second. The average neutron energy is approximately 5.4 Mev.

III. DOSE MONITORING SYSTEMS

Several methods of dose monitoring were required throughout these experiments. The dose standard was a Victoreen Model 570 r-meter with associated medium- and high-energy chambers. To extend the range of this instrument, a 1-cc air-equivalent ionization chamber was constructed, and the ion current from this device was read across precision capacitors with an electrometer. For rate studies, an aluminum thimble ionization chamber was constructed with a 1-mm gap, and up to 20 esu/pulse could be measured with 85% collection efficiency. A thin-window ionization chamber was constructed to determine the contamination of the cesium and cobalt sources, and a graphite-CO_2 ionization chamber was assembled to provide a gamma-ray measurement in a mixed neutron and gamma-ray field.

Neutron flux measurements required a different system of instrumentation. Fast neutrons were detected by the (n,p) reaction of sulfur which has an activation threshold at 3 Mev. The resultant product is a phosphorous atom which decays by the emission of a 1.71-Mev beta particle. This laboratory maintains a Nuclear Accident Dosimetry (NAD) system which is calibrated in neutrons per centimeter square versus counts per minute so that no calibration effort was required. Thermal neutrons were detected by gold and cadmium-covered gold foils which were similarly counted on the calibrated NAD system.

The electron beam of the LINAC required an additional method of dosimetry. A simple aluminum block was placed in the electron beam, and the current produced by the electrons stopped in the block was measured.

A. STANDARDS

The standard used for energy-dependence studies was a
Victoreen Model 570 r-meter with associated medium- and high-
energy chambers. This r-meter was calibrated at the National
Bureau of Standards. The 1-cc air equivalent ionization cham-
ber described later was carefully calibrated with the r-meter
and was used as the secondary standard for high and low dose
where an r-meter is unsuitable.

B. ELECTROMETER SYSTEM

General Radio Electrometers, Model 1230-A, were used
to measure the charge collected in the ionization chambers.
A typical circuit is presented in Figure 2. The coaxial
cable used to connect the ionization chamber to the elec-
trometer is Amphenol Type 21-541 low-noise cable. Regulated
power supplies providing up to 1000 volts of either polarity
were used to provide the collecting field. Goodall Type
820-UB polystyrene capacitors in the range of 0.001 to
0.1 μf were used depending on the magnitude of the total dose
to be integrated. Each capacitor was intercompared with a
General Radio Standard Air Capacitor Model 1403-A to an
accuracy of 0.01% by using the circuit shown in Figure 3.

C. 1-CC AIR EQUIVALENT IONIZATION CHAMBER

For measuring dose at high energies, a 1-cc air-equivalent
ionization chamber was used. This is a 3-terminal ionization
chamber similar in design to that used by Wyckoff.[3] The
chamber, shown in Figure 4, is constructed of an air-equivalent
material developed by Shonka[4] and has a response essentially
independent of energy from 40 kev to 1.25 Mev.

12
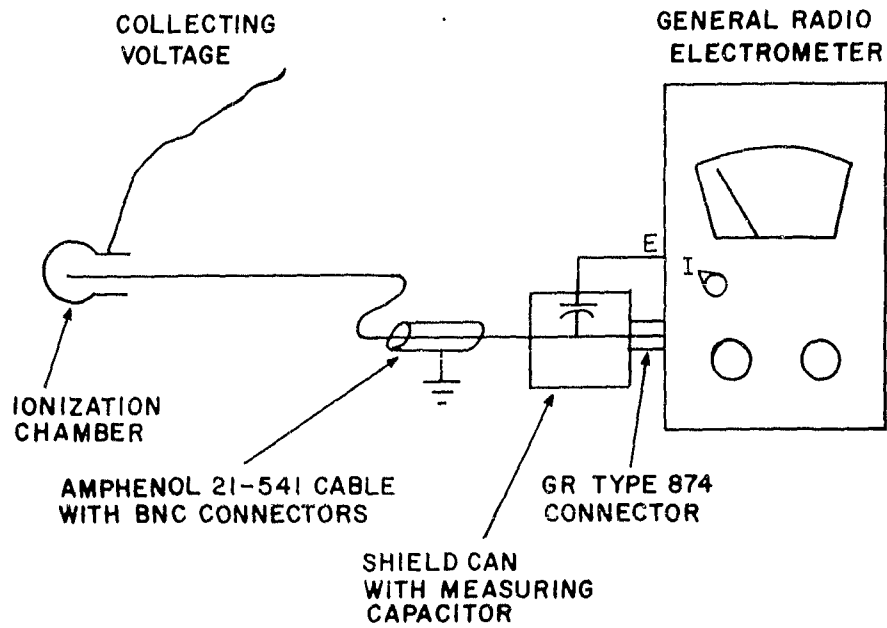
FIGURE 2. TYPICAL ELECTROMETER CONNECTION FOR MEASURING DOSE
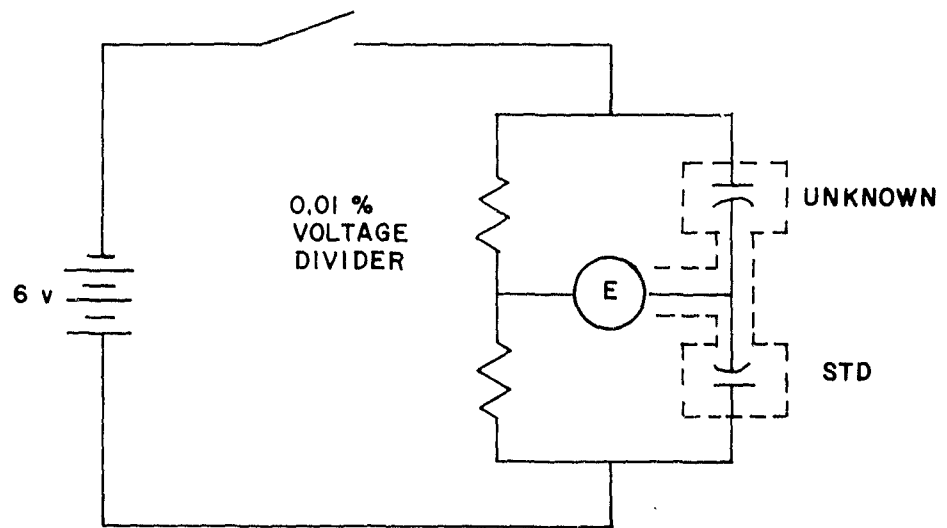
FIGURE 3. CIRCUIT USED FOR DETERMINING D-C CAPACITANCE OF MEASURING CAPACITORS

13
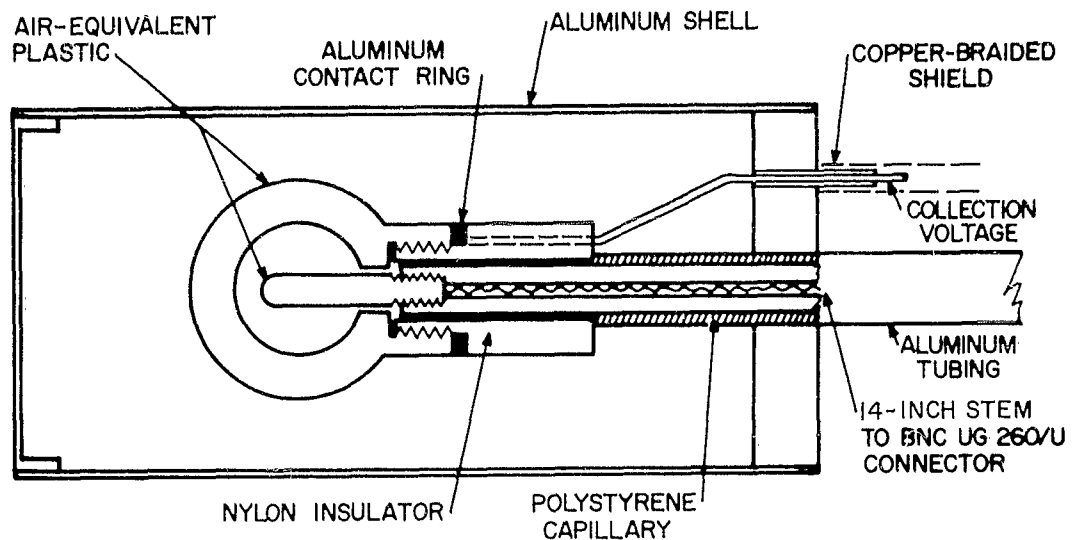
FIGURE 4. I-CC AIR-EQUIVALENT IONIZATION CHAMBER AND ALUMINUM
R F NOISE SHIELD

D. ALUMINUM THIMBLE IONIZATION CHAMBER

In rate-dependence studies some instrument whose response is independent of dose rate must be used. The condenser r-meter is not well suited to applications requiring very long exposures because of nonlinear effects resulting from radiation-induced leakages in the insulating materials. It is even more difficult to use the condenser r-meter at very high dose rates where an appreciable correction must be made for general recombination. For these reasons, a 3-terminal ionization chamber with a very small air gap and negligible stem leakage was constructed. This chamber, shown in Figure 5 was used as a monitor in the determination of rate response.

14
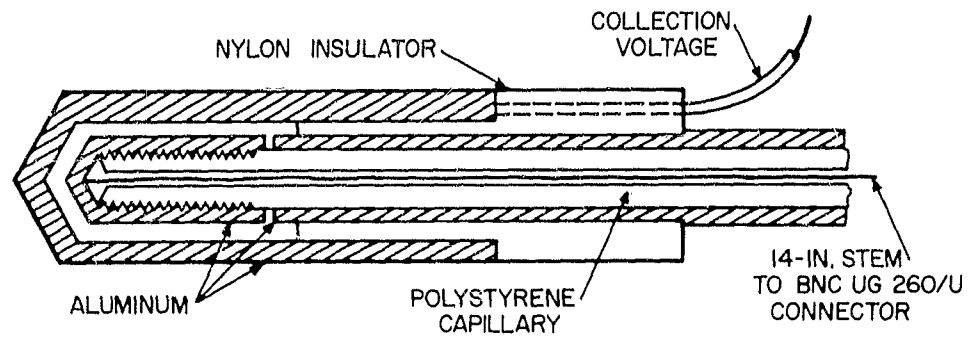
FIGURE 5. ALUMINUM THIMBLE IONIZATION CHAMBER FOR MONITORING HIGH DOSE RATES

E. THIN-WINDOW IONIZATION CHAMBER

A thin-window ionization chamber (Figure 6) was con-structed utilizing standard guarded electrode design and with a 1/4-mil, aluminum-coated Mylar window. This chamber was used to determine the low-energy gamma-ray and electron con-tamination of the various cesium and cobalt sources used. The results of these evaluations are given in Appendix B.
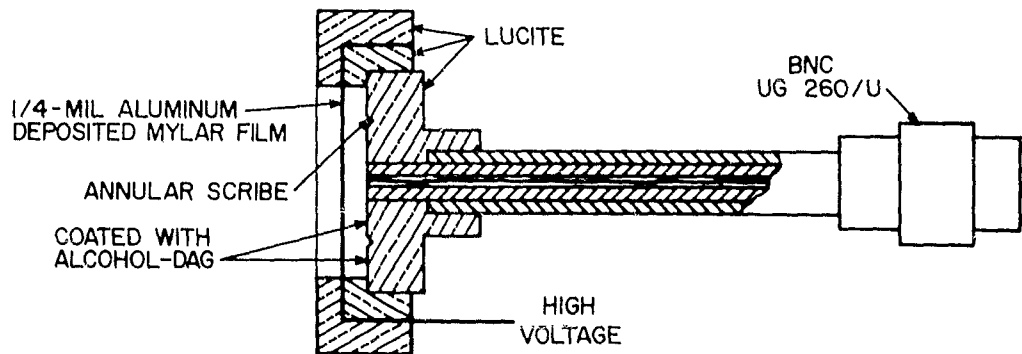
FIGURE 6. THIN WINDOW IONIZATION CHAMBER

MONITOR CHAMBER

FIXED REVERSIBLE CHAMBER VOLTAGE

E

TEST CHAMBER

VARIABLE NEGATIVE CHAMBER VOLTAGE
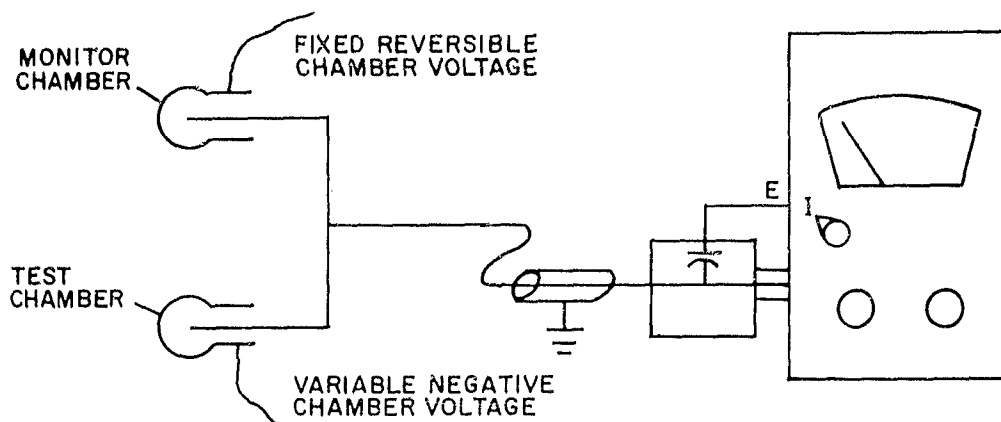
FIGURE 7. CIRCUIT USED FOR DETERMINING IONIZATION CHAMBER COLLECTION CHARACTERISTICS

F. DETERMINATION OF COLLECTION CHARACTERISTICS, ENERGY RESPONSE, AND RATE DEPENDENCE OF THE AIR EQUIVALENT AND ALUMINUM THIMBLE IONIZATION CHAMBERS

The precise measurement of the collection characteristics was performed by using a difference circuit (Figure 7). The operation of the circuit depends upon establishing approximately the same ion current in each chamber near saturation. This condition is established by proper positioning of the two chambers in the x-ray beam. These collection studies were made to determine precisely how the collection current in the test chamber varies with the applied collecting voltage. In practice, it is necessary to provide a monitor chamber to correct for changes in the dose rate of the x-ray generator. The ratio of two electrical signals is not so simple to determine as the difference between two signals. This fact has been incorporated in the circuit design (Figure 7). Readings of the sum and difference of the ionization current are made by reversing the polarity of the collecting voltage on the monitor chamber. The ratio of current in the test chamber, T, to the current in the monitor chamber, M, is determined by the relation

$$\frac{T}{M} = 1 - \frac{2(T-M)}{(T-M) - (T+M)} \qquad (1)$$

16

The energy dependence of the ionization chambers was compared with the Victoreen Model 570 r-meter. The response of the air equivalent ionization chamber is shown in Figure 8, and the response of the aluminum thimble ionization chamber is shown in Figure 9.

The determination of the rate dependence of dosimeters at high dose rates necessitates the collection efficiency of the secondary standard ionization chamber be determined. The collection efficiency of several types of ionization chambers under several conditions is treated rigorously by Boag[5], and the mathematical treatment used here is taken from his work.

A distinct difference in collection characteristics exists for ionization chambers under continuous or pulsed irradiation. For continuous irradiation, the collection efficiency for a particular ionization chamber is determined uniquely by the dose rate and the collecting voltage. For pulsed irradiation such that the pulse length is short with respect to the transit time of the positive ions, the collection efficiency is determined uniquely by the collecting voltage and the dose per pulse.

The collection efficiency may be determined with precision under steady-state conditions by the experimental method described. Absolute values of collection efficiency may be derived by plotting the reciprocal of the ion current in the test chamber as a function of the reciprocal of the collection voltage, and extrapolating the data to infinite collection voltage. The extrapolated value of the ion current may be taken to represent 100% collection, and values of the collection efficiency, f, may be plotted as a function of the inverse collection voltage. Such a plot for the air equivalent ionization chamber is shown in Figure 10. It is possible to

17
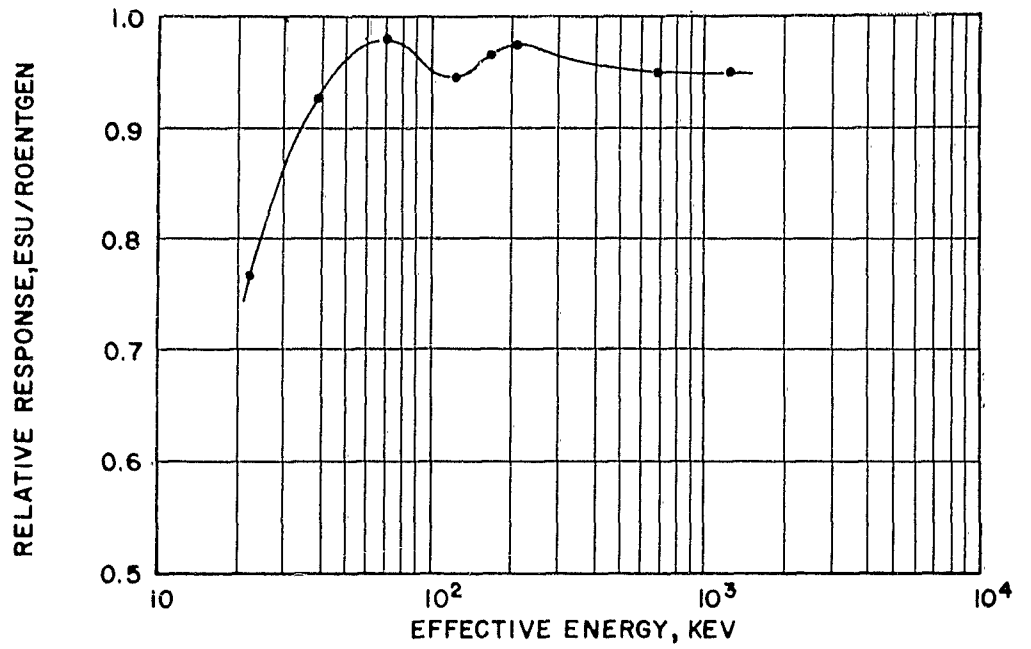
FIGURE 8. RELATIVE RESPONSE OF I-CC AIR EQUIVALENT
IONIZATION CHAMBER
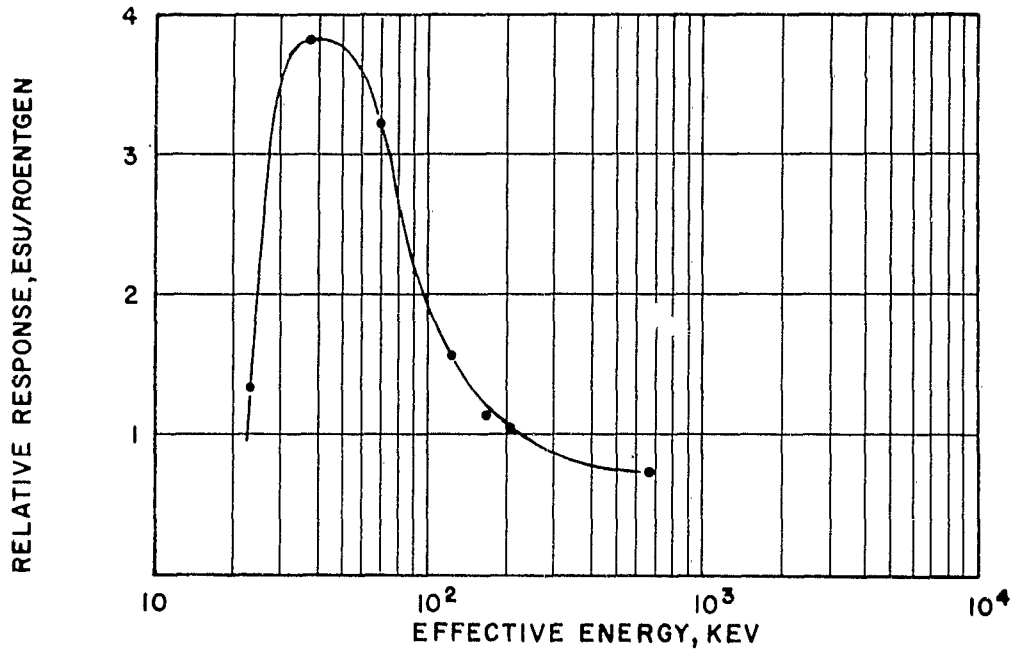
FIGURE 9. RELATIVE RESPONSE OF ALUMINUM
THIMBLE IONIZATION CHAMBER

18
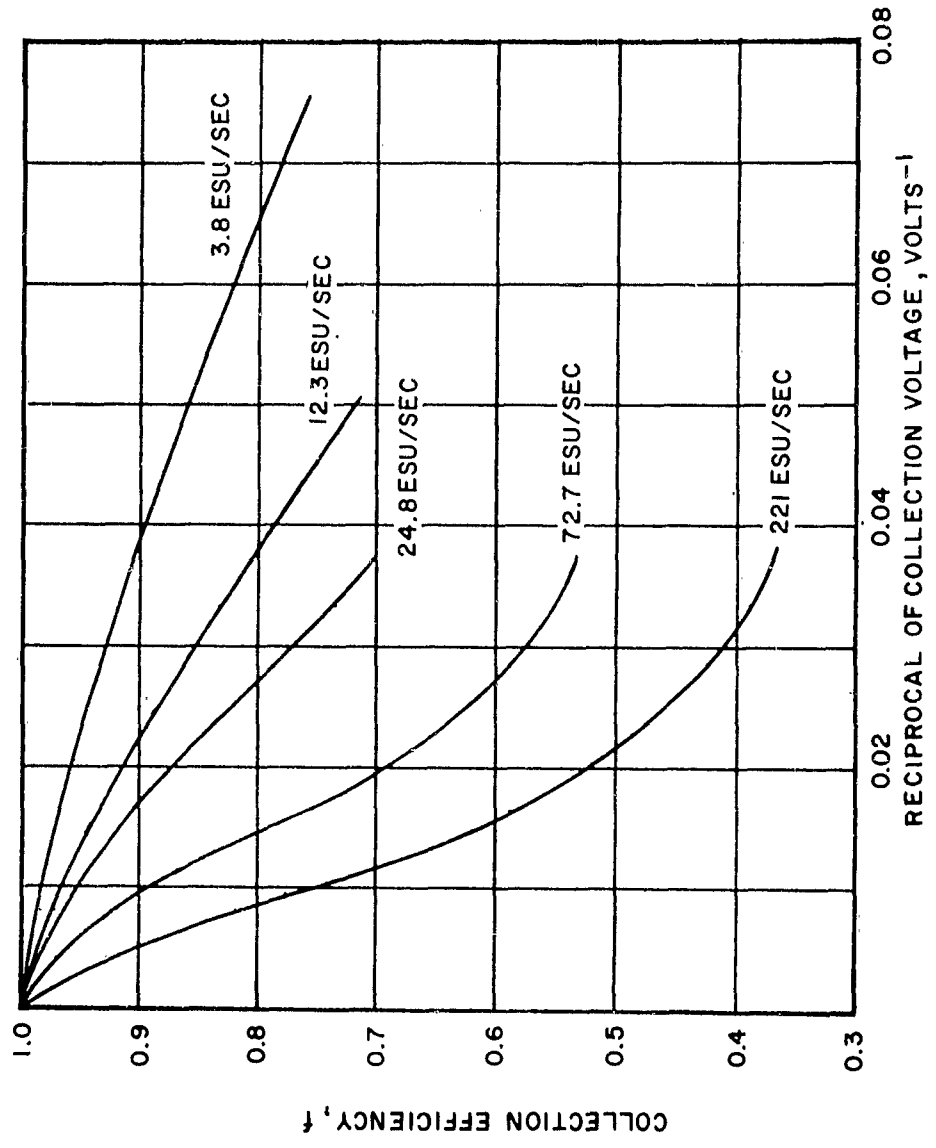
FIGURE 10. COLLECTION EFFICIENCY AS A FUNCTION OF I/V FOR AIR EQUIVALENT IONIZATION CHAMBER

19

extend the experimental data to predict the response of the chamber for different values of dose rate and collecting voltage and also to predict the response under pulsed conditions. For continuous radiation,

$$f = 1 - \frac{f^2 \xi^2}{4} \qquad (2)$$

where f is the collection efficiency and ξ is a parameter defined by

$$\xi = md^2 \ (\ \sqrt{q}/V) \qquad (3)$$

where

m = a constant, characteristic of the ionization chamber filling gas (air),

d = effective spacing of the ionization chamber,

V = applied voltage, and

q = charge density per unit time.

These two equations then define the relationship between the collection efficiency and the collection voltage when the constants m and d are evaluated.

The constants m and d may be evaluated by plotting ξ as a function of $\sqrt{q}/V$, and by determining the slope of the line. These plots are shown in Figure 11a for the air-equivalent ionization chamber and in Figure 11b for the aluminum thimble ionization chamber.

The resulting values of md^2 are 8.51 for the air equivalent ionization chamber and 0.922 for the aluminum thimble ionization chamber. These constants were used to construct the general collection efficiency curves for the two chambers shown in Figure 12.

20
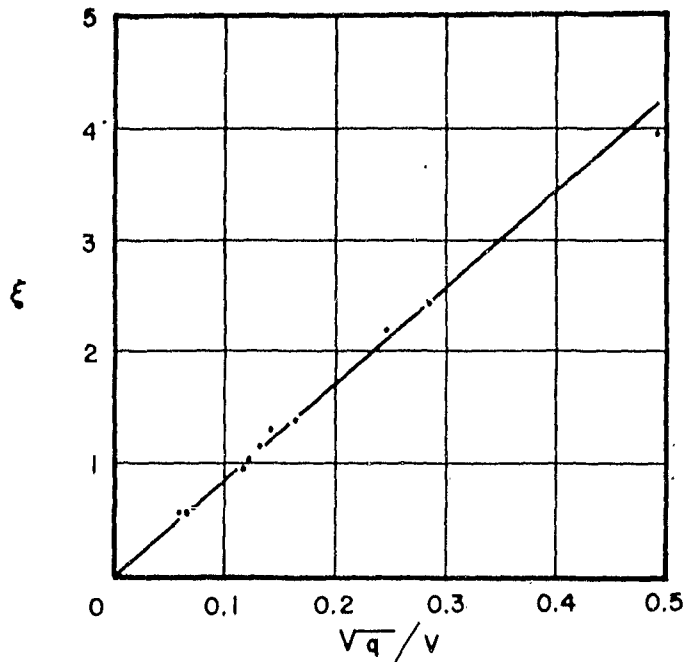
A. AIR-EQUIVALENT IONIZATION CHAMBER
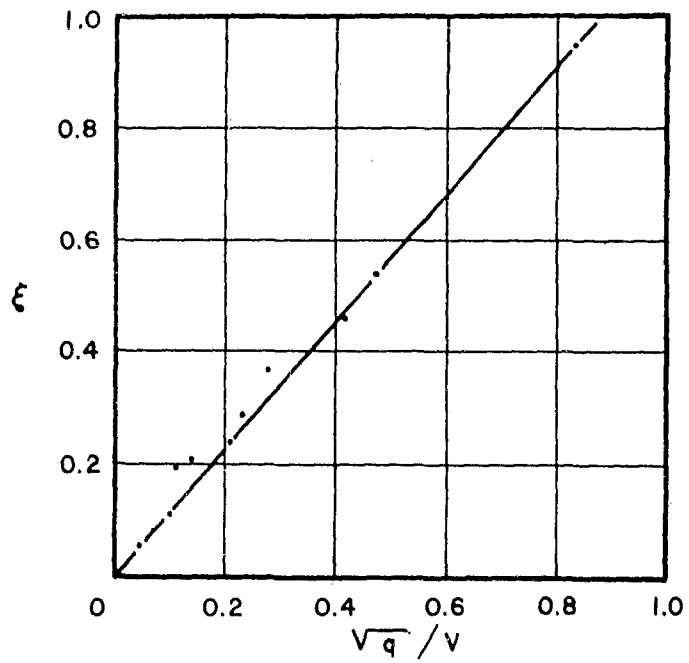
B. ALUMINUM THIMBLE IONIZATION CHAMBER, 0.66 CC

FIGURE II. DETERMINATION OF COLLECTION CONSTANTS

21
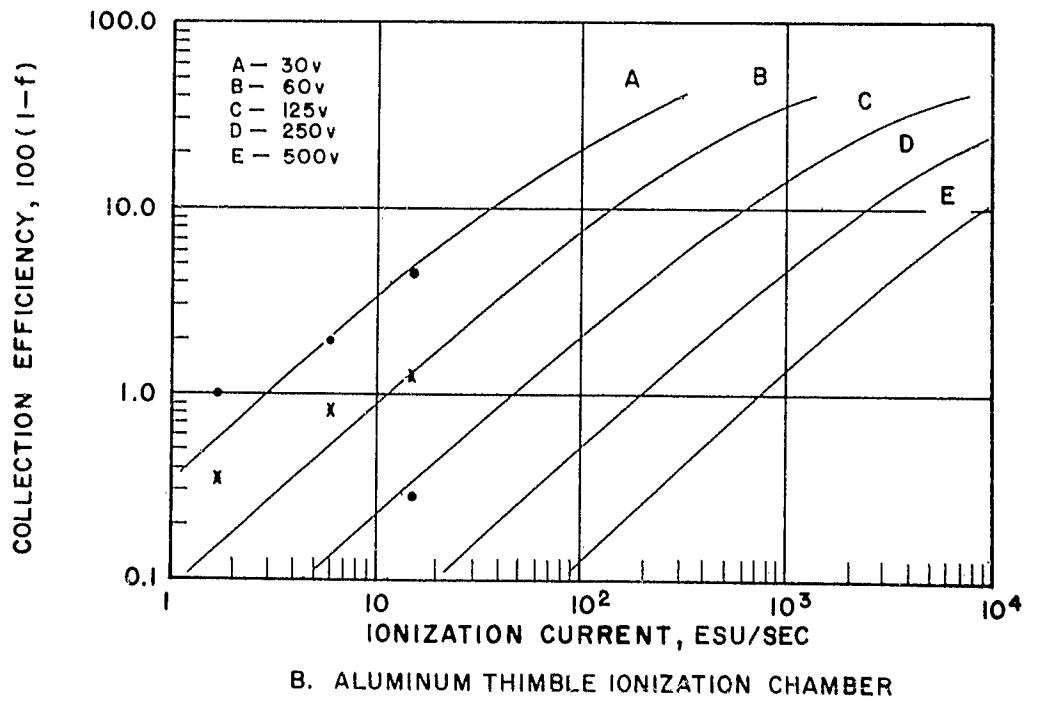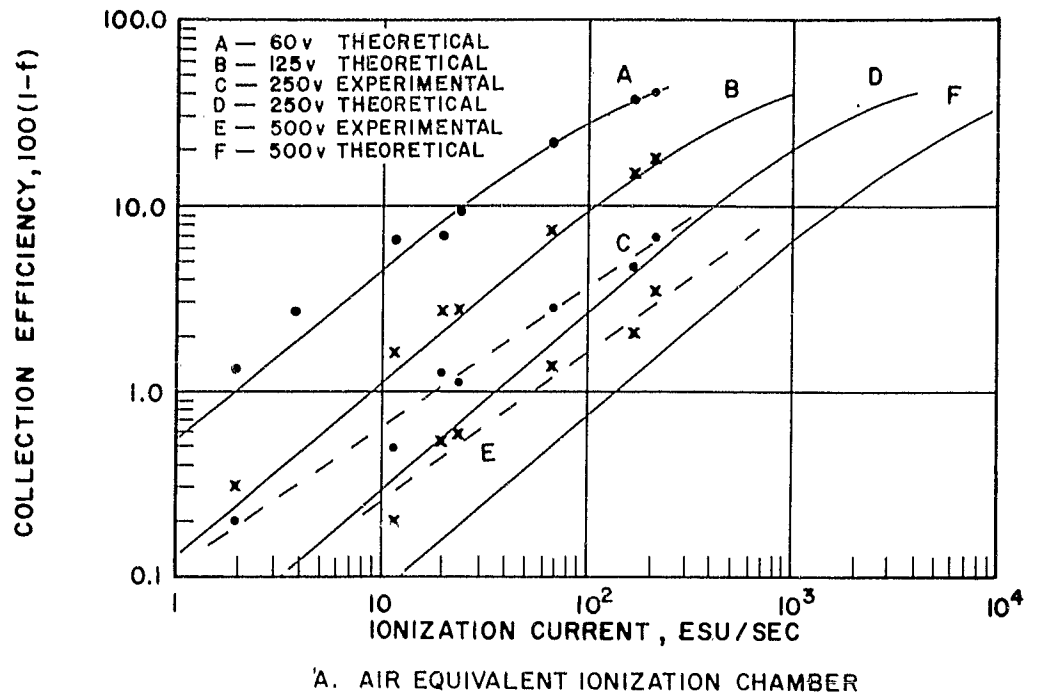
FIGURE 12. COLLECTION EFFICIENCY DURING CONTINUOUS
IRRADIATION

22

For pulsed radiation, the equations analogous to 2 and 3 are

$$f = \frac{1}{u} \log_e (1 + u) \qquad (4)$$

where f is the collection efficiency and u is a parameter defined by

$$u = \frac{Rd^2}{V} \qquad (5)$$

where

u = a constant, characteristic of the filling gas (air)

d = effective plate spacing in the ionization chamber

V = applied voltage

R = charge per unit volume per pulse

Boag gives a value of 15.9 for m and 1000 for μ. These constants are dependent on the ion mobilities and recombination coefficients only, and the ratio of m to μ would be expected to remain constant for air. The constant μd^2 for pulse collection, therefore, was obtained by the relation

$$\mu d^2 = \frac{1000}{15.9} (md^2). \qquad (6)$$

By utilizing this constant, the collection efficiency for the collection of short pulses of radiation was calculated for both ionization chambers. A plot of the efficiency is shown as a function of charge per pulse for several collecting voltages in Figure 13.

The validity of the predicted response under pulsed conditions was checked for both ionization chambers with the Fexitron Flash X-Ray. The x-ray system was operated at
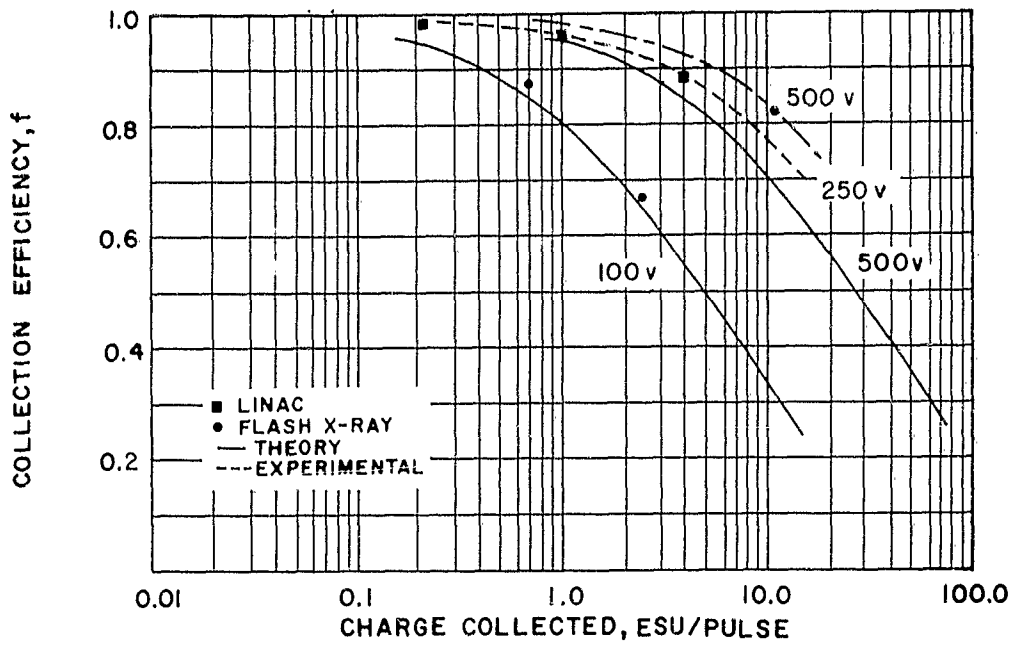
A. AIR EQUIVALENT IONIZATION CHAMBER
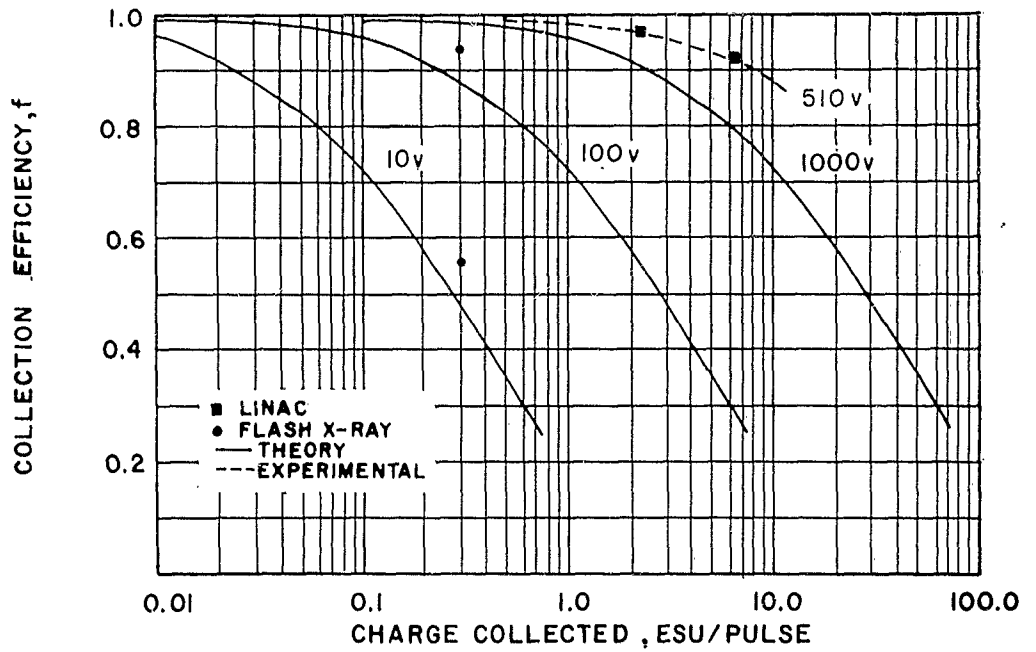
B. ALUMINUM THIMBLE IONIZATION CHAMBER

FIGURE 13. COLLECTION EFFICIENCY DURING PULSED
IRRADIATION

600 kvp and with a pulse width of 0.20 μsec. The total dose
per pulse was 240 mr at the position of measurement. Collection voltage on the aluminum thimble ionization chamber was
varied from 5 to 500 volts, while the air equivalent ionization chamber was maintained as a monitor at a constant
collecting voltage of 420 volts. Subsequently, the voltage
on the air equivalent ionization chamber was varied from 70
to 420 volts while the aluminum thimble ionization chamber was
maintained at a collection voltage of 500 volts. The resultant
experimental determinations of collection efficiency are shown
in Figure 13. Experimental results from the LINAC are included,
as well as additional flash x-ray points determined later.

It is of interest to note that the experimental efficiencies
are actually better than those predicted from the Boag theory.
This may be caused by differences in assumed-to-actual chamber
geometry as well as the validity of the assumptions required
in formulating the theoretical response of the air-equivalent
and aluminum thimble ionization chambers.

G. 50-CC GRAPHITE-CO_2 IONIZATION CHAMBER

In one phase of radiation detector evaluation, the
plutonium-beryllium neutron source and the Van de Graaff
accelerator were used. It was necessary to determine accurately
the neutron flux and the gamma dose rate. Fast neutron flux
can be quite accurately determined by sulfur activation, but
there is no gamma detector available that is insensitive to
neutrons. This problem was solved by using a detector with
known neutron response.

A 50-cc graphite ionization chamber was constructed
(Figure 14). The chamber was normally operated at atmospheric
pressure with a continuous flow of CO_2. The gamma-ray sensitivity of the chamber was easily determined by using an air
fill and a cobalt-60 source. The measured value was 44.78

esu/r, which agreed closely with the calculated value of 45.13 esu/r. When used with CO_2 the sensitivity was 69.53 esu/r. For self-consistency in mixed field evaluation, the charge collected was converted to CO_2 rads using the factor of 0.891 rad/r.
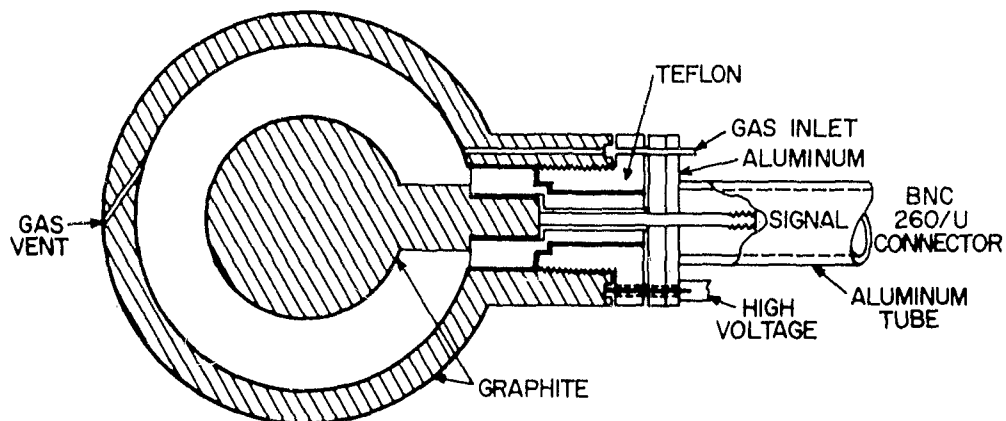
FIGURE 14. 50-CC GRAPHITE IONIZATION CHAMBER

The Pu-Be neutron source was used to determine collection characteristics of the chamber. Ion collection in the chamber is intimately connected with the linear energy transfer (LET) of particles producing the ionization, and the presence of small quantities of high LET particles may often be determined by observing how charge collection varies with a change in collection voltage. (Figure 15).

Practically all the ionization produced by the gamma rays from the Pu-Be source can be collected with a 10-volt collection voltage. Further increase in collection voltage indicates two other types of ionizing radiation, i.e., the recoil nuclei and their low energy delta rays.

This single experiment determined both the gamma dose rate and the neutron response of the chamber. Figure 16

26
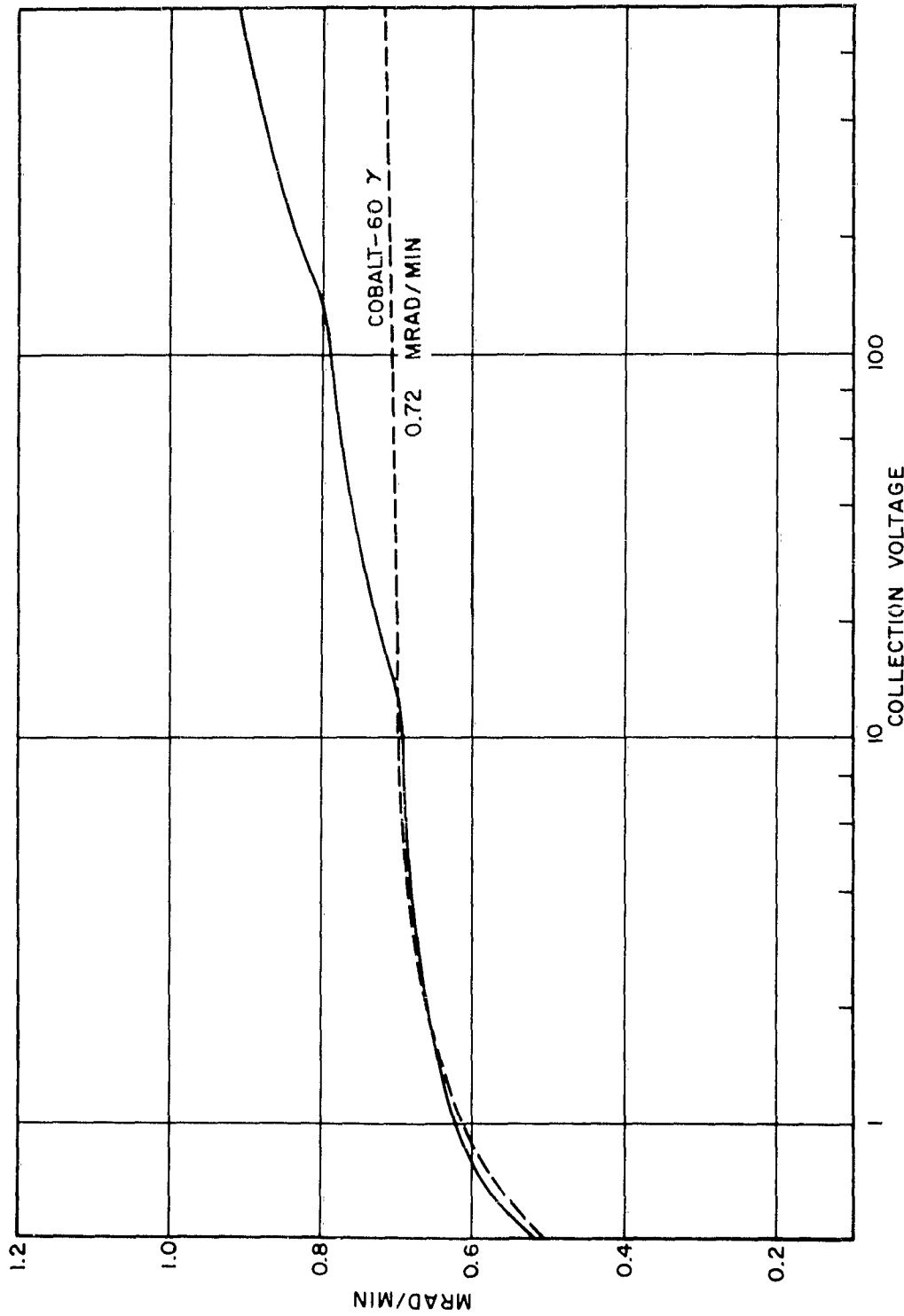
FIGURE 15. COLLECTION CHARACTERISTICS OF 50-CC GRAPHITE-CO₂ IONIZATION CHAMBER 10 CM FROM Pu-Be FAST NEUTRON SOURCE

27

FIGURE 16. COLLECTION CHARACTERISTICS OF 50-CC GRAPHITE-CO_2 IONIZATION CHAMBER 10 CM FROM Pu-Be FAST NEUTRON SOURCE

28

shows charge collected plotted as a function of the inverse
of the collection voltage. This method of plotting is useful
in stripping out the mixed-field components and in extrapola-
ting the collection curve to an infinite voltage for deter-
mination of the collection efficiency. Identification of
the gamma ray contribution to the collection field requires
the chamber collection characteristics in a Pu-Be gamma ray
field be known. Figure 17 shows collection losses for
cobalt-60 gamma rays. These data are presented for inter-
polation in Figure 18. Application of these data is shown
by the dashed line in Figure 15. The good correlation be-
tween the shape of the first Pu-Be plateau and a gamma-ray
collection characteristic for the same intensity serves to
identify that portion of the mixed field as gamma rays.

H. SULFUR THRESHOLD FOILS FOR FAST NEUTRON DOSIMETRY

1. Neutron Flux from the Pu-Be Source

The neutron flux monitored by sulfur threshold detectors
must consider both the activation cross section for the sulfur
(n,p) reaction as well as the neutron spectrum of the source.
This laboratory maintains calibrated counters for NAD
service. These instruments utilize a standard 1-1/2-inch-
diameter by 3/8-inch-thick sulfur foil and provide a neutron
flux number for a fission spectrum irradiation. A 3.0-Mev
threshold in conjunction with a 300-mb cross section is con-
sidered. To determine the flux from the Pu-Be source it is
necessary to combine the sulfur cross section and source
spectrum to obtain an effective activation cross section.
Once determined, the flux number from the NAD system can
be corrected by the ratio of the two cross sections.

29
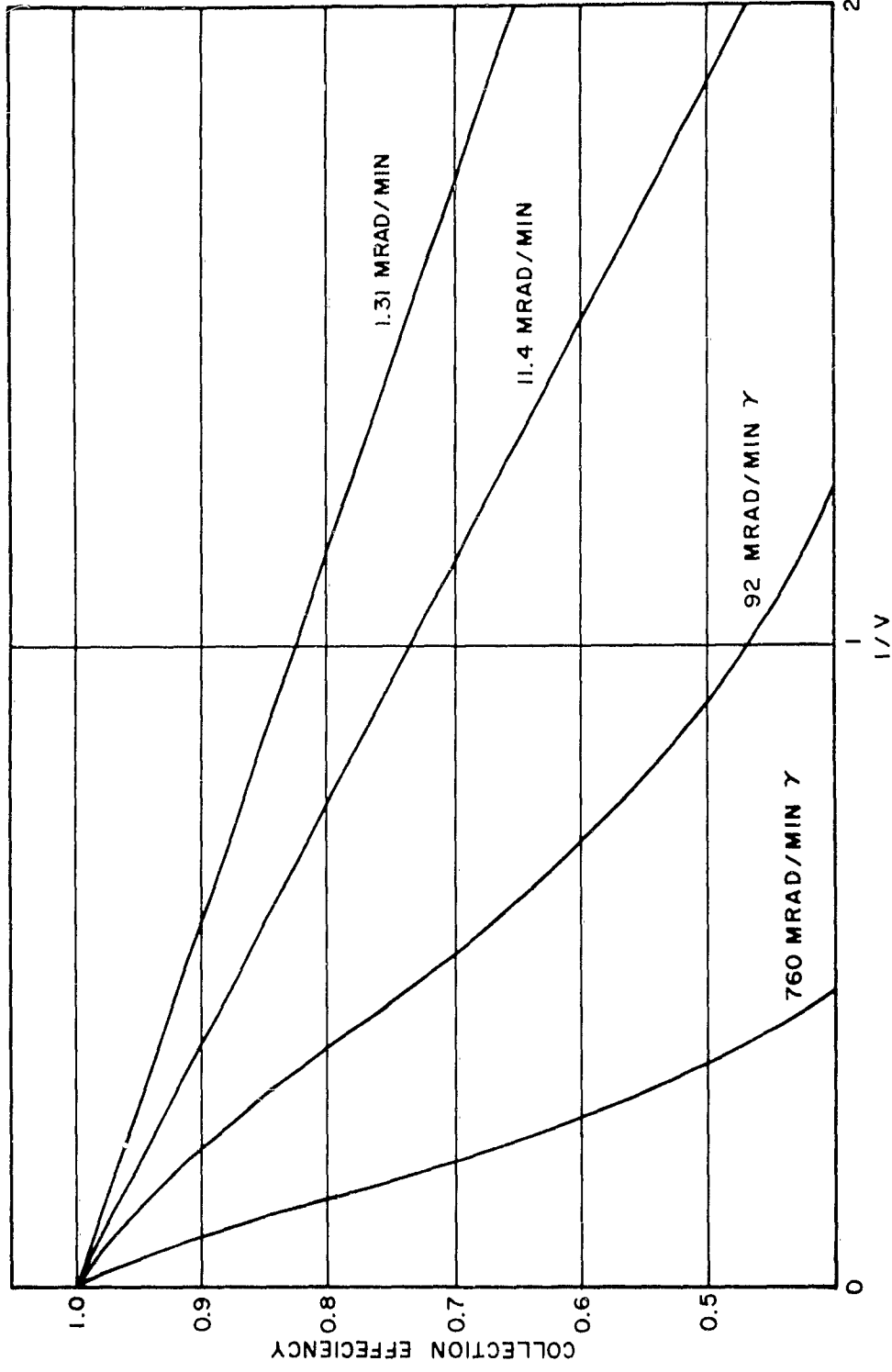
FIGURE 17. COLLECTION CHARACTERISTICS OF 50-CC GRAPHITE-CO_2 IONIZATION CHAMBER USING Co^{60} GAMMA RAYS

30
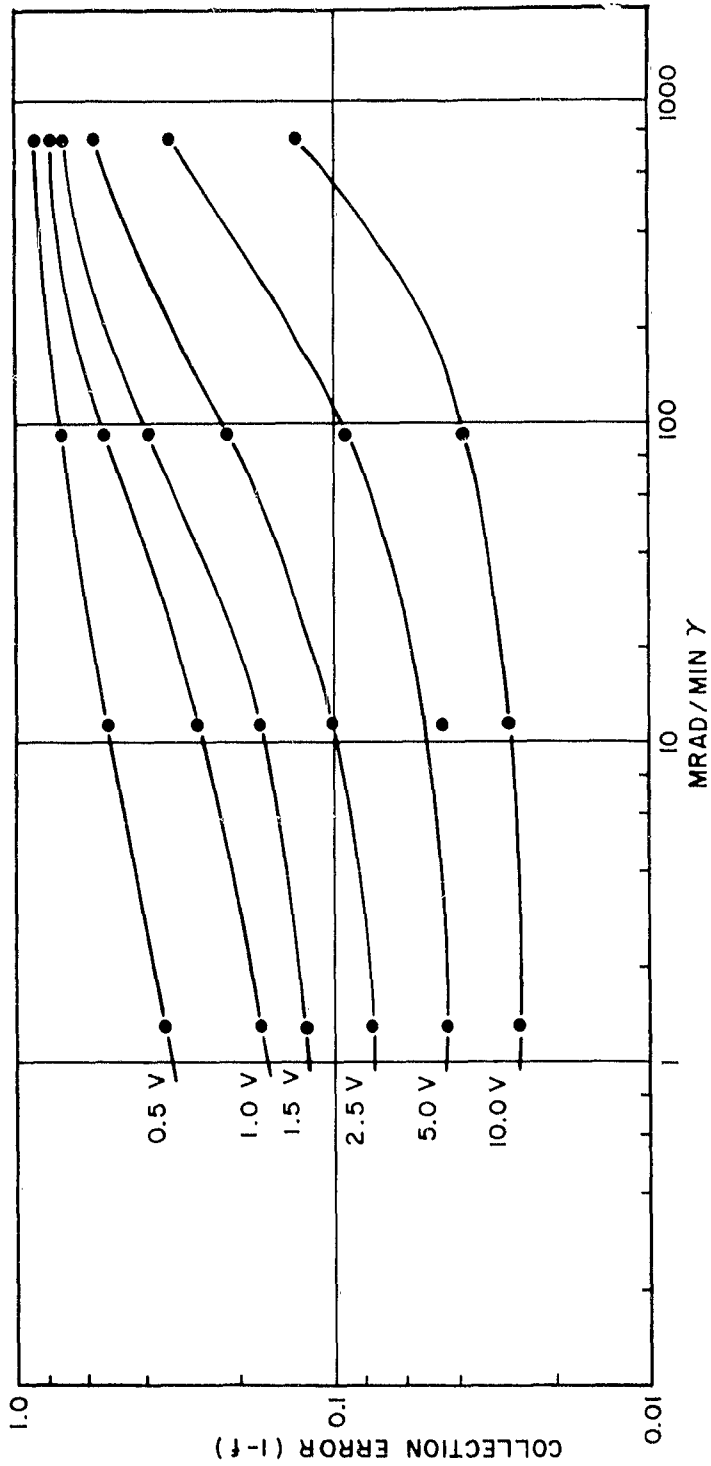
FIGURE 18. COLLECTION CHARACTERISTICS OF 50-CC GRAPHITE-CO_2 IONIZATION CHAMBER USING Co^{60} GAMMA RAYS

31

The sulfur activation cross section as a function of neutron energy was taken from a report by Troubetzkoy, et al.,[6] and the Pu-Be spectrum from Stewart.[7] Figure 19 shows a histeogram of these data. An effective cross section of 207 mb was determined by folding the two curves at 0.1-Mev intervals. The source has a nominal value of 1.4×10^7 neutrons/second while by the method outlined above, a value of $1.58 \times 10^7 \pm 6\%$ neutrons/second was determined.

2. Neutron Flux from the 400-kv Van de Graaff

The same sulfur threshold technique was used in determining the integrated neutron output from the 14-Mev (d,t) reaction of the Van de Graaff. Although the neutron production is isotropic, the neutron energy has a particular distribution about the target. The neutron energy at 90° from the target, however, is predominantly 14 Mev. By carefully placing the sulfur detector at this position and by making the appropriate ratio of activation cross section from fission spectrum (300 mb) to 14 Mev (248 mb), a flux number can be obtained and correlated to a beam monitor for normalizing data on different runs during a series of experiments.

I. THERMAL NEUTRON DETECTORS

Gold and cadmium-covered gold foils are used in a subtraction technique which allows a determination of the neutron flux for neutron energies less than 0.5 ev. Another term sometimes used in thermal neutron studies is the cadmium ratio or, specifically, the fraction of activity of a bare gold foil divided by the activity of its associated cadmium-covered gold foil.

This number may be used as a figure of merit for a thermal neutron source. For example, the cadmium ratio for the particular cavity used in the General Dynamics/General Atomic

32
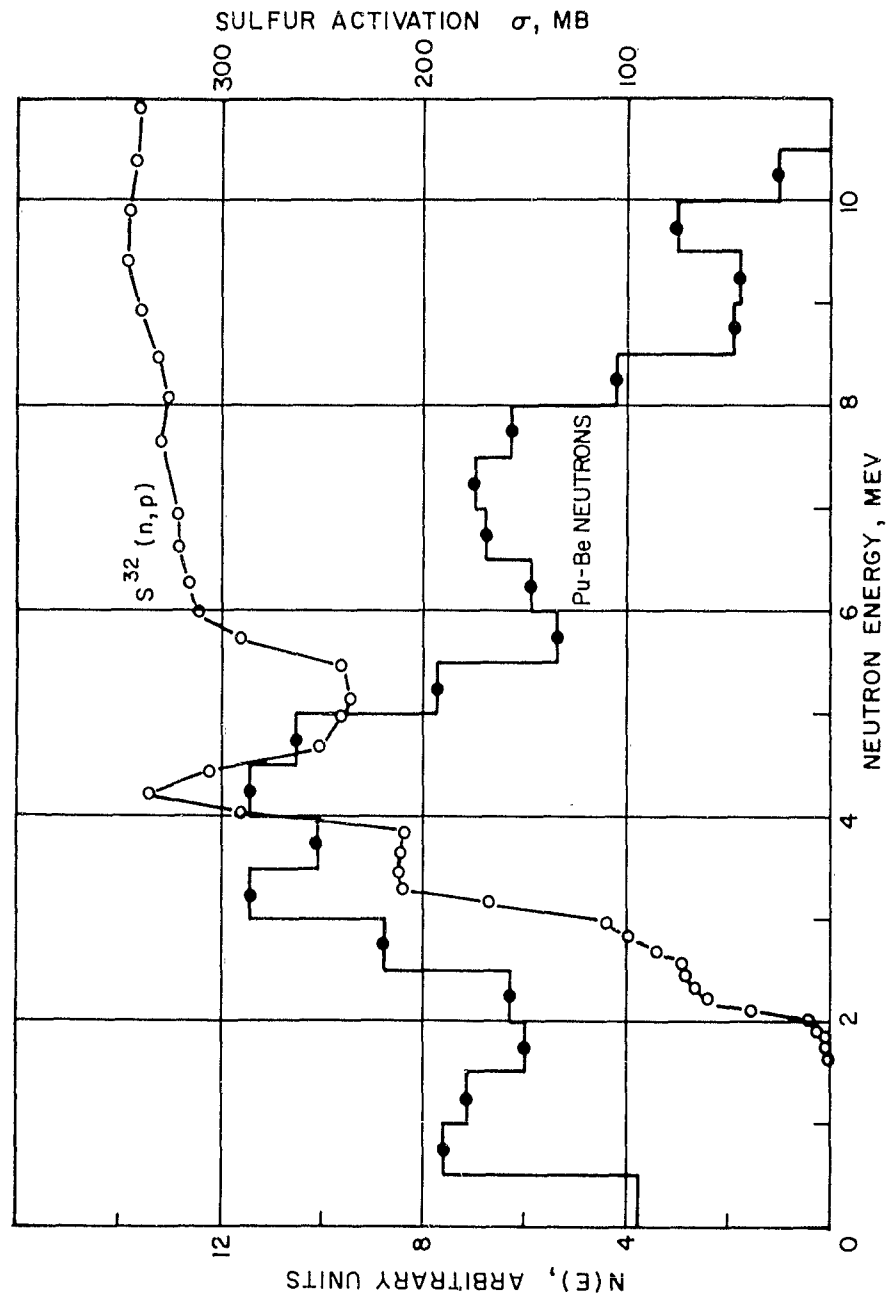
FIGURE 19. Pu–Be NEUTRON SPECTRUM AND SULFUR (n, p) CROSS SECTION

33

thermal neutron facility was 520 while the paraffin geometry with the Pu-Be source was about 15.

Because gold has several large resonances at higher neutron energies, for comparison this number should be examined with a knowledge of the source and its spectrum. It is obvious however, that a large number in any case is representative of a good source of thermal neutrons.

J. NEUTRON FLUX MONITOR

To perform precise measurements on the 14-Mev (d,t) neutron beam, a monitor is necessary. The monitor used in these experiments was a lead-shielded plastic fluor coupled to a photomultiplier tube. The charge and current were read on two General Radio electrometers. Since all the detectors involved were sensitive to total dose or flux, the charge for a particular exposure was used to normlize the data. Figure 20 shows the monitor system.

Some calibration factors for the Van de Graaff accelerator are shown in Tables 2 and 3. These data result from exposures of sulfur pellets at 31.6 and 100 cm from the target. The standard deviation for counting the sulfur was approximately 3 and 7% for the sulfur exposed at 31.6 and 100 cm, respectively.

TABLE 2. Neutron Flux Determination for the
Van de Graaff Beam Monitor

	31.6 cm	100 cm
Sulfur Pellet No.	1S20	1S21
Exposure Duration, min	13	15.06
Monitor Charge, coul	3.913×10^{-4}	5.456×10^{-4}
Total Flux, n/cm^2	6.5×10^{7}	0.97×10^{7}
Ratio of Total Flux to Monitor Charge	1.662×10^{11}	1.776×10^{10}

TABLE 3. Absorbed Dose Determinations (Normalized for the Van de Graaff Mixed Field to 3×10^{-5} monitor coulombs/minute)

	31.6 cm	100 cm
Total CO_2 rads/min	0.0088	0.00107
CO_2 rads/min/from neutron flux	0.00838	0.000895
Net CO_2 rads/min from gamma	0.00042 ± 0.00025	0.000175 ± 0.000063
Gamma/neutron ratio (CO_2 rads)	0.5	0.195
Gamma/neutron ratio (tissue rads)	0.018	0.070
Gamma/neutron ratio (number flux assuming 1-Mev gammas)	0.20	0.78
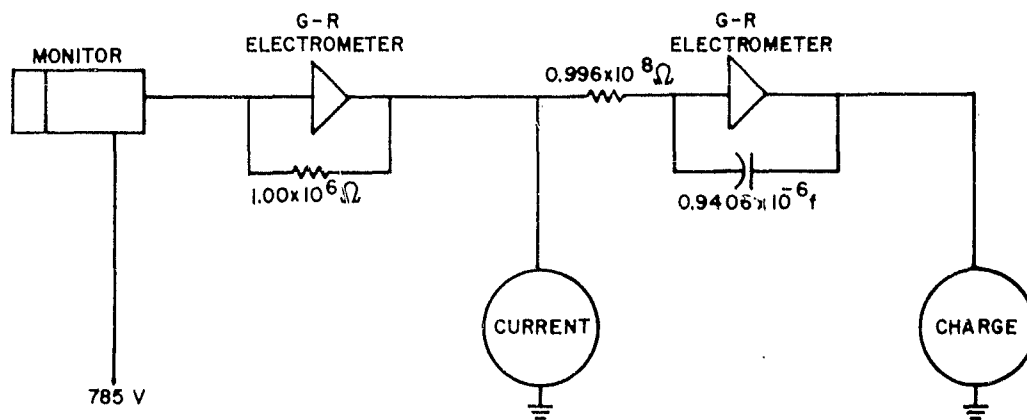
FIGURE 20. VAN DE GRAAFF MONITOR

35

K. LINAC ELECTRON BEAM MONITOR

The monitor used in the LINAC electron beam experiments was a 200-cm^2, 1-inch-thick aluminum block. To preclude collection of free ions in the air, a thin aluminum shell, insulated from the block and at ground potential, was used. Only electrons of the beam were then stopped and collected by the block. Correlation of the current collected was made to the air equivalent ionization chamber also enclosed in a thin metallic shell at ground potential. The monitor was placed at 200 cm and all exposures were made at interposed positions.

In later experiments, this block was modified to incorporate only a 1-inch-diameter active section in the center. For rate studies, the silver-activated glass rods and cobalt glass were affixed to this area by double-faced masking tape. In effect then, the dose delivered to the dosimeters was also measured by the electrons stopped in this small volume. Uncertainty in beam location is not a source of error in this method.

The thermoluminescent dosimeter samples were placed at the edge of this area because they were more massive and would introduce an error into the number of electrons collected. Evaluation of data from this portion of the experiment indicated that beam position was critical only at distances of 15 cm or less from the beam port.

IV. DOSIMETRY SYSTEMS READOUT INSTRUMENTATION

A. SILVER-ACTIVATED GLASS-ROD READER

A Bausch & Lomb Microdosimeter Reader Model 1 is the basic instrument used for determining the glass rod fluorescence. Early in the program, efforts were made to enhance the readout resolution and stability. The reader was powered from a Sorenson Model 1001 regulated 115-volt, a-c power supply, and the filament of the differential amplifier tube was separately energized from a 6-volt, 100-amp-hr battery. The nulling accuracy was improved by using a light beam galvanometer in lieu of a standard, panel-mounted meter. A 5-mm deflection of the light beam was equivalent to a single division of the readout dial.

The early efforts to improve stability, sensitivity, and linearity of the microdosimeter reader were not entirely satisfactory. A new modular system was constructed from available components and proved to be superior to all previous configurations. This consisted of two operational amplifiers receiving the photomultiplier signals directly, and the output fed to a digital ratiometer. Excellent long-term stability and repeatability and accurate readout to four significant figures were easily achieved. The system is illustrated in Figure 21. The sensing electrometer is operated with a 10^7- or 10^8-ohm input resistor and a 0.1- or 0.01-μf capacitor to establish a time constant of 1 second. The electrical stability is approximately 0.2r at the level of the background fluorescence of an unirradiated rod. At high dose levels, the stability is principally limited by the photomultiplier tubes and their associated circuitry. For short periods the stability is approximately 0.1% and may be several percent over long periods of time.
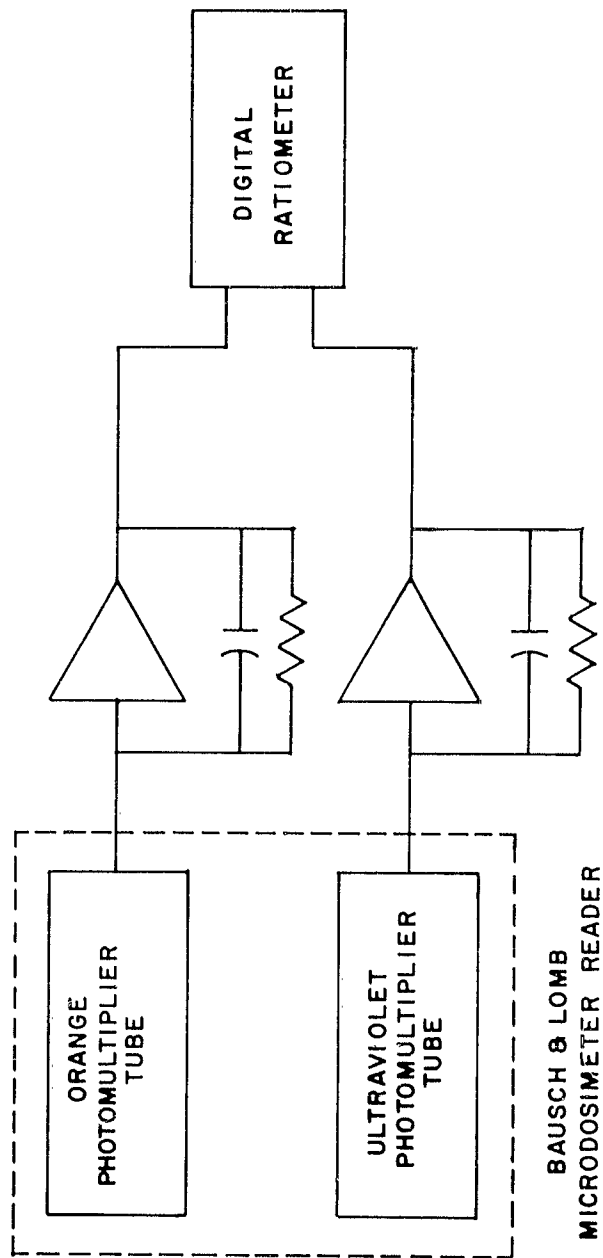
FIGURE 21. GLASS ROD MICRODOSIMETER READING SYSTEM

The most accurate technique for determining the fluor-
escence of the rods was to take two readings at 180° rotational
difference on each end of the rod, a total of four readings
per rod, and average the results (Appendix C). The fine
resolution of the readout system makes absolute cleanliness
essential. Each rod was cleaned ultrasonically in alcohol
and rinsed in a fresh absolute alcohol bath, dried in a
stream of dry nitrogen, and carefully placed in the micro-
dosimeter reader with special tweezers.

B. COBALT GLASS PLATE READER

The original unit used for readout of the cobalt glass
plates was a Bausch & Lomb Spectronic 20 spectrophotometer.
Readings were made in terms of optical density at a wave-
length of 400mμ At this wavelength, the plates had a back-
ground density of approximately 0.07 and the density could
be read to an accuracy of 0.002 density unit.

In determining cobalt glass characteristics at low and
medium energies, the sensitivity of the Spectronic 20 was
seen to be lower than was desired. Relatively large doses
were required to produce density changes that could be
measured with this machine. The more sensitive Beckman DK-2
recording spectrophotometer was utilized by modifying a
Spectronic 20 chuck to fit in the sample holder. The DK-2
was operated in the transmission mode at a wavelength of
400 mμ, with the photomultiplier tube as detector and a
slit width of 0.03 mm. The glass was read in two orien-
tations such that the ends of the glass are in alternate
positions. A separate unirradiated glass dosimeter read in
similar fashion was used as a reference for all measurements.
A measurement was obtained by first adjusting the DK-2 for
100% transmission of the reference on the most sensitive

39

scale (0.95 to 1.05). The sample to be irradiated was read
with the same sensitivity settings. Prior to the reading of the
irradiated sample, the DK-2 was again adjusted to 100%
transmission with the reference dosimeter. The sample was
then measured with the same sensitivity settings. The logarithm
of ratio of the sample transmission before and after irradi-
ation (that is, the optical density) was used as a measure
of the dose. Measurements of low doses (1000 to 10,000r)
can be made with a reproducibility of approximately 0.05%
which is 0.0002 density units. Glass plates were cleaned
before reading by washing in absolute alcohol and wiping
with a Kimwipe. Subsequent handling was performed with
ivory-tipped or plastic tweezers. The difference of trans-
mission readings of alternate ends was found to correlate
with the cleanliness of the glass dosimeter as well as
severely chipped edges and striations in the glass. In
some instances non-uniform irradiation sometimes encountered
in a LINAC beam will produce a similar effect.

C. CaF_2(Mn) THERMOLUMINESCENT DOSIMETER READER

The basic thermoluminescent dosimeter (TLD) is an evacu-
ated glass ampule which contains the manganese-activated,
calcium fluoride phosphor deposited on a metal substrate.
Electrical leads are connected in such a manner that the
substrate can be heated to the necessary readout temperature.

The readout device consisted of a regulated current supply
and timer which provides a reproducible heating cycle. This
heat cycle lasts for 20 seconds and the peak fluorescence
occurs in approximately 10 seconds. A 6199 photomultiplier
with a blue filter was used to monitor the blue-green
fluorescence and a General Radio DC Amplifier, Model 1230A,
was used in conjunction with a strip chart recorder for

40

determing the peak signal. A shutter system was incorporated
so that the dosimeter could be inserted and removed without
changing the voltage or input signal level to the photomultiplier
tube. It also provided a means of adjusting the amplifier
and recorder for zero input signal. Doses of approximately
2 to 4r were used for the experiment involving energy response
and shield evaluations. Backgrounds were negligible for
these measurements, and the heat cycle was sufficiently long
to erase the dosimeter completely for the next exposure.
To obtain confidence in the data, the dosimeter was allowed
to cool at room temperature for a minimum of 15 minutes after
readout before a subsequent exposure.

V. SILVER-ACTIVATED PHOSPHATE GLASS
MICRODOSIMETER SYSTEM

A. SILVER-ACTIVATED GLASS ROD DOSIMETER

The silver-activated glass rod dosimeter is a small cylinder 1-mm in diameter and 6-mm long. The glass composition is

Material	Weight %
$Ba(PO_3)_2$	23.15
$K\ PO_3$	23.15
$Al(PO_3)_3$	46.3
$Ag\ PO_3$	7.4

Irradiation by x-rays, gamma rays, or nuclear particles cause metastable energy levels to be produced in the glass. By illuminating the irradiated glass with ultraviolet light, these metastable levels give rise to an orange fluorescence. The system is based on the proportional response of this fluorescence to the exposure dose.

An inherent background fluorescence apparently caused by the glass constituents provides a predose reading of approximately 25 r. For expected low dose exposures, each rod is preread and the background level recorded.

To determine the minimum error obtainable from a glass rod taken at random, a linear measurement and weight analysis was performed on a group of 50 rods. The diameter of each rod was measured with a Bausch & Lomb DR-25B optical gage. Accuracy to 10^{-5} inches was possible and an average diameter for the group was 0.03972 inch ± 0.69%. In turn, 50 rods were weighed individually on a Mettler balance. An average weight for a glass rod was 0.01375 gram, ± 1.6%. On the basis of

these data for one-rod statistics, it appears that the limit of the system is 3 to 4% without further grading of the glass rod dosimeters.

In an effort to provide better self-consistency in the study, a rod selection system was initiated based on individual rod response. To facilitate this selection, a large group of undosed rods were exposed to a nominal radiation exposure. The rods were read and placed into groups having the same response. The fluorescence of the rods was quenched by baking overnight at a temperature of 850°F. The spread within the groups was 3% at selection. The groups were systematically exposed to the same Co-60 dose to verify the selection processes. In addition, a relative response index was determined for each group.

This system was used until the rotational dependence study was performed (Appendix C). At that time the multiple reading technique took precedence. Before that, however, a large number of glass rods were read by the above procedure, and a distribution curve for a 1000r dose was obtained. Figure 22 shows the number of glass samples in 2% intervals as a function of glass rod response.

B. SILVER-ACTIVATED GLASS ROD SYSTEM LINEARITY

To measure effectively the rate and energy dependence of a dosimeter system independently of any possible nonlinear characteristics one of two procedures may be used. All exposures are made so that a constant dosimeter response is effected; the exposure dose is then the dependent variable of the experiment. In practice, this technique is somewhat difficult, and the alternate technique is to measure the linearity at a constant energy and dose rate and use the resulting data to arrive at an apparent dose which can be compared to the true dose. The latter method has been used in most of these studies. A

43
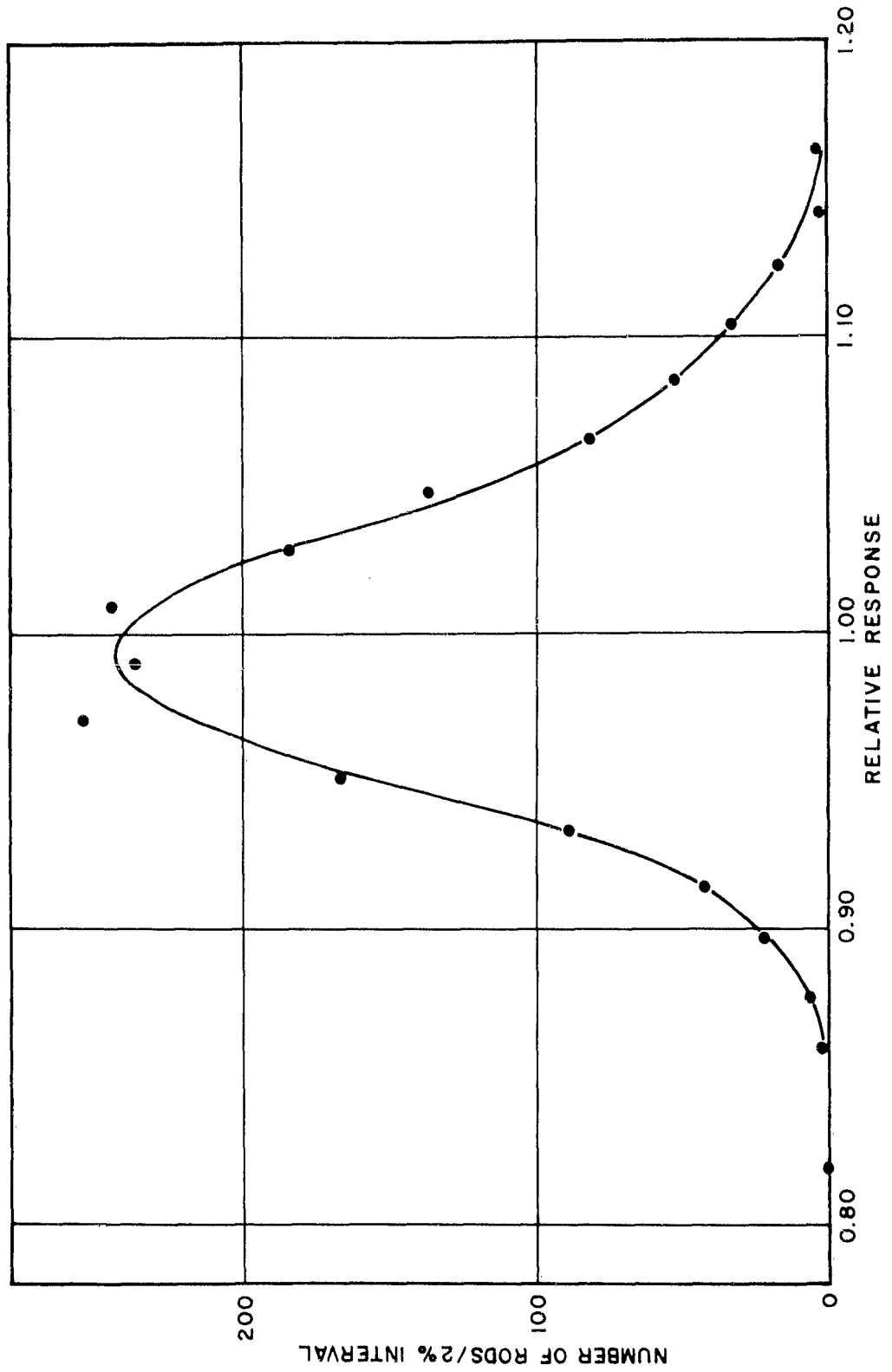
FIGURE 22. RESPONSE DISTRIBUTION OF 1584 SILVER-ACTIVATED GLASS MICRODOSIMETERS EXPOSED TO THE SAME DOSE OF X-RADIATION

44

curve of dosimeter response as a function of exposure dose for the silver glass system is shown in Figure 23A. In practice, the differential calibration curve is better suited for precise comparisons. Such a curve is shown in Figure 23B for the silver glass system. These data were obtained at a constant dose rate of 1 r/sec. Exposures of 1 to 30,000 seconds with a 50-curie Co-60 source were utilized.

C. EVALUATION AND RELIABILITY LIMITS

Normally, the lowest dose that may be read out without loss of precision is 10r. However, if rods of selected minimum background are used it is possible to achieve consistent results as low as 2r. At this level the difference ratio figure is only 0.00025.

The practical upper limit of response is approximately 25,000 to 30,000r. Beyond this dose, the readout ratio becomes nonlinear.

D. FLUORESCENCE BUILDUP

It is well known that the use of the silver glass system has required correction for an inherent buildup of fluorescence during the first 24 hours after irradiation. To ensure that errors were not incurred as a result of uncertainties in the magnitude and rate of this buildup, an experiment was devised to measure this buildup from a few seconds after a short exposure to greater than one day. The readout system was placed near the x-ray machine and equipped with a recorder for recording the fluorescence during the first few seconds after the exposure and before the digital ratiometer had settled out. The first useful recorder data were obtained 8 seconds after the first second of a 2-second exposure. Useful data were obtained on the digital ratiometer after 20 seconds and further

45
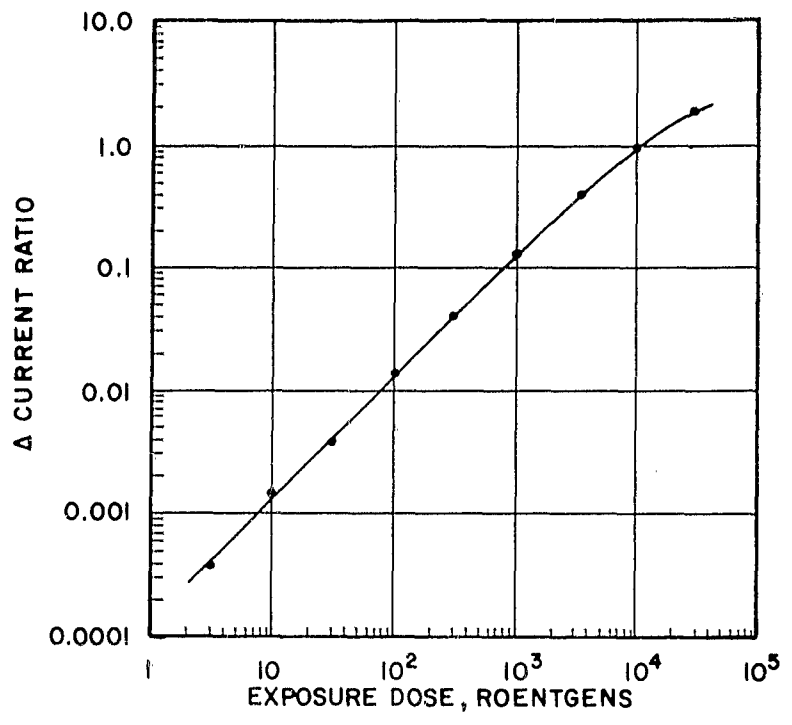
A. CALIBRATION CURVE
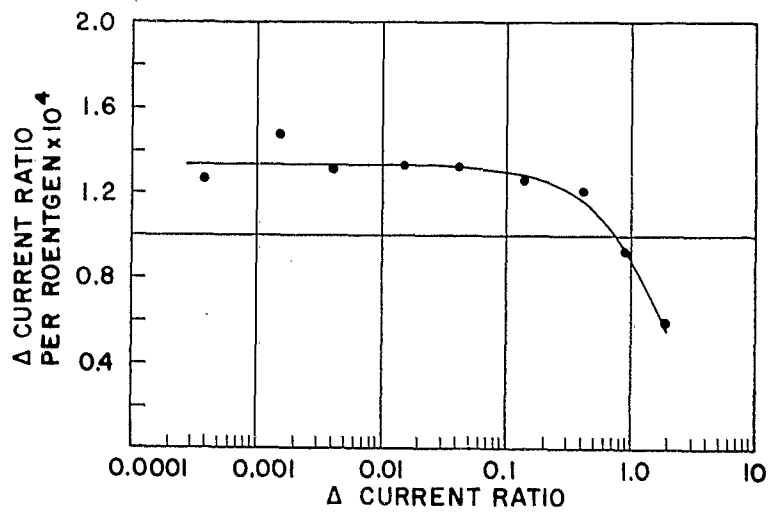
B. DIFFERENTIAL CALIBRATION CURVE

FIGURE 23. SILVER-ACTIVATED GLASS ROD MICRODOSIMETER
Co^{60} RADIATION CALIBRATION CURVES

46

readings were taken at intervals throughout the first day. To avoid the possibility of removing the fluorescence centers caused by prolonged exposure to the ultraviolet radiation, the glass rod chucking mechanism was withdrawn during the interval between readings after the first 5 minutes. The resulting fluorescence buildup curve is shown in Figure 24.

The data of Figure 24 were noted to resemble the growth of a daughter product in radioactive decay, and an effort was made to find the half-life of the parent state. The results of an analysis indicate that the growth curve actually is the result of the decay from four discrete, non-fluorescent states each with widely differing half-lives. The results of the stripping processes are shown in Figure 25 and 26. The empirical equation for the fluorescence buildup becomes

$$F = F_{max} (1 - A_2 e^{-\lambda_2 t} - A_3 e^{-\lambda_3 t} - A_4 e^{-\lambda_4 t}$$

$$- A_5 e^{-\lambda_5 t}). \qquad (7)$$

This is the equation for the decay of four parent states to a single daughter state which is initially 60% populated. A summary of the half-lives and initial populations of the five states is shown below:

Term	Half-Life, minutes	Initial Population, A
5	0.143	0.100
4	0.697	0.141
3	3.83	0.1088
2	34.0	0.0544
1	Long	0.596

47
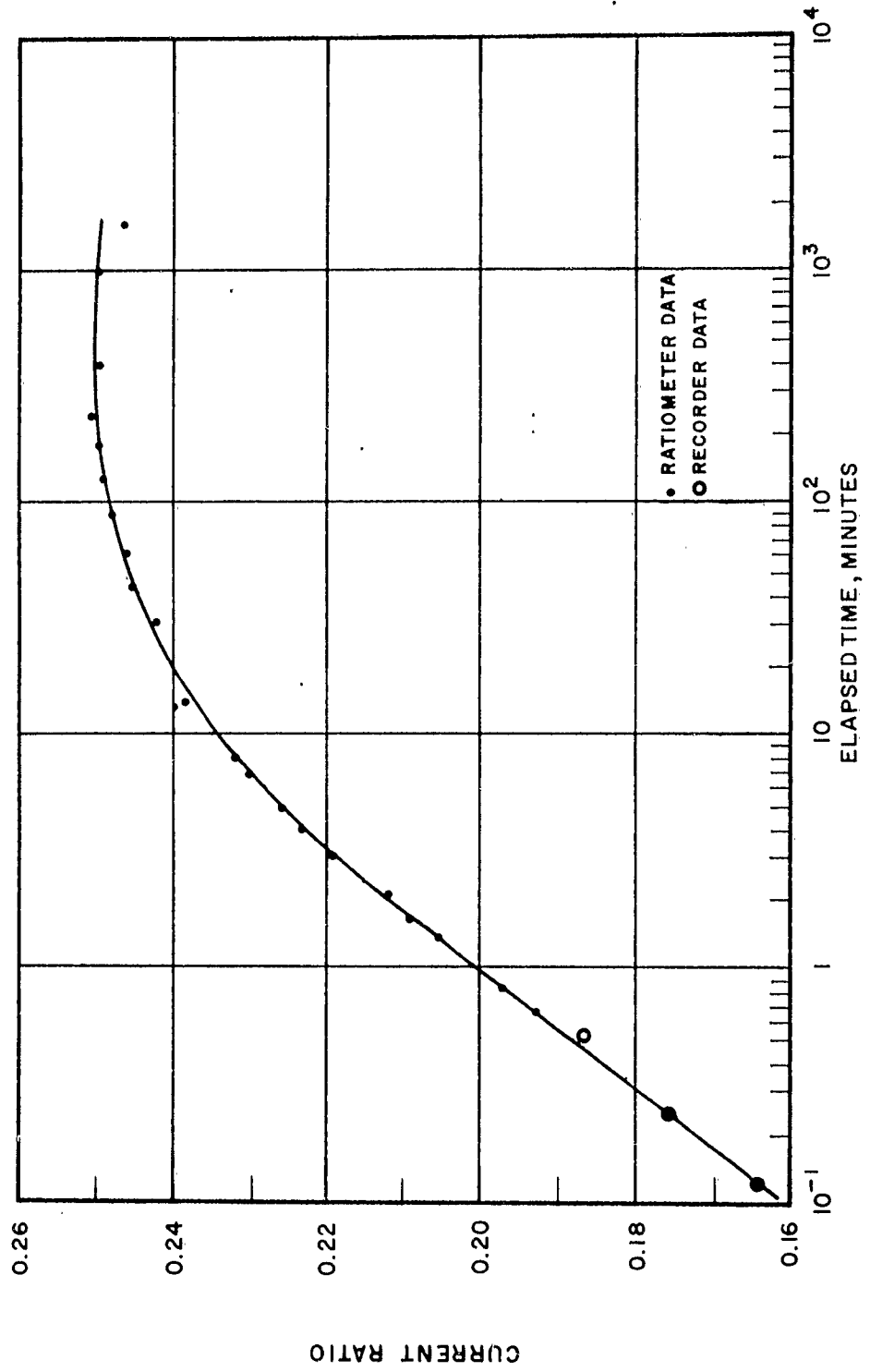
FIGURE 24. FLUORESCENCE BUILDUP IN BAUSCH & LOMB HIGH-Z GLASS ROD MICRODOSIMETERS, 2-SECOND X-RAY EXPOSURE

B. SECOND RESIDUAL COMPONENT, $T_{1/2}=3.83$ MINUTES

A. FIRST RESIDUAL COMPONENT, $T_{1/2}=34.0$ MINUTES

FIGURE 25. FLUORESCENCE BUILDUP CURVES

49

FIGURE 26. FLUORESCENCE BUILDUP CURVES

B. FOURTH RESIDUAL COMPONENT, $T_{1/2} = 0.143$ MINUTES

A. THIRD RESIDUAL COMPONENT, $T_{1/2} = 0.697$ MINUTES

E. ENERGY RESPONSE

Energy response of the glass rods was determined by exposing a calibrated group of five rods at each of the energies listed in Table 1. These data were normalized for group response as described and also to Co-60 response. The resulting response curve is shown in Figure 27 with a theoretical curve based on the ratio of absorbed dose in the glass to absorbed dose in air. There is good agreement between the two curves at energies above 100 kev. Thornton and Auxier[8] have shown that the difference at lower energies is caused by the finite width of the spectrum used and the self-attenuation of the glass rods.

The response at 662 kev reported earlier was distorted by the Cs-137 beam contamination. This distortion was rectified in later work (Appendix B), and a new response for this energy point is presented.

The response to energies above 1.25 Mev were made with 5, 10, and 15 Mev bremsstrahlen from the LINAC. These data for bare rod response are also presented in Figure 27. The bare rods were exposed in equilibrium with 1.5 cm of glass.

F. RATE DEPENDENCE

The requirements for determining the rate dependence of a dosimeter system are twofold. First, it is necessary that a rate-independent monitor be available to measure the total dose delivered to the dosimeter system. Second, it is necessary that a radiation source be available which can deposit a measureable dose from a constant energy spectrum over a range of dose rates from 10 to 10^7 r/sec. Although the first requirement seems to be met adequately by the aluminum monitor chamber, no single machine is available which will meet the second requirement. Therefore, it is necessary to evaluate carefully

51
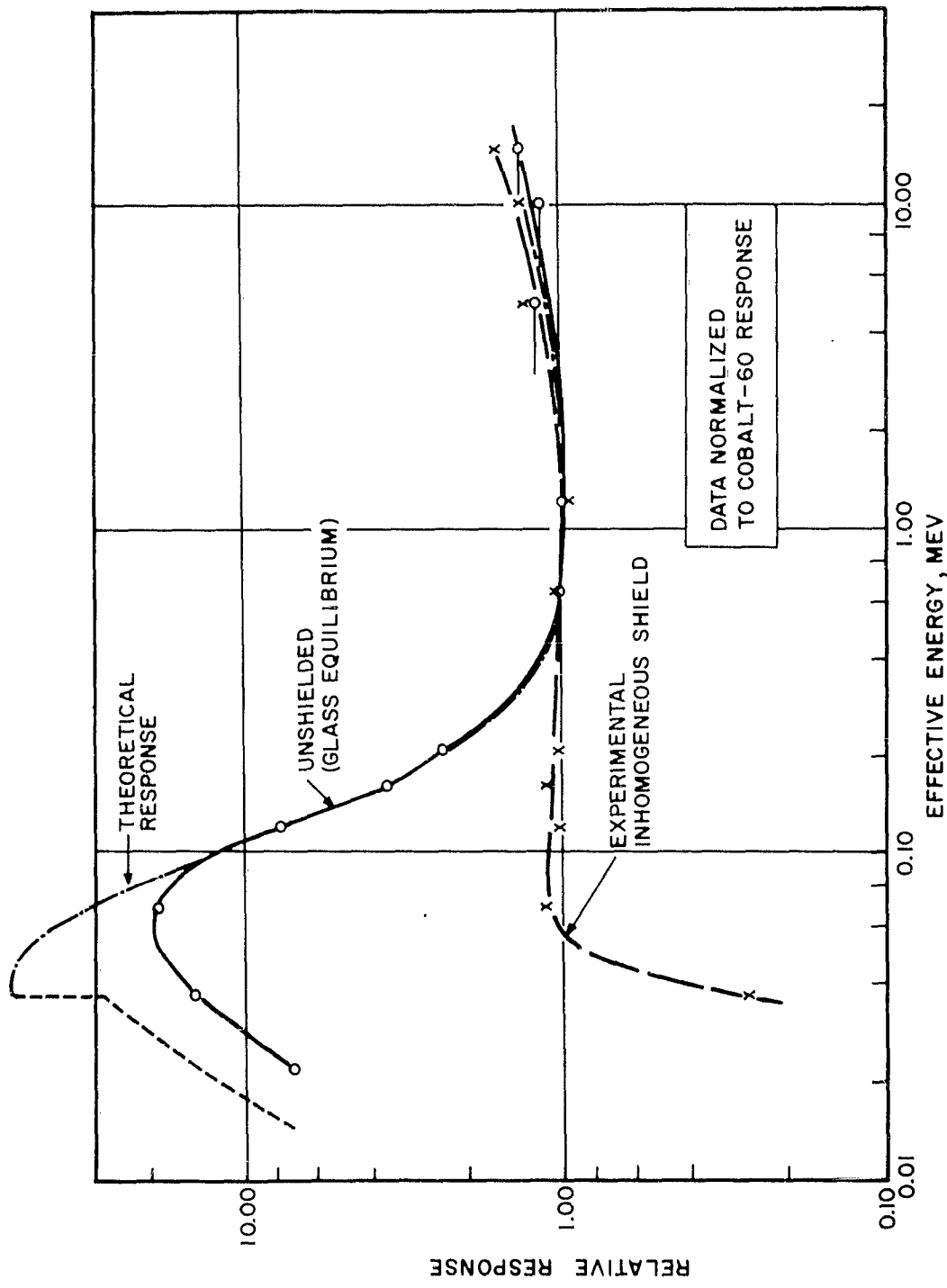
FIGURE 27. ENERGY RESPONSE OF SILVER-ACTIVATED GLASS ROD DOSIMETERS

52

the response of the dosimeter at some overlapping rate on each piece of generating equipment.

Some advantage may be taken of the high response of most of the dosimeters to soft x-rays to deposit dose at a relatively high rate. For example, the dose rate at the window of the x-ray tube on the 250-kv constant potential x-ray generator is 370 r/sec at 220 kv and 20 ma. For this particular spectrum the silver-activated glass dosimeters have a response relative to Co-60 of 13.5. This response results in an apparent dose rate of 5000 r/sec with the above technique. The x-ray tube current may be easily varied throughout the range from 20 ma to 2 μa. This then provides effective dose rates to the glass rods of 5000 to 0.5 r/sec.

This experiment was performed with the glass rods placed directly on the window of the x-ray machine, and the data are shown in Figure 28. Additional data were obtained with a flash x-ray system where the dose rate was of the order of 10^7 r/sec. A comprehensive experiment was performed with shielded and unshielded dosimeters. The bare rod over-response for the 600-kv flash x-ray was determined to be 8.73. Five pulses were necessary to provide a satisfactory exposure of the dosimeters.

Further rate studies were performed using 15 Mev bremsstrahlung from the LINAC. Exposures were made at distances of 15, 50, 150, and 500 cm. At 150 and 500 cm the air-equivalent ionization chamber was adjacent to the test dosimeter system in the beam. The air-equivalent ionization chamber was then used as the standard. For exposures at the shorter distances, the aluminum ionization chamber was compared to the air-equivalent ionization chamber and used at the test position. The air-equivalent ionization chamber was used as a monitor at a distance of 200 cm. Since the monitor saw radiation transmitted through the dosimeter packet, the composition of the dosimeter packet was simulated with similar materials for the standardizing exposures.

53
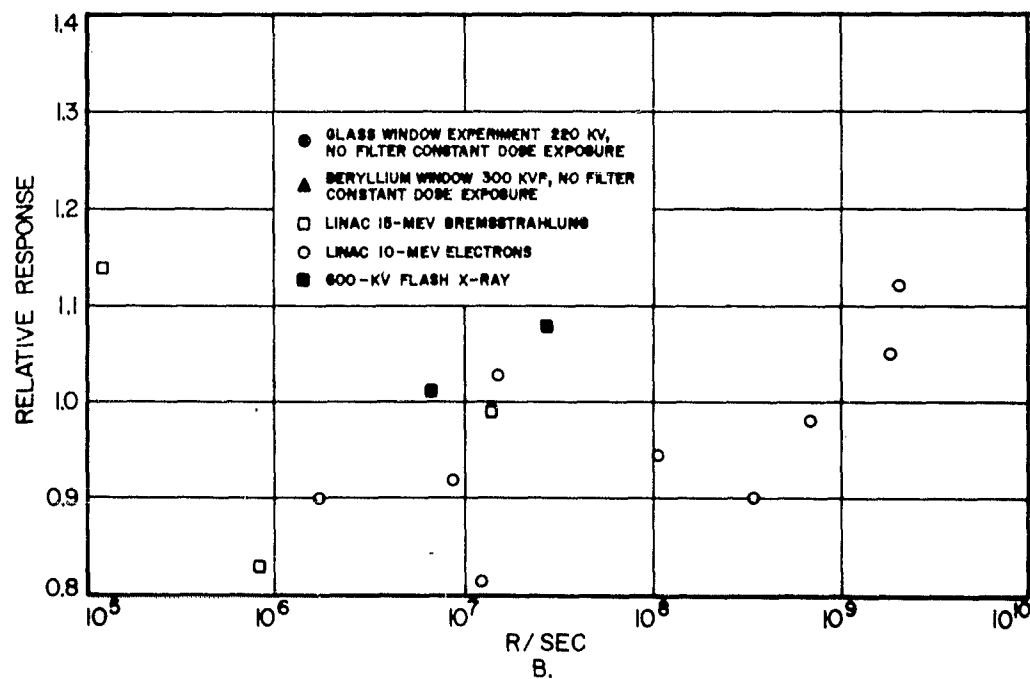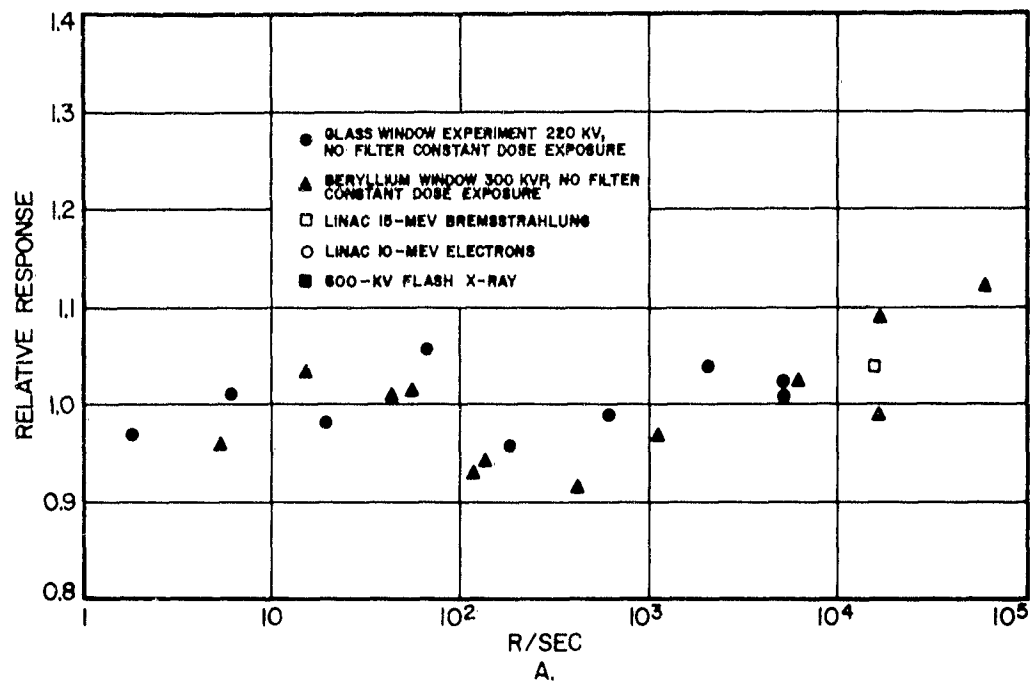
FIGURE 28. RATE DEPENDENCE OF SILVER-ACTIVATED GLASS ROD DOSIMETERS

54

The silver-activated glass rod dosimeters were exposed in equilibrium with 1.5 cm of glass at each of the above distances. A sufficient number of pulses were given each group so that all dosimeters received the same dose. A 1-μsec pulse width was used except for the 500-cm point, here the pulse was increased to 2 μsec. Rates of 10^4 to 10^7 r/sec were obtained with this technique.

To extend the study for higher rates, the electron beam of the LINAC was used directly. It is assumed that the mechanism for dosimeter response is identical to or, at least, very similar to photon irradiation.

The dose delivered to the samples was determined by collecting all the electrons in a given solid angle of the beam. This was approximated by a 1-inch-diameter by 1-inch-thick aluminum plug in a large (6- by 6-inch) plate of aluminum. The range to energy factor for 10-Mev electrons is 2 Mev-cm^2/gm, which gives a sensitivity for the aluminum stopping plug of 13.15 r/esu (air).

The glass rods were mounted directly against this monitor and placed at varying distances in beams of 1 and 500 ma with pulse widths of 1 and 0.1 μsec, respectively.

An average over-response of 70% was noted for the bare silver glass rods. The data were normalized to this figure and correlated to dose rates of 10^6 to 10^9 r/sec.

A wider divergence of data was noted for exposures made at 15 cm or less and is attributed to the inaccuracies of beam size and location. The data are shown in Figure 28.

G. SHIELD DESIGN AND CONSTRUCTION

Several cylindrical shields were constructed of materials of widely differing atomic numbers to determine a satisfactory shield which would compensate the energy-response of the dosimeter.

55

Energy-dependence curves were determined for several shields and for several combinations of shields. The most descriptive are shown in Figure 29. (The additonal experiments with assorted shield combinations are described in Appendix D.) After analyzing the results of these experiments, the following conclusions were made:

1. A single, homogeneous high-Z shield results in a response curve with a peak at about 70 kev and a valley in the region of 100 to 150 kev;

2. No low-Z material provides sufficient attenuation above 200 kev;

3. A low-Z material placed outside a high-Z shield tends to obscure the deep valley in the shielded response curve, but results in cutoff at a higher energy.

4. A low-Z material with a small attenuation in the useful range of the system must be interposed between the shield and dosimeter.

After considering the above conclusions, an experimental inhomogeneous shield (Figure 30) was fabricated. The shield contains thick lead to provide attenuation to unity response at about 200 kev, an open area to allow the response to rise to unity at about 70 kev, and a thin tantalum layer on the outside to broaden the spectrum to obscure the region of low response between 100 to 150 kev. The tantalum also serves to attenuate the peak response in the 70-kev region and allows a larger gap in the lead shield than would be used otherwise. A large gap is desirable when considering the directional response of the shield.

Energy response of dosimeters in this experimental shield to 5, 10, and 15 Mev bremsstrahlen were obtained on the LINAC. These data are shown in Figure 27 with the bare rod response.

The success of this shield concept resulted in the design and construction of the prototype shown in Figure 31. The end cap configuration was based on a window-type geometry similar to the lateral portion of the shield. The results of the first rotational response evaluation of this shield indicated that a larger window area was required on the end cap. There is reason for concern here
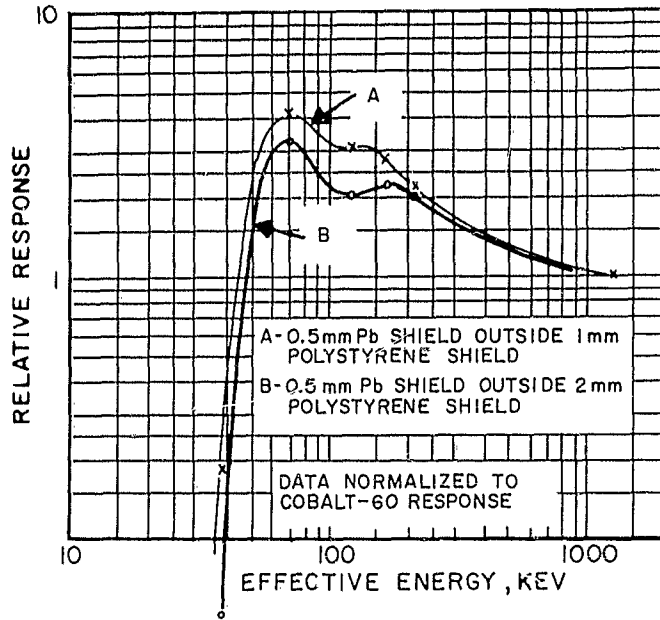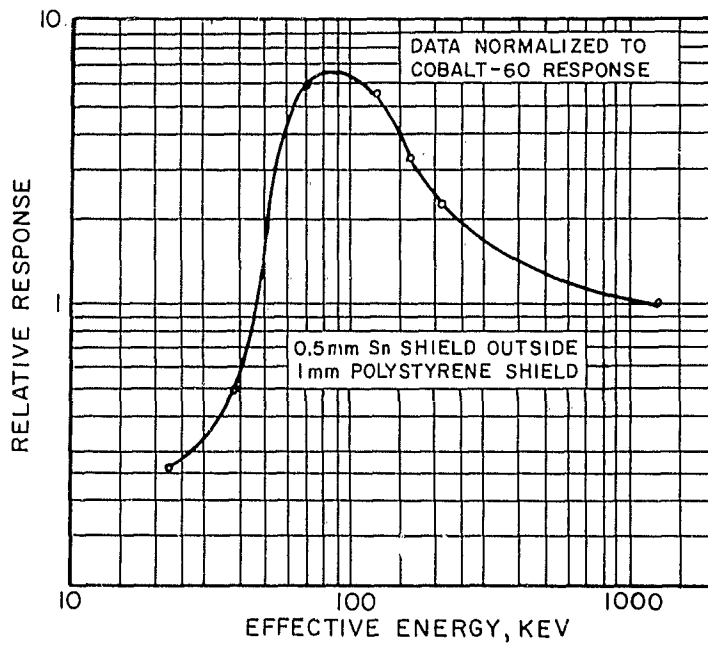
FIGURE 29. ENERGY RESPONSE OF SILVER-ACTIVATED GLASS
ROD MICRODOSIMETERS IN EXPERIMENTAL SHIELDS

57

C.

D.

FIGURE 29. ENERGY RESPONSE OF SILVER-ACTIVATED GLASS
ROD MICRODOSIMETERS IN EXPERIMENTAL SHIELDS

58

TANTALUM
LEAD
PLASTIC
ALUMINUM

SCALE, mm   0   1   2
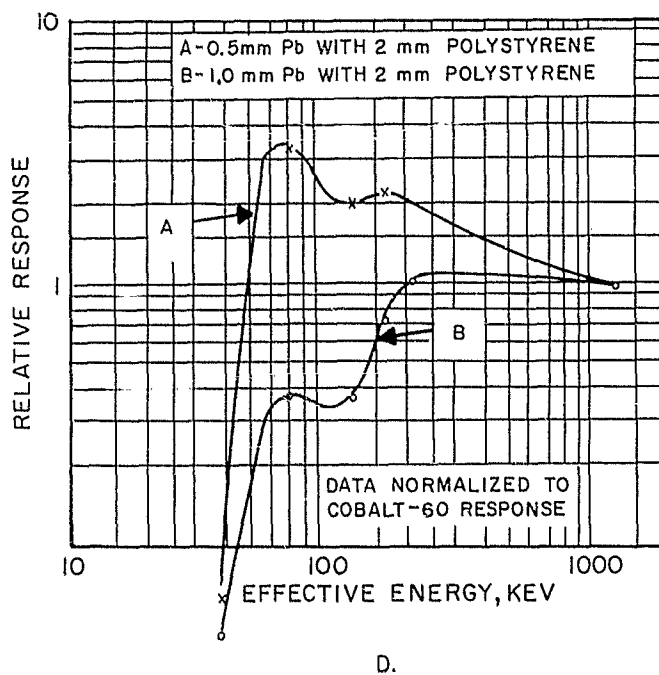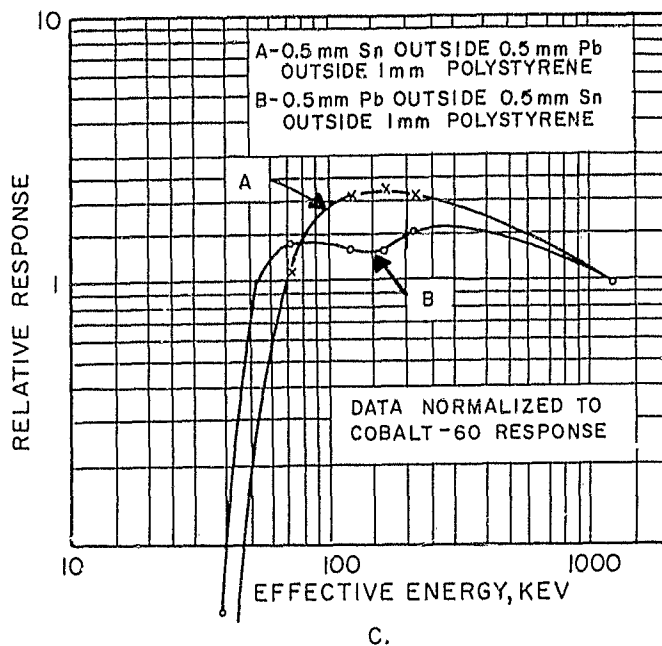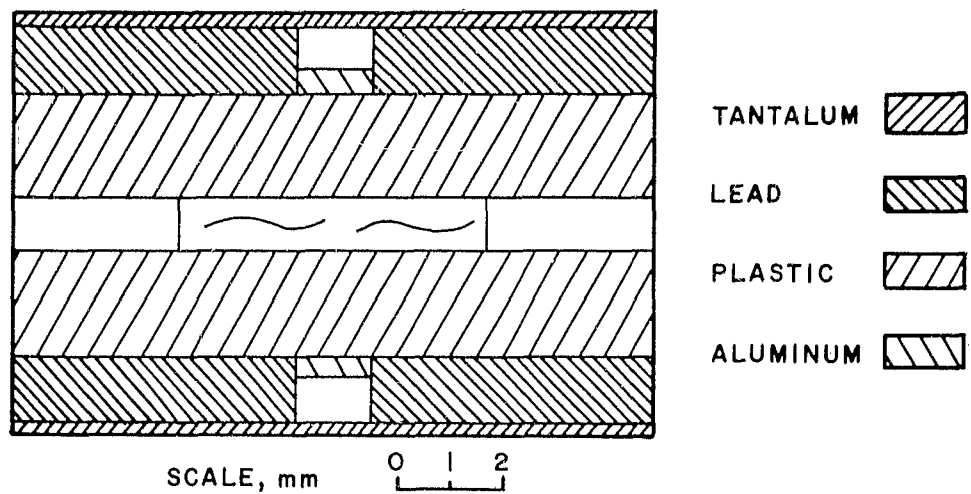
FIGURE 30. EXPERIMENTAL INHOMOGENEOUS SHIELD FOR GLASS
ROD MICRODOSIMETER

TANTALUM
LEAD
PLASTIC

SCALE, mm   0   1   2
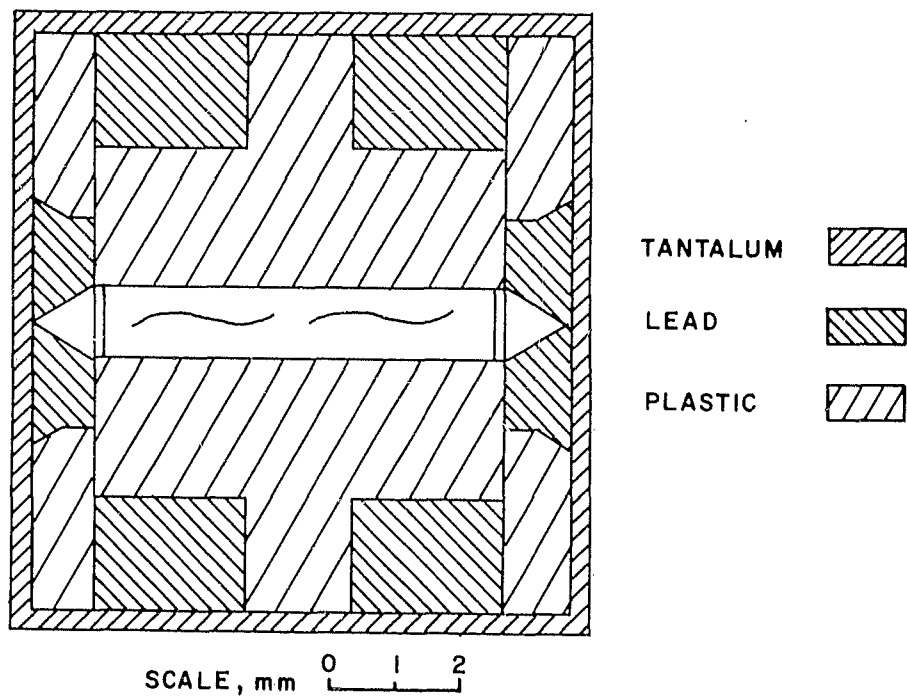
FIGURE 31. PROTOTYPE INHOMOGENEOUS SHIELD FOR GLASS
ROD MICRODOSIMETER

59

A.

B.
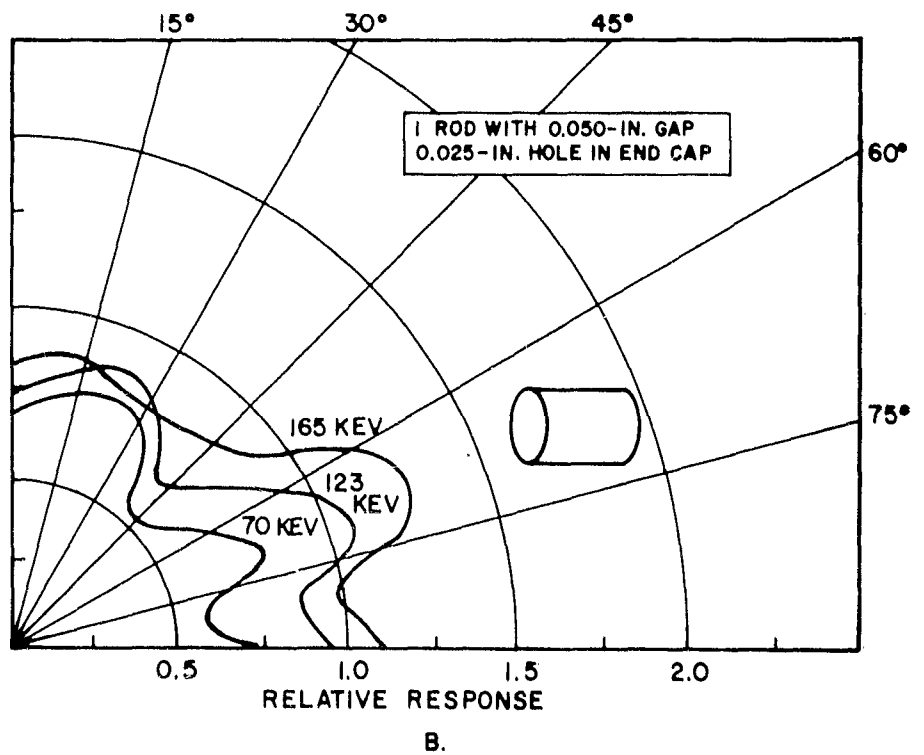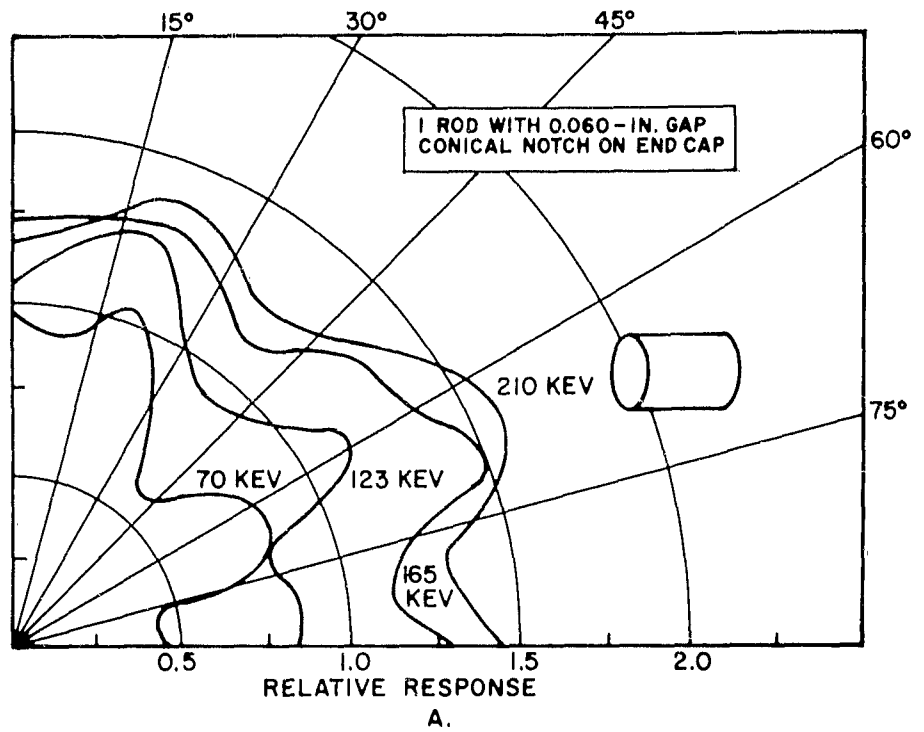
FIGURE 32. ANGULAR DEPENDENCE OF PROTOTYPE INHOMOGENEOUS SHIELD

because almost all the rod will show through this area at normal incidence to the end cap.

Figure 32 shows the angular response of the prototype shield and a modification to it which reduced the side gap from 0.060 to 0.050 inch and perforated the lead end cap with a 0.025-inch hole.

It was suggested at this time to increase the number of glass rods contained in the shield to take advantage of the statistics fo a single exposure. Rather than drill separate holes for additional glass rods, it was decided to increase the center hole to accept three glass rods to maintain the maximum amount of plastic between the rods and the metal portion of the shield. An angular response for this configuration was performed and is shown in Figure 33.
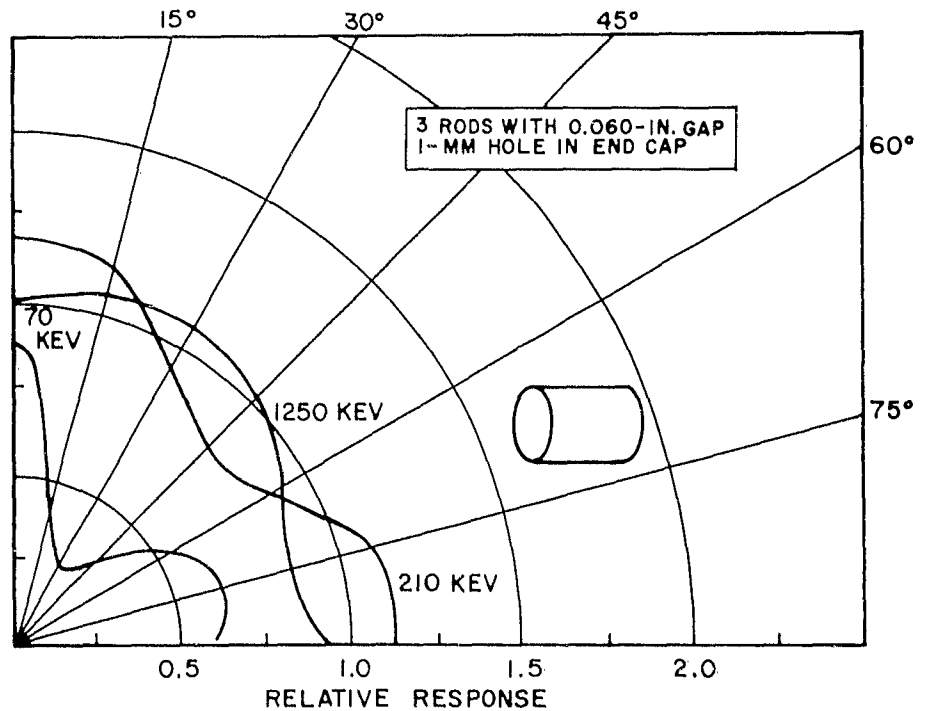
FIGURE 33. ANGULAR DEPENDENCE OF FINAL INHOMOGENEOUS SHIELD

61

The gap was increased to 0.060 inch for this evaluation. The
shield now appeared to be satisfactory for controlling the
energy response of the silver-activated glass rod dosimeters
to an accuracy of better than ±20% for effective energies be-
tween 50 kev and 5 Mev. Figure 34 shows the final shield
configuration; Figure 35 shows the energy response.

It was suggested that the inhomogeneous shield may be ex-
pensive to build and that a homogeneous shield would be more
economical. Energy response evaluations of the several shields
investigated previously were reviewed and additional combina-
tions tried (Appendix D). The two most promising are shown in
Figure 36. It was advised that the lead shield was sufficient
and a design is shown in Figure 37. This is a simple, homo-
geneous, lead shield 0.035 inch thick, with a plastic insert
to contain 3 glass rods, and an aluminum outer protective con-
tainer. To facilitate a durable yet simple construction, a
sleeve of aluminum has been included around the lead core.
This sleeve necessitates an overlap of the lead end cap with-
out making a special step in the aluminum end caps. The effect
of this excess lead is shown in Figure 38.

H. SILVER-ACTIVATED GLASS DOSIMETER NEUTRON RESPONSE

Silver-activated glass dosimeters were exposed to the
fast neutron flux of the Pu-Be source for four days. The ex-
posure was made using a minimum of support material for the
source, and the glass rods were supported on thin paper
at distances of 3, 5, 7, and 10 cm from the center of the
source. Figure 39 shows the results of this exposure. Be-
cause of the finite size of the source, the exposures made
at 3, 5, and 7 cm could not be used directly to calculate
the response of the glass rods to the fast neutrons. The
results of the neutron response of the five glass rods which
were exposed at 10 cm from the source are shown in Table 4.

62

Labels within figure:

0.010 IN.
0.055 IN.
0.040 IN.
0.069 IN.
0.350 IN.
0.415 IN.
0.060 IN.
0.015 IN.
0.015 IN.
0.010 IN.
0.080 IN.
0.043 IN.
0.040 IN.
0.215 IN.
0.060 IN.
0.240 IN.
0.415 IN.

TANTALUM   PLASTIC

LEAD   ALUMINUM
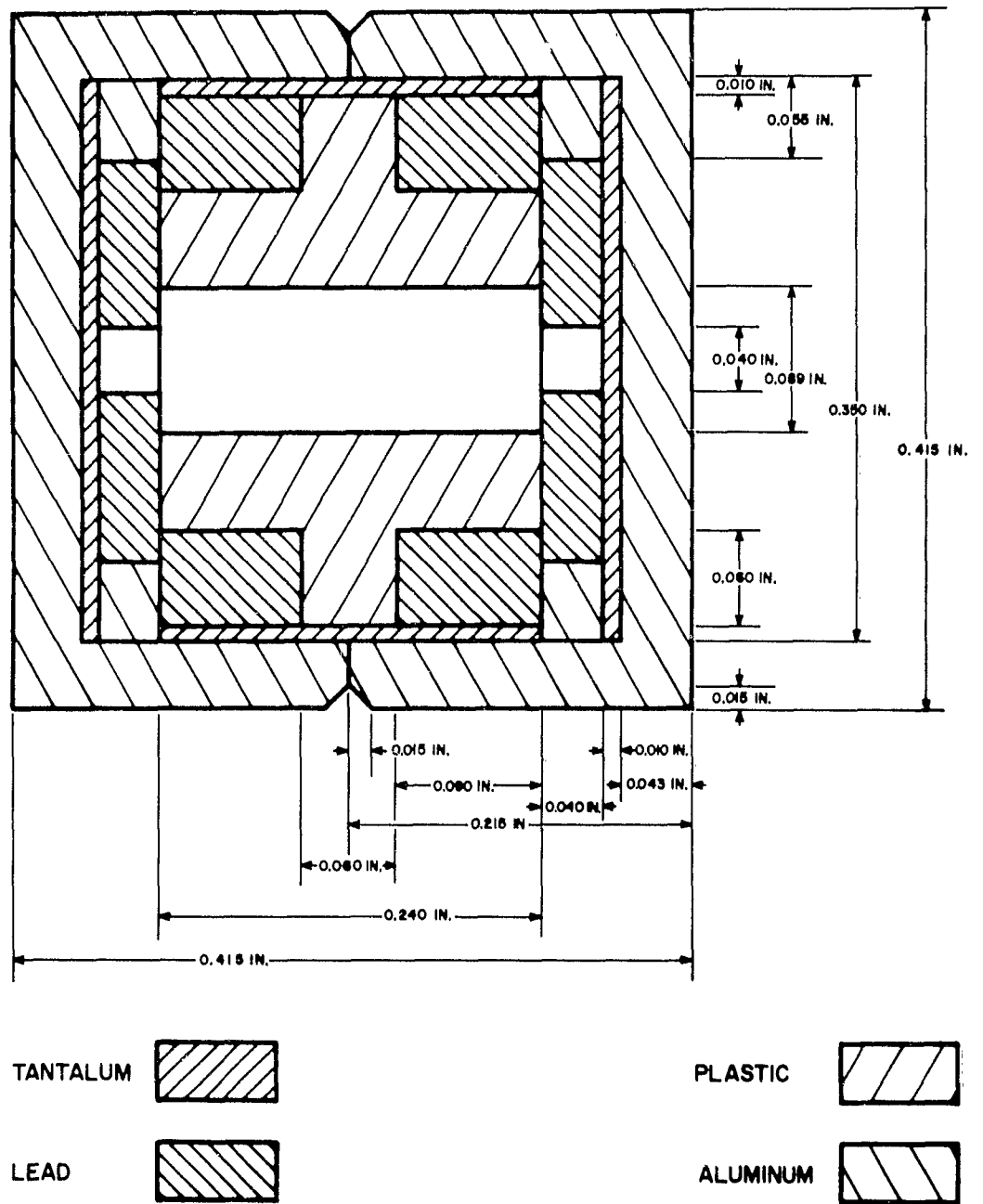
FIGURE 34. FINAL INHOMOGENEOUS SHIELD FOR THREE GLASS
ROD MICRODOSIMETERS

63

FIGURE 35. RESPONSE OF GLASS ROD MICRODOSIMETER IN FINAL INHOMOGENEOUS SHIELD (LATERAL INCIDENCE)

DATA NORMALIZED TO
COBALT–60 RESPONSE

EFFECTIVE ENERGY, KEV

RELATIVE RESPONSE

64
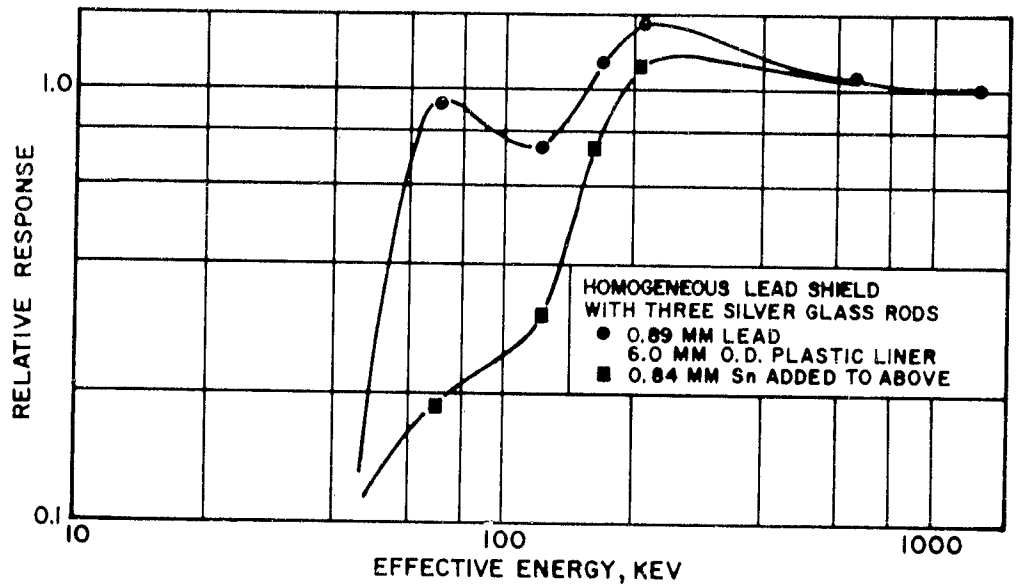
FIGURE 36. RESPONSE AS A FUNCTION OF ENERGY FOR
HOMOGENEOUS LEAD SHIELD

TABLE 4. Calculation of Pu-Be Neutron Response of
Silver-Activated Glass Microdosimeters

Average apparent exposure dose, r	5.08
Total exposure time, hr	112.7
Apparent exposure dose rate, mr/min	0.75
Measured gamma dose rate (graphite ion chamber), mr/hr	0.70
Neutron flux (sulfur activation), n/cm^2	7.55×10^5
Neutron response of glass, $r/n/cm^2$	0.066×10^{-9}

The measured response of the bare glass rods is small and the
exact value becomes somewhat uncertain because of the difficulty
in establishing the gamma dose to the glass.

65
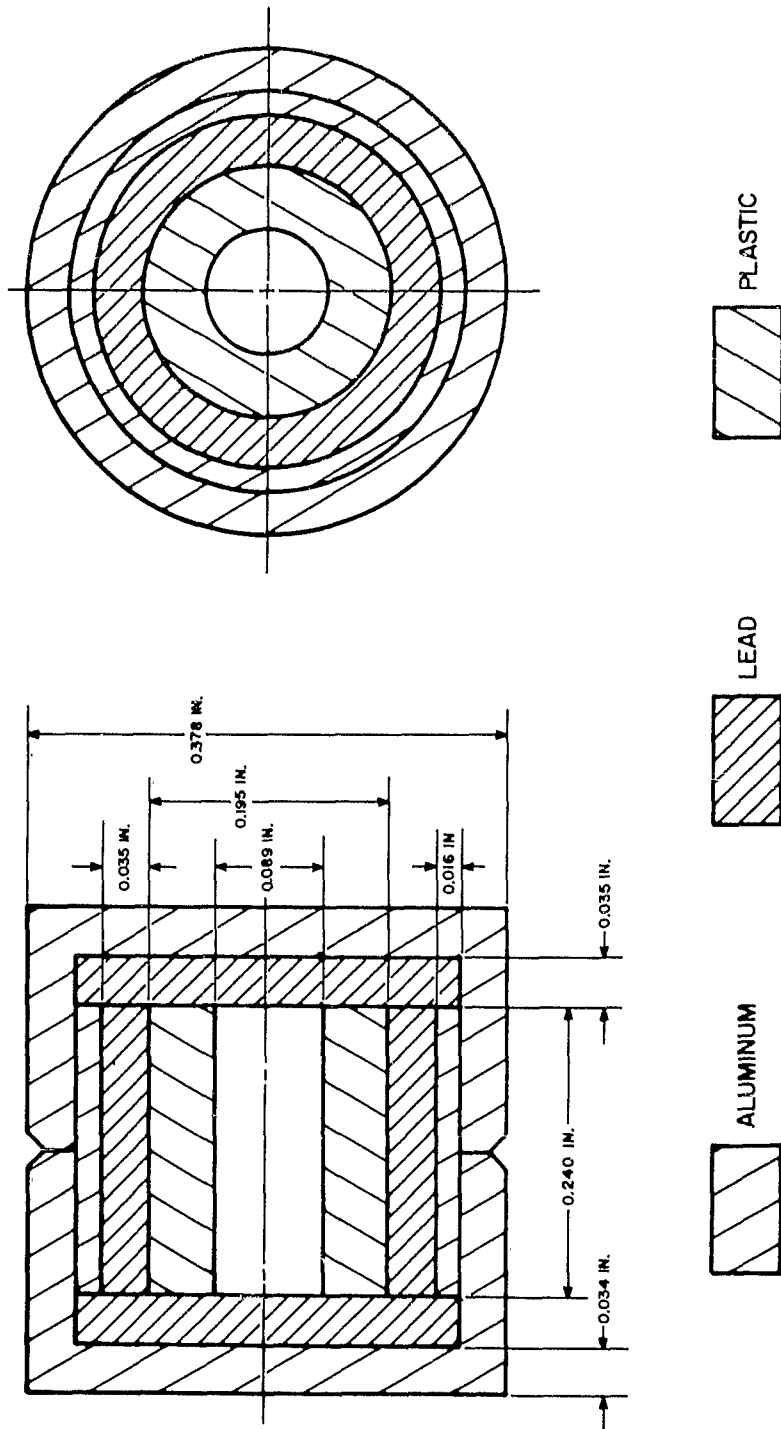
FIGURE 37. SILVER-ACTIVATED GLASS ROD HOMOGENEOUS LEAD SHIELD

66
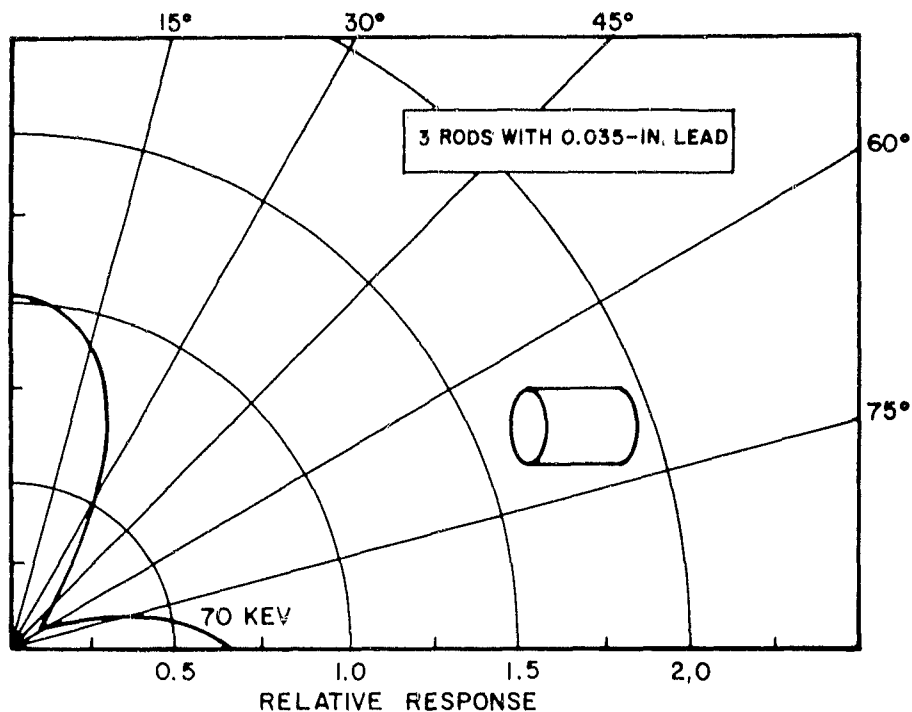
FIGURE 38. ANGULAR DEPENDENCE OF HOMOGENEOUS
LEAD SHIELD

Glass rods were exposed to 14-Mev neutrons using 6-mm-o.d.
graphite equilibrium shells and the homogeneous lead shield.
The graphite shells ensured electron equilibrium for high-energy
gamma rays, which may be present. In addition, paper-wrapped
bare rods were also exposed at 3 cm. For these exposures the
gamma component was negligible. The neutron response of the
silver-activated glass rods was (a) 0.77×10^{-9} r/n/cm^2 in
the graphite shell, (b) 1.60×10^{-9} r/n/cm^2 in the homogeneous
shield, and (c) 0.88×10^{-9} r/n/cm^2 for the paper wrapped rods.

The response of the dosimeter rods in the homogeneous
shield seems to indicate that the hydrogeneous plastic liner

67
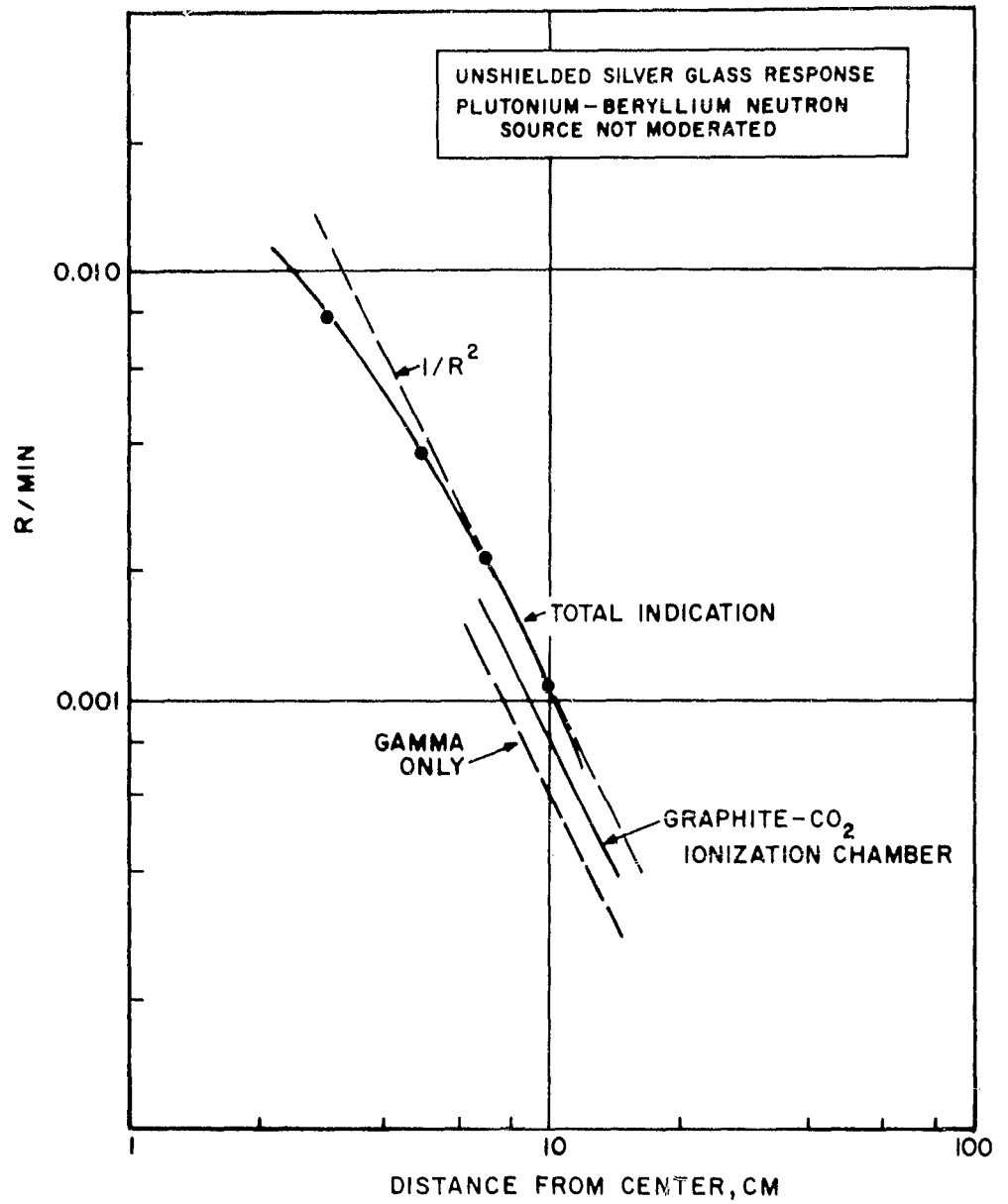
FIGURE 39. SILVER-ACTIVATED GLASS ROD RESPONSE
FROM Pu-Be NEUTRONS

68

used in the core of the energy discrimination shield is a source of recoil protons and results in an increase in absorbed dose in the rod. The use of graphite as a core material may reduce this effect for fast neutron environment.

A similar experiment was performed with three different shield configurations. The results of this experiment were:

Inhomogeneous Shield with plastic insert	8.3×10^{-9} r/n/cm^2
Homogeneous Shield with plastic insert	7.1×10^{-9} r/n/cm^2
Homogeneous Shield with graphite insert	5.9×10^{-9} r/n/cm^2

The effects of the plastic liner can be seen in these data, however, they are not so pronounced.

The first data were obtained from a cursory experiment while these last data were based on a good source-to-sample distance (10 cm) and a 1-hour exposure. The neutron dose at the samples was 7.55×10^9 n/cm^2.

The thermal neutron response was determined at the General Dynamics/General Atomic thermal column where the ratio of thermal-to-fast-neutrons was determined to be 520. The method of evaluating the neutron response of the silver-activated glass rods required two exposures: one with the gamma-ray energy discrimination shield and another with this shield in the Lithium-6-enriched LiF shield. This shield has a thermal neutron attenuation factor of 426. The difference in dosimeter response of these two measurements is attributed

to the thermal neutrons and is described mathematically.

Let

$(R)_{Li-6}$ be the dosimeter response in the energy discrimination shield and thermal neutron shield

$(R)_B$ be the dosimeter response in the energy discrimination shield

n be the neutron dose of the thermal column exposure

γ be the inherent gamma dose of the thermal column exposure

Then

$$(R)_B = \gamma + n \tag{8}$$

and

$$(R)_{Li-6} = \gamma + \frac{1}{426} n \tag{9}$$

by subtracting Eq. (9) from Eq. (8) the neutron dose is

$$(R)_B - (R)_{Li-6} = n - \frac{1}{426} n \tag{10}$$

The last term is less than 1% and can be ignored.

The results of these measurements are:

Silver-activated glass rods in the inhomogeneous shield with plastic insert	3.54×10^{-10} r/n/cm^2
Silver-activated glass rods in the homogeneous shield with plastic insert	2.38×10^{-10} r/n/cm^2
Silver-activated glass rods in the homogeneous shield with carbon insert	2.36×10^{-10} r/n/cm^2

VI. COBALT GLASS DOSIMETER SYSTEM

A. COBALT GLASS DOSIMETER

The cobalt glass dosimeters used in this study are made by Bausch & Lomb as a small 1.5 by 6 by 15 mm plate. The composition of the glass (Batch F-0621) is:

Material	Mole%	Weight%
SiO_2	62.5	57.75
Na_2O	10.6	10.13
B_2O_3	20.8	22.33
Al_2O_3	6.0	9.42
Co_3O_4	0.1	0.37

Since the readout mechanism is based on the density of the plate, its uniformity of thickness and flatness will affect its over-all accuracy in measuring a radiation dose.

Fifty cobalt glass dosimeters were measured for thickness, using a Bausch & Lomb DR-25B Optical Gage. The average thickness was 0.05934 inches ± 0.64%. Flatness was also checked on several samples and found to be better than ± 0.0001 inch thick.

Since the plates are 1.5 mm thick, it is of some interest also to know what the attenuation of x-rays is for the dosimeter at various energies. Attenuation of radiation as a function of energy was determined by limiting the x-ray beam with a small aperture. Transmission of the beam for no dosimeter and up to three dosimeter plates was measured. Figure 40 shows these data.

The cobalt glass dose range is between 10^3 to 2×10^6R, where an absorption band is built up in the ultraviolet region and gradually spreads into the visible. Figure 41 shows this spreading effect by a composite of several dosimeters with

71·
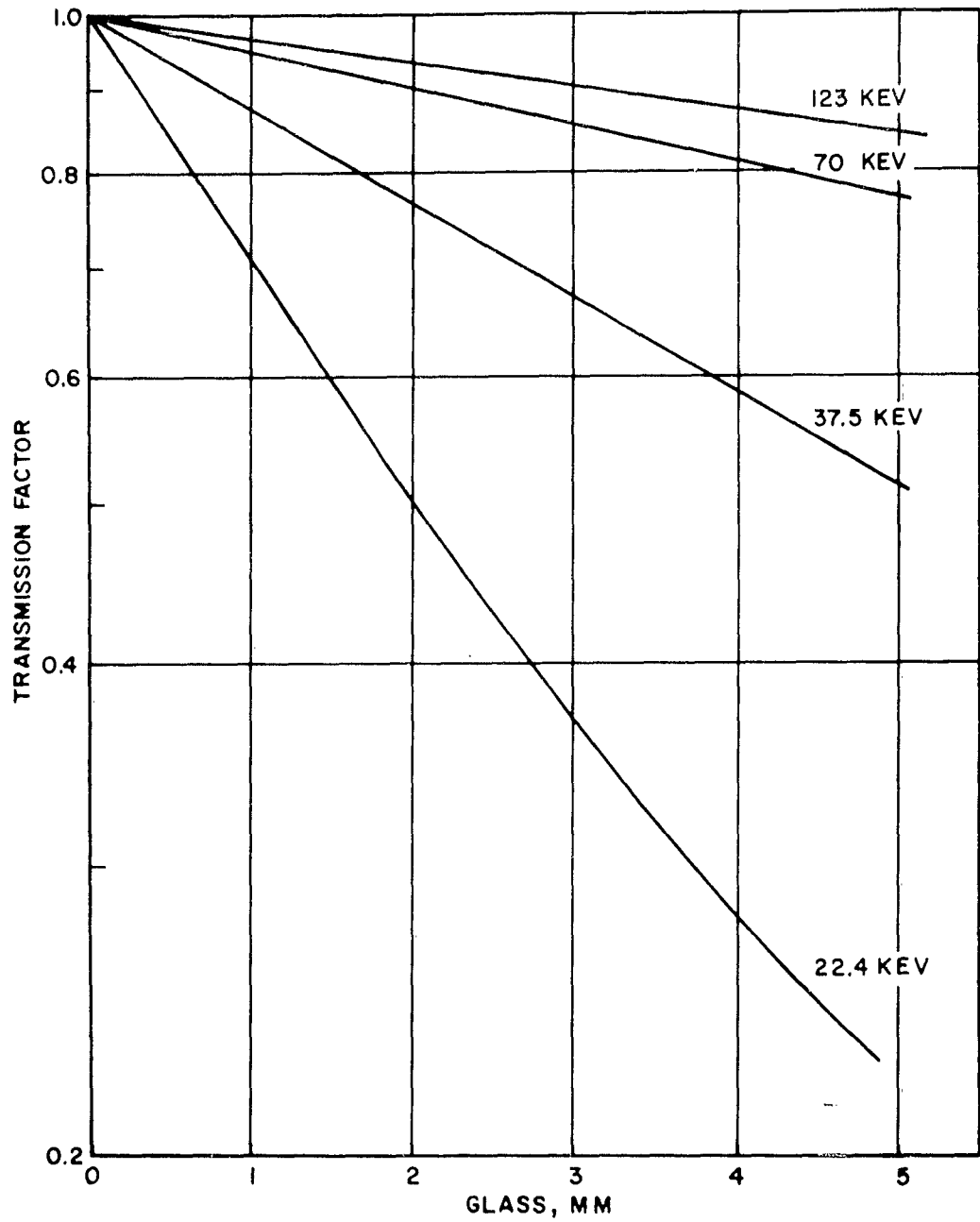
FIGURE 40. ATTENUATION OF X-RAYS THROUGH COBALT GLASS DOSIMETERS

72

increasing exposures in this range. Historically, the glass
has been read at 400 mμ although other wavelengths have been
noted in the literature. For these investigations this wave-
length has been adequate; however, in an attempt to increase
the range, the 750-mμ wavelength was investigated. As in-
dicated on Figure 41, the transmission is over 40% at this
point for a dosimeter with a 10^7r dose. Unfortunately,
fading of the dosimeter is severe for these large doses.
Adequate calibration necessitates a close control on ex-
posure time and delay to readout.

B. COBALT GLASS DOSIMETER SYSTEM LINEARITY

The derivation of the cobalt glass linearity data using
Co-60 radiation would be very time consuming if readily avail-
able sources were used. High doses can be readily obtained
from an x-ray generator by using short distances and low
filtrations. The effective dose can be varied over the
required limits by changing only the exposure time. A
calibration curve can be made with this technique and be
normalized to a single Co-60 data point. The calibration
curve used in these studies was derived in this manner.
Densities ranging from 0.001 to 2.2 were obtained. These
data were then normalized to the density produced by a
100,000r, Co-60 exposure. A curve showing cobalt glass
dosimeter response as a function of exposure dose is shown
in Figure 42; a differential curve of the same data plotted
as a function of density change is shown in Figure 43.

These two curves have been revised to account for the
density fading of dosimeters which have been highly dosed and
to incorporate a better Co-60 normalization. A recheck of
the cobalt point, using the Cottage Hospital teletherapy unit
with a superior time-distance relation for exposure, revealed

73
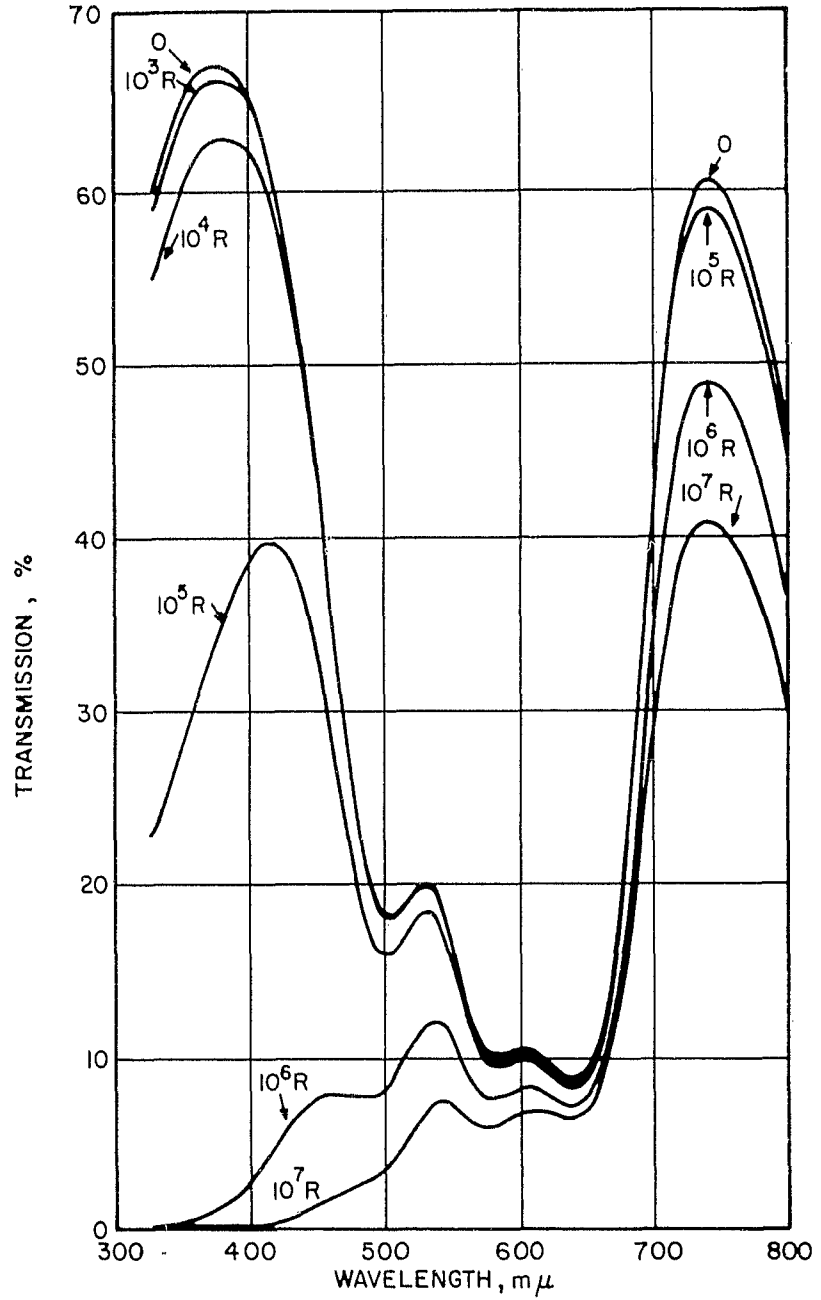
FIGURE 41. TRANSMISSION SPECTRUM FOR COBALT GLASS DOSIMETERS

74
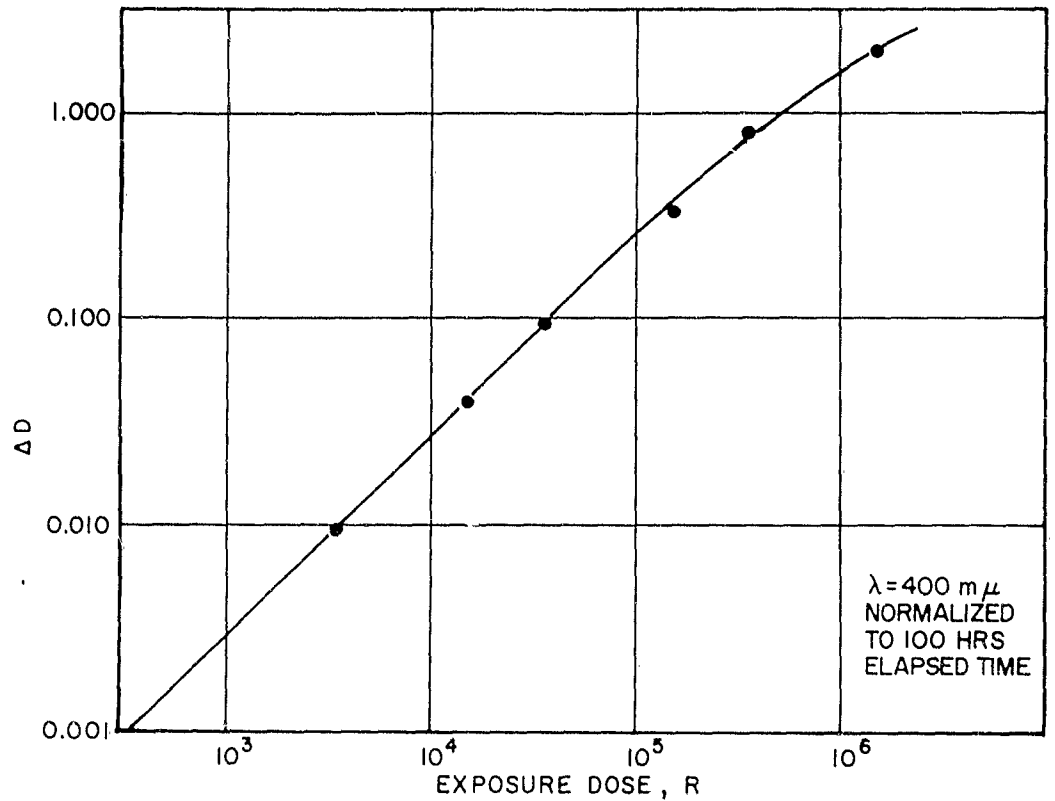
FIGURE 42. COBALT GLASS UNSHIELDED CALIBRATION CURVE
FOR Co^{60} RADIATION (REVISED)
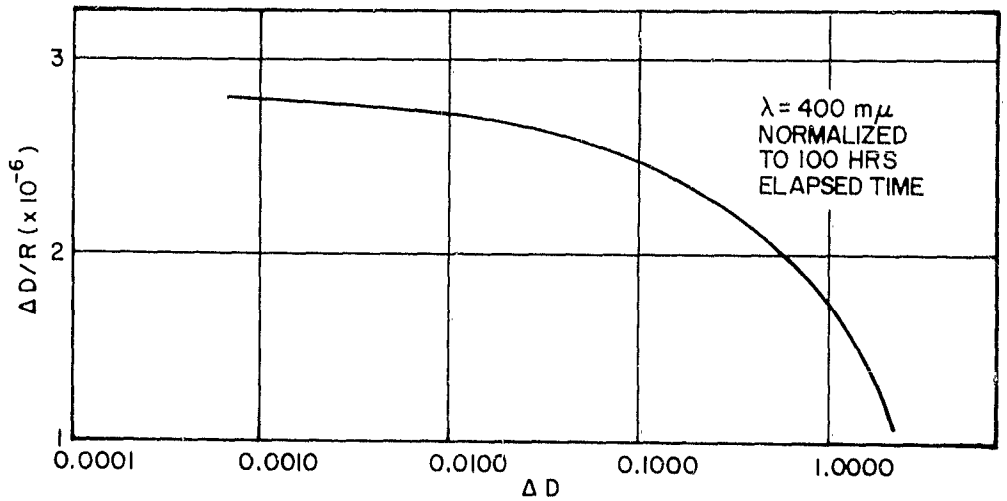
FIGURE 43. COBALT GLASS UNSHIELDED DIFFERENTIAL CALIBRATION
CURVE FOR Co^{60} RADIATION (REVISED)

75

an error of approximately 18% for the previously reported data. Recent studies of the density fading of dosimeters dosed above 10^5r indicate a drastic dependence of exposure time and delay-to-reading. A method of normalizing all readings to 100 hours elapse time has changed the linearity curve for doses above 10^5r.

C. EVALUATION AND RELIABILITY LIMITS

The DK-2 readout system can discern changes reliably in optical density of 0.1% which corresponds to a dose of approximately 400r and is the lower working limit of the system. The normal fluctuations in glass density for random undosed samples of glass raise this level to about 1000r although selected dosimeters can read a 400r dose under ideal conditions. At doses in excess of 2×10^6r, the glass plate becomes too dense to transmit enough 400 mμ light to be detected. To extend the range, the peak at 750 mμ was used, where the absorption band had not reduced its transmission properties as much as the 400 mμ wavelength. A calibration for these higher doses was made only to realize that fading which was thought to have stabilized had not done so. Density records were kept on three samples dosed to different levels for over three months. The dose was originally delivered by an exposure on the window of the 250-kv x-ray machine at 220 kv and 10 ma for 10^2, 10^3, and 10^4 seconds. Effective doses for these exposures were 4×10^4, 4×10^5, and 4×10^6r, respectively. Figure 44 shows this fading as a function of transmission factor for the three samples.

At this time, it was accepted that the 400-mμ wavelength reading was only slightly affected at very early times. A recheck of some previous data indicated that fading was also

76

present in the 400-mμ wavelength at extended times. An experiment was arranged to look at the rate of fading as a function of time for the 400-mμ region. The transmission factor is used since it changes at a faster rate than the logarithm of this number. Figure 45 shows the results of these measurements.

From these data, the curve for optical density as a function of dose will be time dependent at doses greater than 10^5 r. Since irradiation time may be considerable for high doses, a fiducial time large to this exposure time would be desirable to reduce errors from fading during exposure. An arbitrary time of 100 hours was selected as a normalizing time and a correction factor is shown in Figure 46. The curves in Figure 46 show the correction factor to apply to the measured density change for various elapsed times by assuming an exposure time short with respect to the delay before reading.
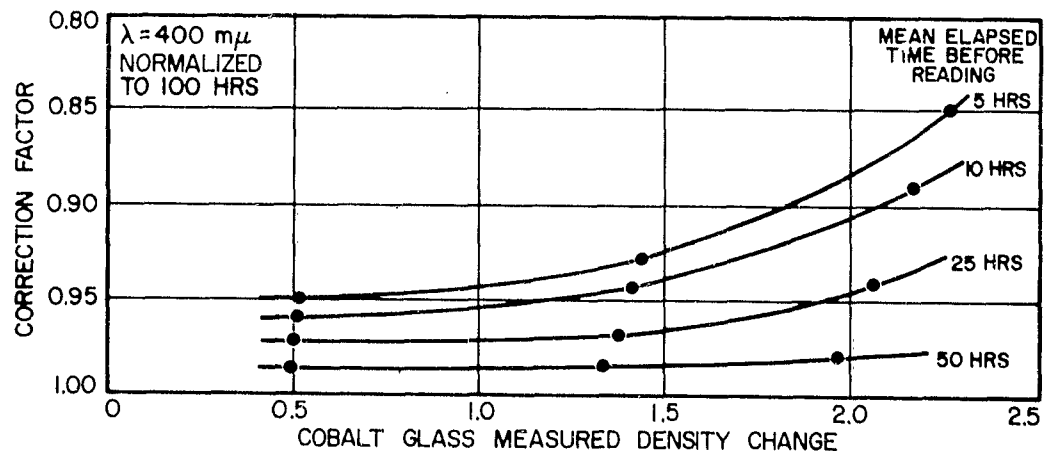
FIGURE 46. FADING CORRECTION FOR COBALT GLASS DOSIMETERS

77
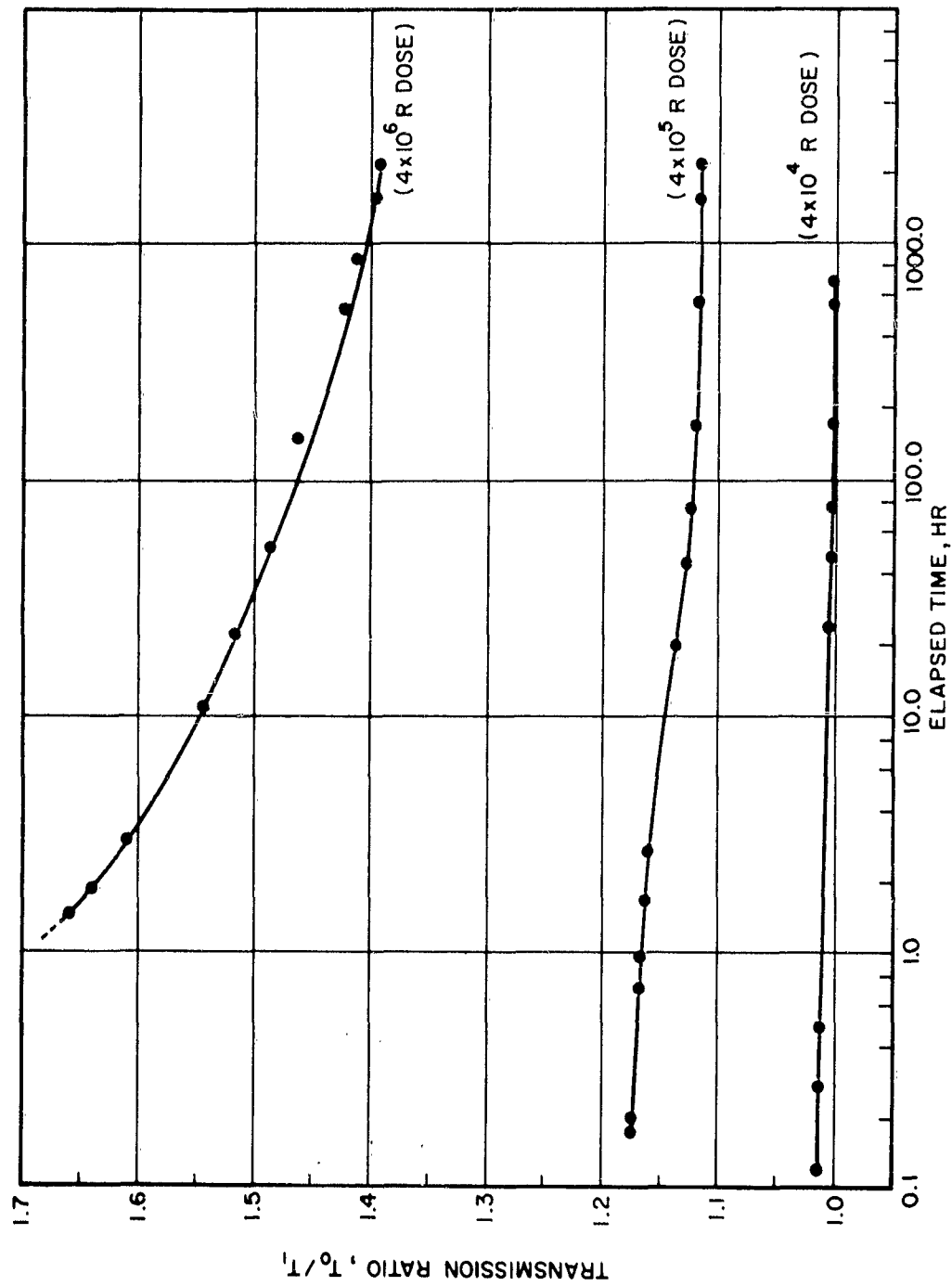
FIGURE 44. COBALT GLASS TRANSMISSION AT 750 mμ AS A FUNCTION OF TIME AFTER EXPOSURE

78
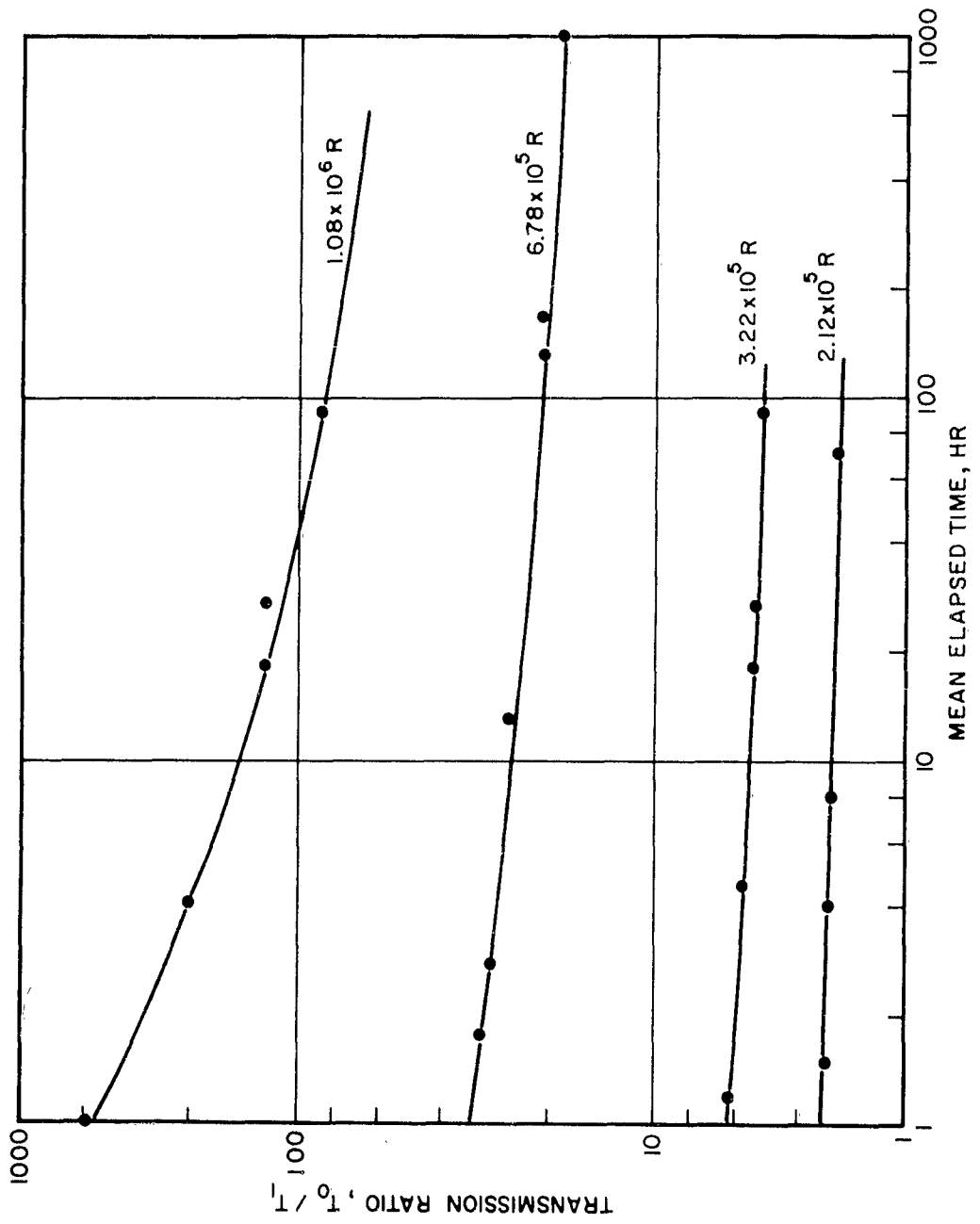
FIGURE 45. COBALT GLASS TRANSMISSION AT 400 mμ AS A FUNCTION OF TIME AFTER EXPOSURE

79

D. ENERGY RESPONSE

A theoretical energy-dependence curve for the 1.5-mm-thick cobalt glass dosimeters is shown with the measured data in Figure 47. The theoretical curve was obtained by taking the ratio of the absorbed dose in the glass to the absorbed dose in air and correcting for self-attenuation in the glass. The measured data represent the average value of five pieces of cobalt glass exposed at each of the six filtered x-ray energies (Table 1). The data at 5, 10, and 15 Mev were obtained for six pieces of cobalt glass placed in equilibrium with 1.5 cm of glass. To augment the data obtained with the monitor at these energies, silver-activated glass rods were also placed adjacent to the cobalt glass. Evaluation of these rods agreed within 10% of the monitor.

E. RATE DEPENDENCE

Cobalt glass pieces were exposed to unfiltered x-rays. A monitor was placed at 1 meter and the dosimeters were placed on the window approximately 5 cm from the target. Rates of 5 to 10^3 r/sec were obtained and the results are shown in Figure 48.

Rate data were obtained at the LINAC with 15-Mev bremsstrahlen. The cobalt glass pieces were placed in 1.5 cm of glass for electron equilibrium and placed at positions of 15, 50, 150, and 500 cm from a Fansteel target. Rates of 10^4 to 10^7 r/sec were obtained in this manner.

Additional rate data were obtained with electrons from the LINAC. Two exposures were made with the dosimeters placed on Styrofoam blocks, and the remainder were affixed to the aluminum monitor block described in Section III-K.
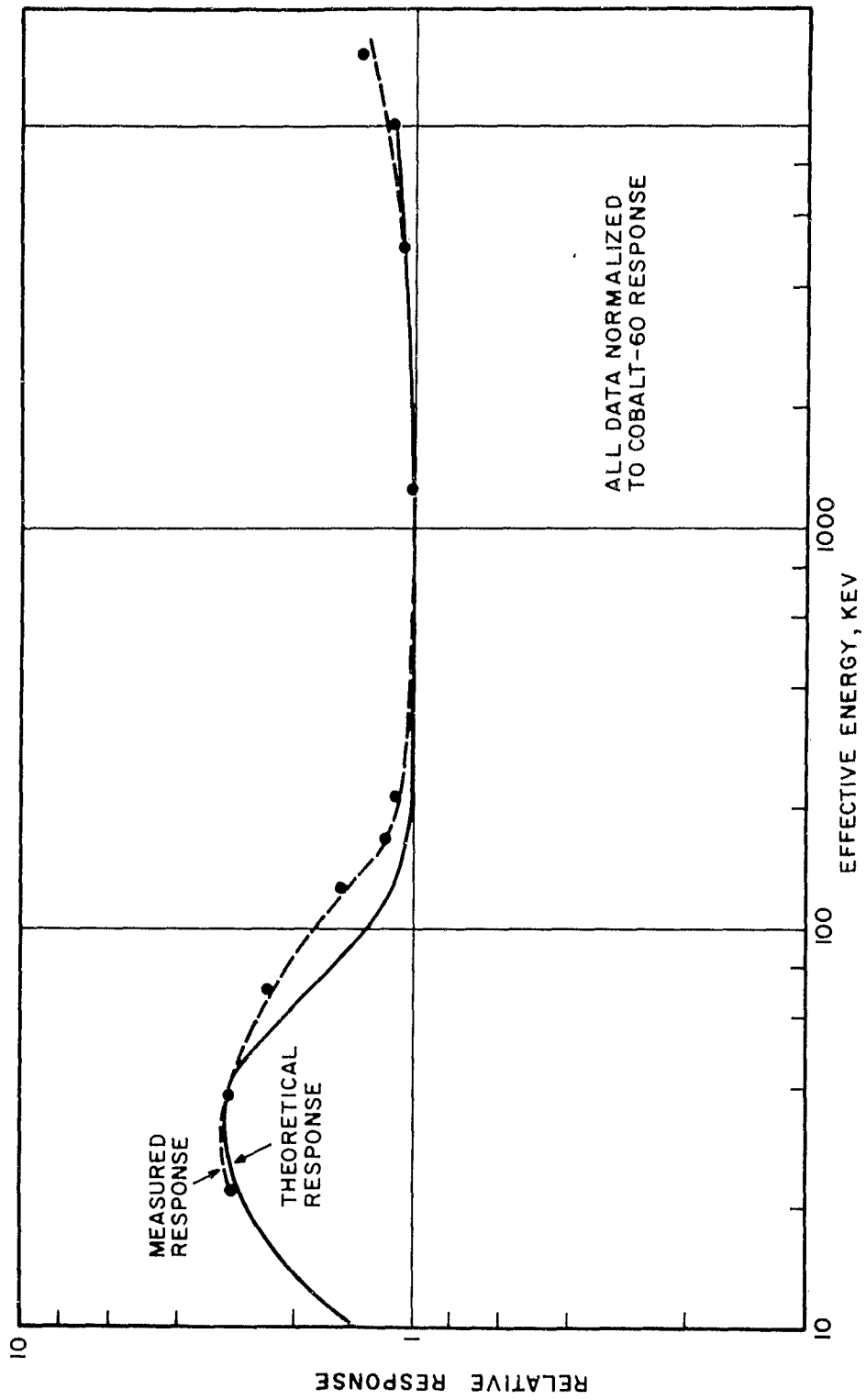
FIGURE 47. ENERGY RESPONSE OF UNSHIELDED COBALT GLASS DOSIMETERS

81
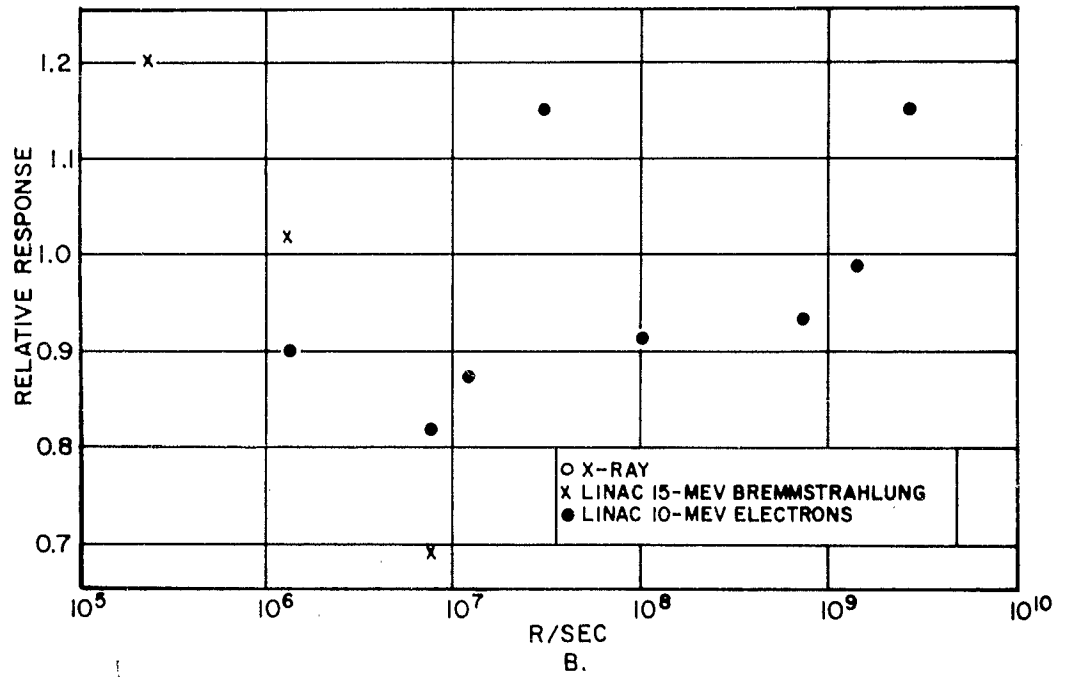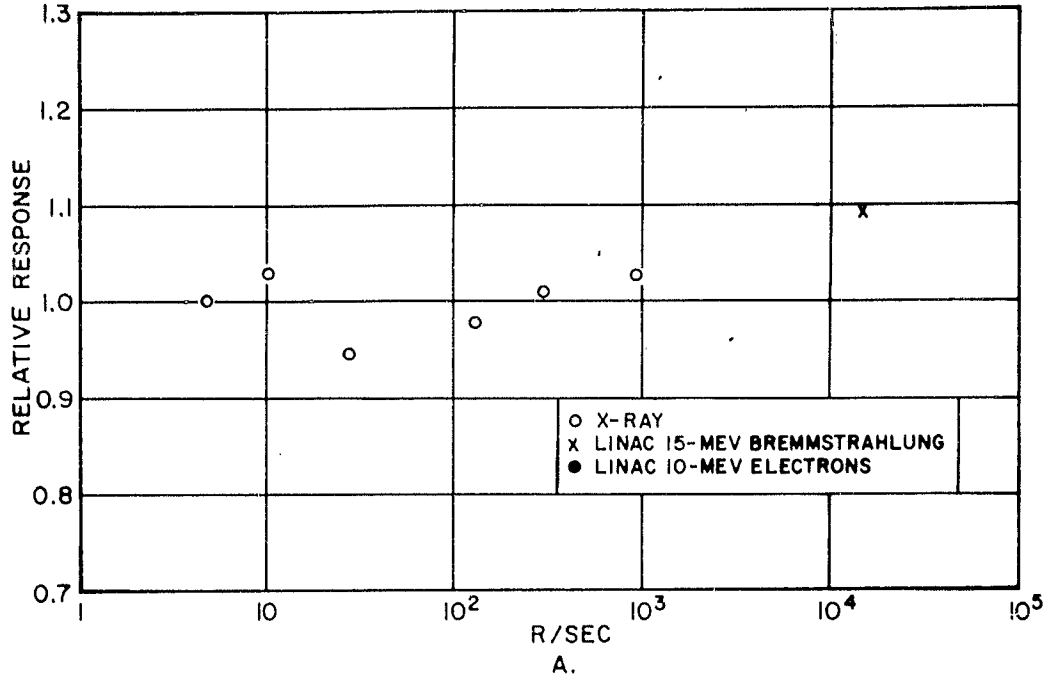
FIGURE 48. COBALT GLASS DOSIMETER RESPONSE AS A FUNCTION
OF DOSE RATE

Figure 48 shows these data, which included rates in excess of 10^9 r/sec. There appears to be no rate dependence up to this point within the limits of experimental error for this dosimeter system.

F. COBALT GLASS ENERGY DISCRIMINATION SHIELD

The first cobalt glass dosimeter shield was a 6- by 11- by 20-mm Teflon box with a cavity large enough for one dosimeter and two thin (0.28 mm) lead shields with 25% open area. This open area consisted of 20 uniformly spaced 0.074 in. diameter.

To obtain an approximation of the response in a reasonable time, the x-ray machine was operated at 220 kv and 20 ma, and increasing amounts of copper filter were added to harden the beam. The response relative to a bare dosimeter exposed to cobalt energy is listed below for specific copper filters:

Filter (gm/cm^2)	Response
0	1.19
0.75	1.21
1.50	1.21
2.24	1.26
3.02	1.25

To facilitate further work, a response for different energies for a condition of no holes was evaluated. These results are tabulated below:

Energy, kev	Response
30	-
50	0.23
100	1.11
150	1.12
200	1.31
250	1.57

Although no normalization was made for cobalt energy in this experiment it is apparent that the low-energy response is overshielded. Several calculations for various degrees of openings to increase the low-energy response were made, until it was discovered that the DK-2 illumination was not ideally uniform and hole positioning would be extremely critical. For this reason, a search for some homogeneous shielding material combination was continued. It also was realized that some medium- or low-Z material was required between the lead shield and the glass dosimeter. This eventually evolved into the "Jelly Roll" shield which incorporated 0.040 inch of aluminum with 0.010 inch of lead wrapped around a single glass plate, Figure 49. The "Jelly Roll" was evaluated for several of the available energy points and results are listed below.

Energy, kev	Response
100	0.882
150	1.157
200	0.915
250	1.413
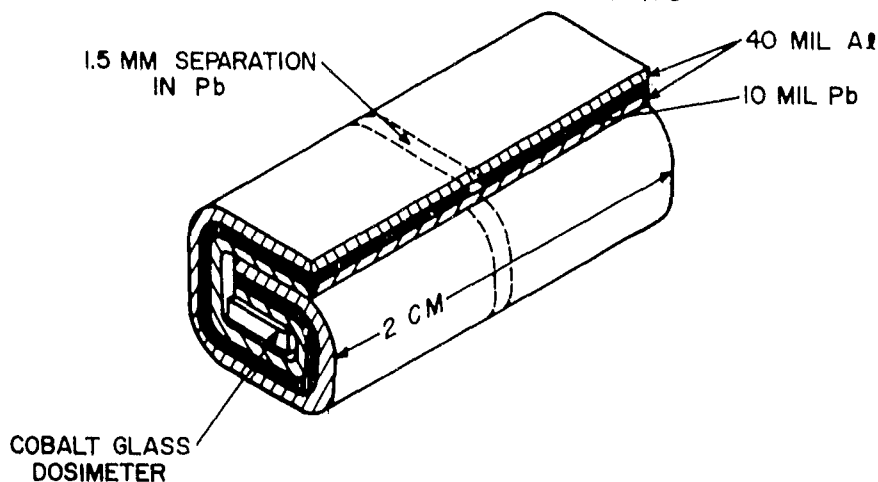
FIGURE 49. EXPERIMENTAL COBALT GLASS SHIELD

This shield was used in the first LINAC experiments and the data are presented with the bare glass data in Figure 50.

84
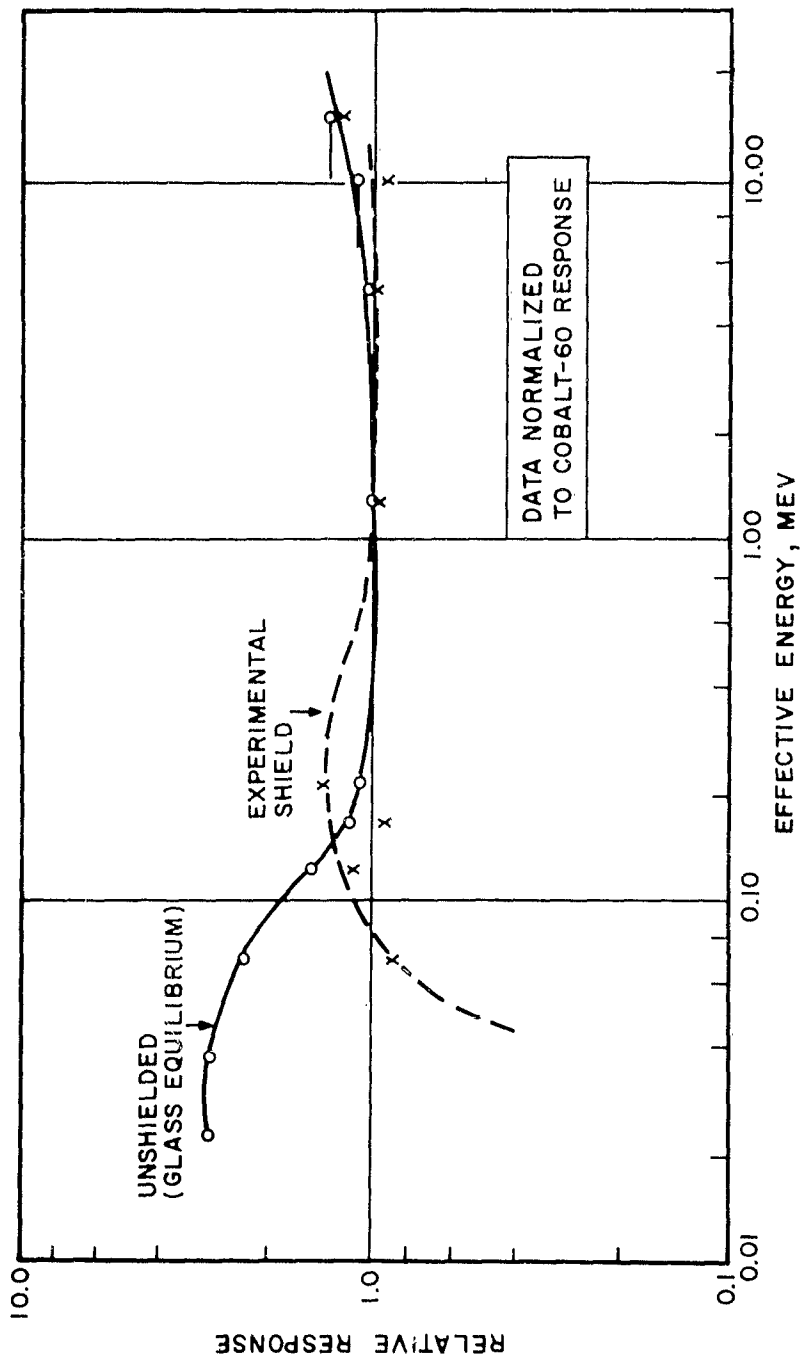
FIGURE 50. ENERGY RESPONSE OF COBALT GLASS DOSIMETERS IN EXPERIMENTAL SHIELD

85

It became apparent that a cylindrical form would be the simplest to fabricate and the separation was omitted in the prototype model. Upon evaluation, this new shield design proved unsatisfactory (Figure 51).

A modified design was constructed to include 3 glass plates. The inner aluminum was replaced by plastic, and the lead thickness was reduced to 0.005 inch. This design now provides a uniform response from 70 to 1250 kev within better than 10% (Figure 52).
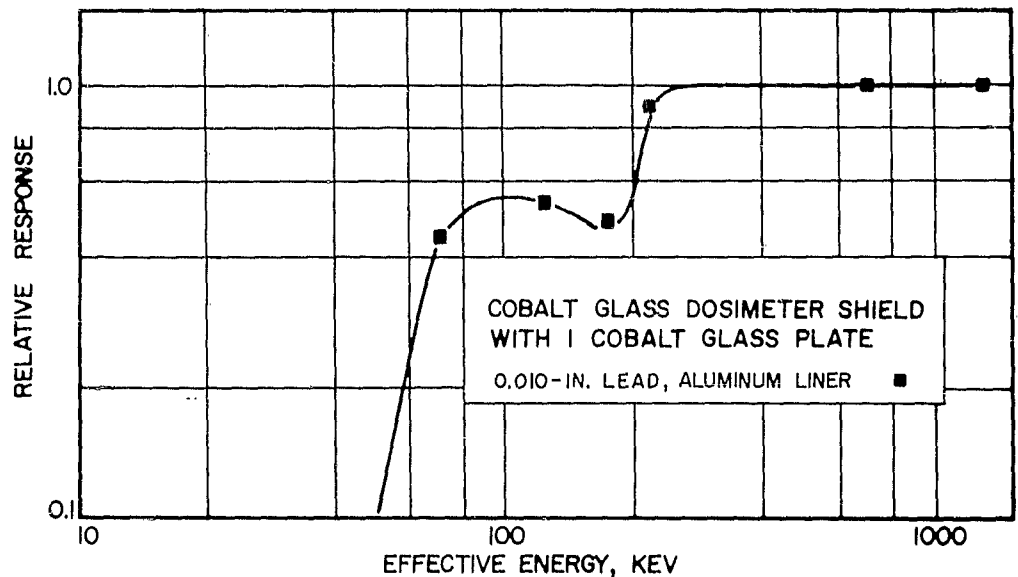
FIGURE 51. RESPONSE AS A FUNCTION OF ENERGY FOR COBALT
GLASS DOSIMETER PROTOTYPE SHIELD

End caps for this shield were constructed in a manner analogous to the basic shield. A Co-60 irradiation with end caps of no lead, 0.003 and 0.005 inch lead for end-on exposure, indicated that the 0.003 inch of lead was most like the side-on response of the dosimeter. Energy dependence for this end cap was evaluated at all the available filtered x-ray energies including the 46 kev point. This shield was also evaluated at the LINAC and the results of these measurements are shown in Figure 52. Since the orientation of the glass plate becomes

86
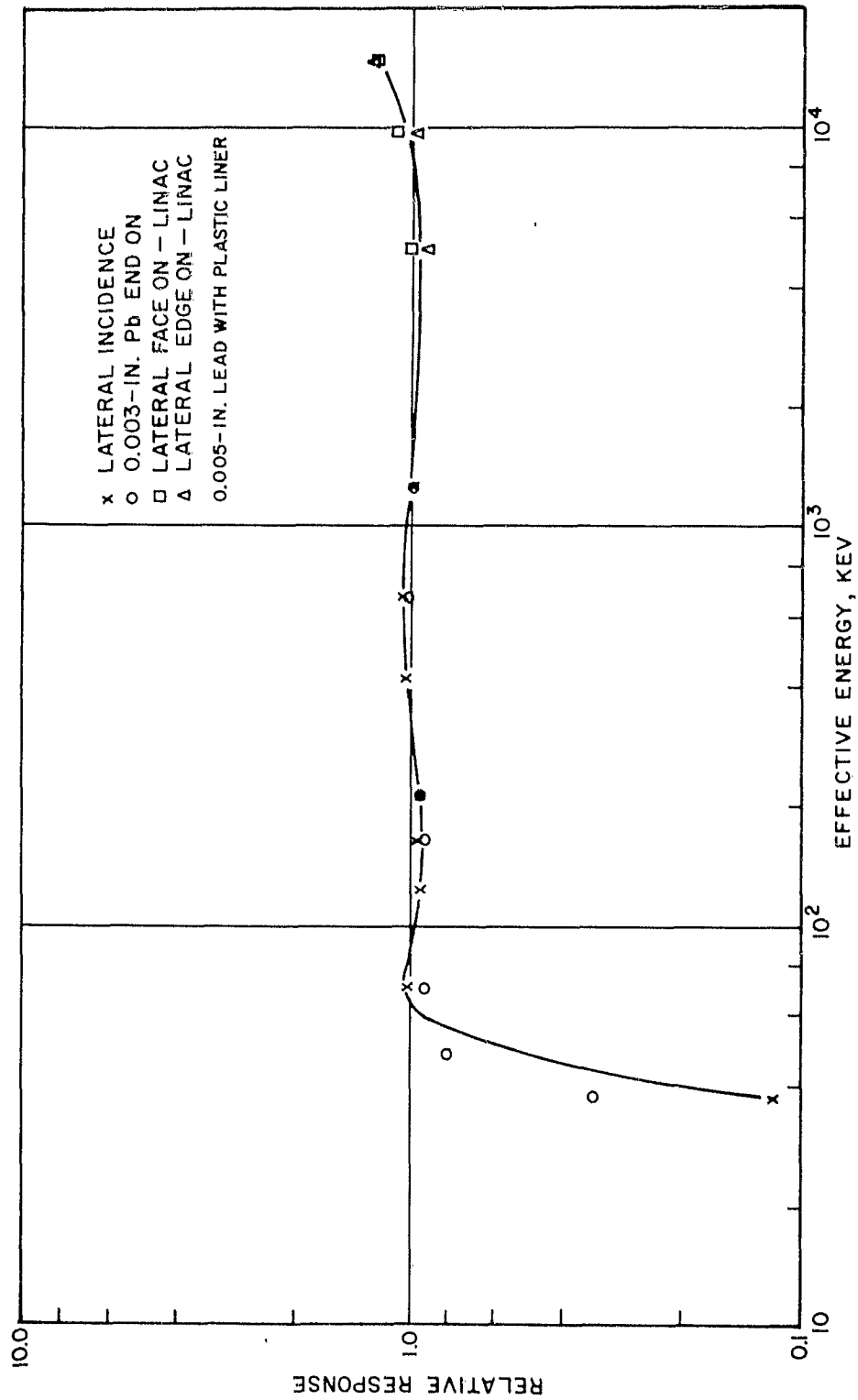
FIGURE 52. RESPONSE AS A FUNCTION OF ENERGY FOR COBALT GLASS DOSIMETER FINAL SHIELD

x   LATERAL INCIDENCE
o   0.003-IN. Pb END ON
□   LATERAL FACE ON – LINAC
△   LATERAL EDGE ON – LINAC
0.005-IN. LEAD WITH PLASTIC LINER

EFFECTIVE ENERGY, KEV

RELATIVE RESPONSE

87

obscure, special attention was given to exposing the shielded dosimeter in the LINAC for lateral face- and edge-on conditions. These data are shown in Figure 52. The final shield design is illustrated in Figure 53, and has a Co-60 response of 0.918.
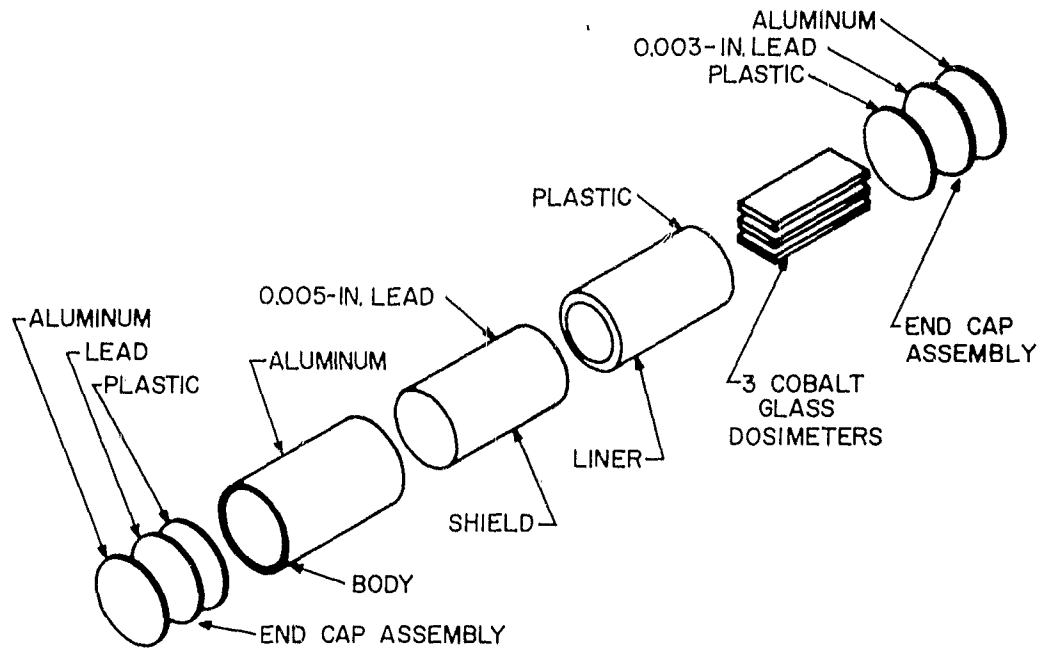
FIGURE 53. COBALT GLASS DOSIMETER FINAL SHIELD CONSTRUCTION

G. COBALT GLASS DOSIMETER NEUTRON RESPONSE

The thermal neutron response of the cobalt glass was determined using the General Dynamics/General Atomic thermal neutron column and the thermal neutron attenuation shield developed for the silver-activated glass rods. The method was identical to that used in determining the silver-activated glass rod response. It was necessary, however, to remove the outer aluminum can when the Li-6-enriched LiF thermal neutron shield was used. The response was determined to be 3.63×10^{-9} $r/n/cm^2$.

An attempt to determine the fast 14-Mev neutron response was successful to the extent that no response of the dosimeters was measureable for a dose of 7.55×10^9 n/cm^2.

88

VII. THERMOLUMINESCENT DOSIMETER SYSTEM

A. Thermoluminescent Dosimeter

The present thermoluminescent dosimeter is basically a small amount of manganese-activated calcium fluoride coated on a nichrome wire spiral and encapsulated in an evacuated bulb. Various types of substrates, such as electrofilm mesh and nickel screen, have been used as prototypes during this study. The development of the final thermoluminescent dosimeter for the Bureau of Ships was coincident with this study and better prototypes became available as time progressed.* The latest prototype element of the Bureau of Ships dosimeter is shown in Figure 54. The system herein described makes use of this element only and does not consider the Bureau of Ships coded handle attachment.
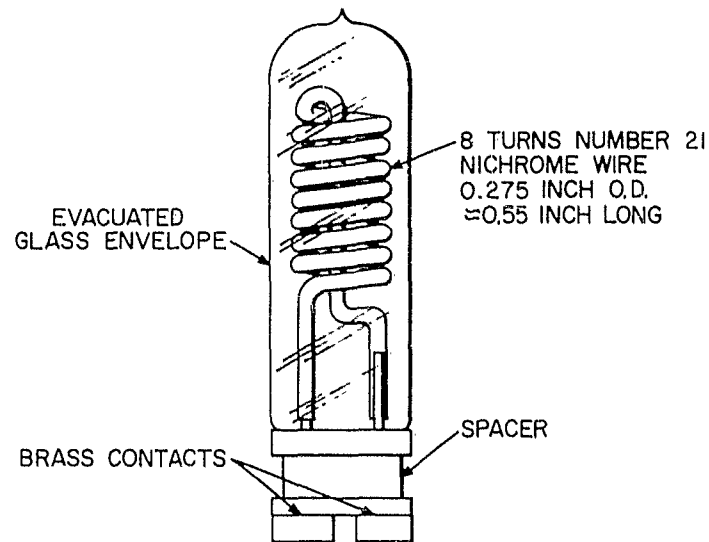
FIGURE 54. PROTOTYPE THERMOLUMINESCENT DOSIMETER ELEMENT

*
Phase II Final Engineering Report for Thermoluminescent
Dosimeter Computer-Indicator System, EG&G Report S-221-R
Oct. 1962.

89

B. THERMOLUMINESCENT DOSIMETER LINEARITY

The thermoluminescent dosimeter is a unique device capable of recording integrated doses of less than 10 mr to greater than 10,000r. In measuring dosimeter linearity, the characteristics of the readout system must also be considered. Photomultiplier tubes do not respond linearly to the entire range of light capable of being emitted by the dosimeter during readout.* The present method of evaluation consists of a blue-filtered photomultiplier tube appropriately adjusted to investigate either the upper or lower dosimeter range. Five thermoluminescent dosimeter units were exposed to cobalt radiation for integrated doses ranging from 1 to 10,000r in decade steps. The photomultiplier tube current per roentgen was uniform within ± 4%. Another series using six different thermoluminescent dosimeters in a range of 100 mr to 1000r in decade steps gave an error of ± 5%. Figure 55 shows these data plotted in microamperes per roentgen as a function of total dose in roentgen.

The use of appropriate standard light sources would provide a check and allow for adjustment if amplifier or system gain should change. Since the thermoluminescent dosimeter must be heated for readout, care must be taken to keep the photocathode at a uniform temperature to prevent dark current and signal current from changing.

C. EVALUATION AND RELIABILITY LIMITS

In determining the accuracy and reliability of the thermoluminescent dosimeter reader, a dosimeter would be exposed and read out successively for several times. The reproducibility of this data was better than ± 4%. Since the reader and dosimeter were being developed, this reproducibility test was often repeated before proceeding with further tests to ensure proper system operation.

* Under Bureau of Ships sponsorship, a sophisticated readout system is being developed to cover this range.

FIGURE 55. LINEARITY OF TWO THERMOLUMINESCENT DOSIMETER GROUPS
WITH DIFFERENT SENSITIVITIES

Prototypes were extremely rare in early investigations; consequently much data was obtained with only a few dosimeters. Between 50 and 100 readout operations were performed on some of these dosimeters. Little change in response was noted for these well-used dosimeters, provided the phosphor was still adhering to the dosimeter heating element.

D. ENERGY RESPONSE

A theoretical energy-response curve for the thermoluminescent dosimeter was derived by utilizing the ratio of absorbed dose in the phosphor to the absorbed dose in air. A comparison of these data to the measured response of an experimental thermoluminescent dosimeter is shown in Figure 56. The loss of response of the empirical curve at low energies is caused by the glass envelope surrounding the thermoluminescent dosimeter material. The two unshielded data points at 15 Mev are for two rate conditions. A response of 1.07 was measured for 1.05×10^7 r/sec and 0.93 for 1.04×10^4 r/sec. As the result of an oversight, no further unshielded data were taken at higher energies.

E. RATE DEPENDENCE

The first rate-dependence data for the thermoluminescent dosimeters were obtained on the LINAC using 15-Mev bremsstrahlen and at exposure positions of 15 and 500 cm. One pulse was delivered to a dosimeter in its shield at the 15-cm point while the two remaining dosimeters were exposed at the 500-cm point in a shielded and unshielded condition for a similar dose. The relative response of these dosimeters is shown in Figure 57 to be better than ± 10% for the dose rate of 10^4 and 10^7 r/sec.
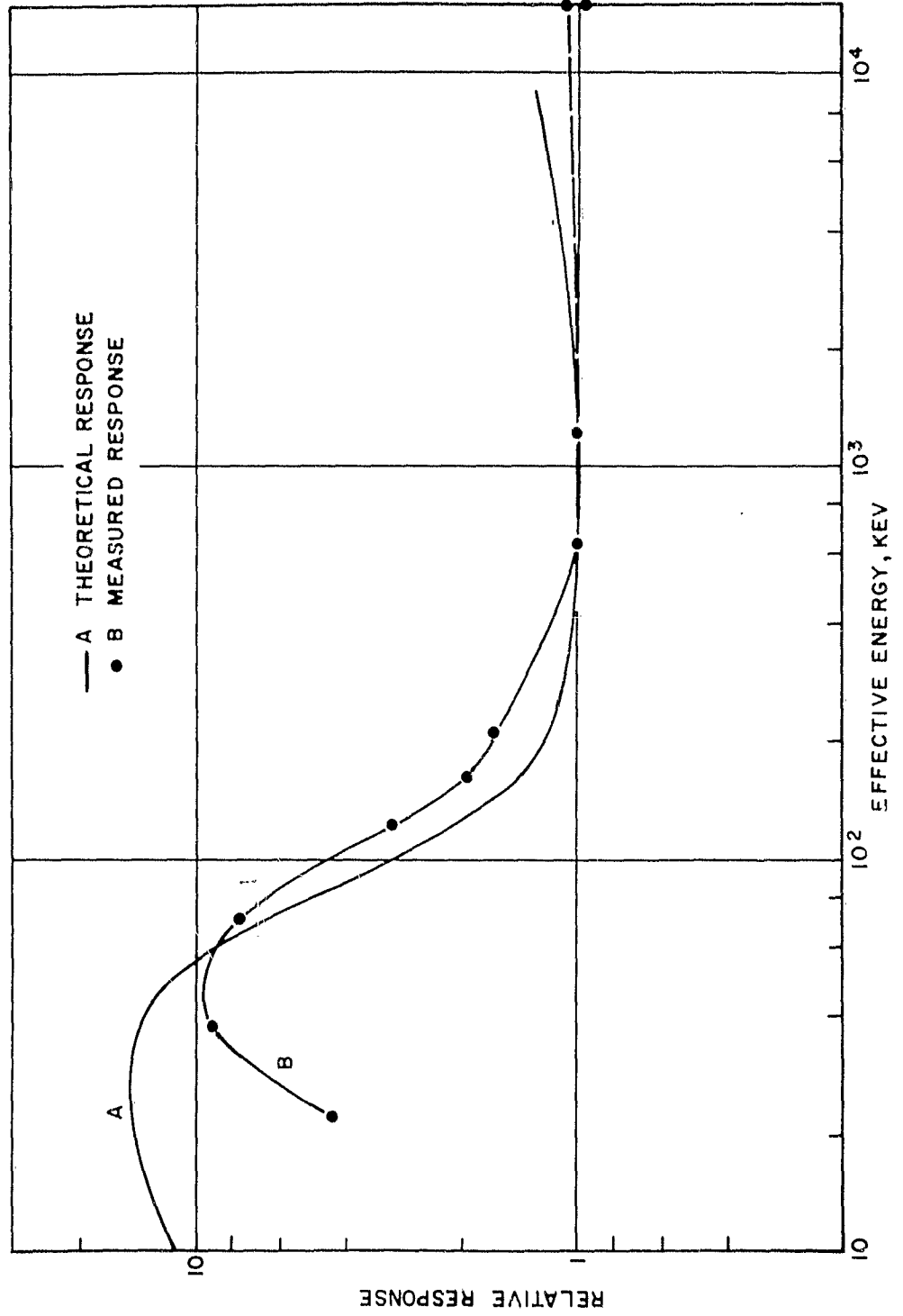
FIGURE 56. ENERGY RESPONSE OF AN UNSHIELDED CaF_2 (Mn) THERMOLUMINESCENT DOSIMETER
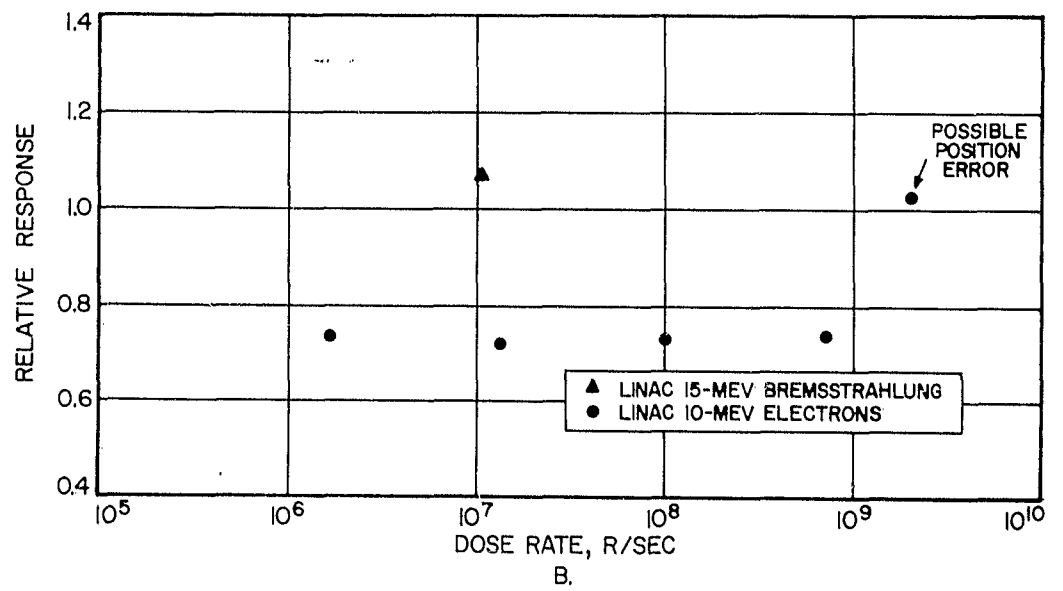
93
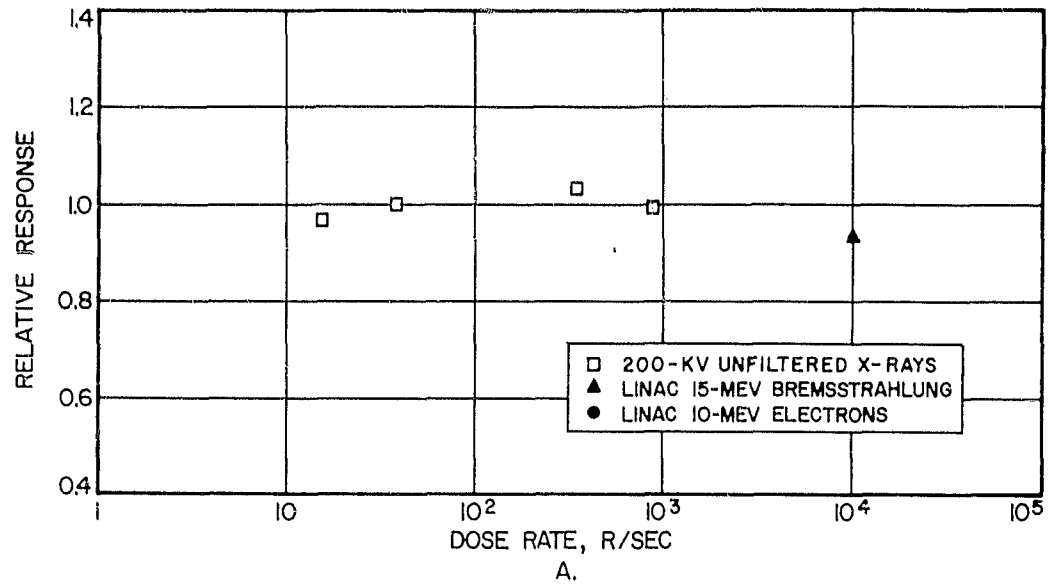
FIGURE 57. RATE DEPENDENCE OF THERMOLUMINESCENT DOSIMETER

94

The LINAC electron beam was used to obtain the remaining thermoluminescent dosimeter rate data (Figure 57). The data at 2×10^9 r/sec are not in agreement because of the very short (15 cm) target distance. Beam position is difficult to locate at this position and the data indicate that the monitor was possibly misaligned. The remainder of the data was taken at greater distances and substantiated the lack of a rate dependence at least up to 10^9 r/sec. The shift in absolute value is presumed to be caused by the glass envelope. All exposures were performed with the bare dosimeter element affixed to the periphery of the sensitive area of the electron beam monitor.

F. ENERGY DISCRIMINATION SHIELD

The first prototype thermoluminescent dosimeter to be evaluated for an energy-response shield was a phosphor-covered mesh of nickel which was split into two conical sections. This configuration presents a directional problem which is apparent from curves A and B in Figure 58A. Several shield configurations were tried as well as different orientations of the dosimeters, Figures 58A and 58B.

Holes were first used to provide the necessary open area of the shield to increase the low-energy response. This design was not too satisfactory for reproducibility and was changed to an annular slot which bisects the midplane of the dosimeter.

The acquisition of six pre-production Bureau of Ships thermoluminescent dosimeters permitted a more concentrated effort on a final shield design. These units had the phosphor coated on a spiral of nichrome wire instead of a nickel mesh. It was necessary to determine the optimum thickness of lead and tin and the open area between the two sleeve sections.
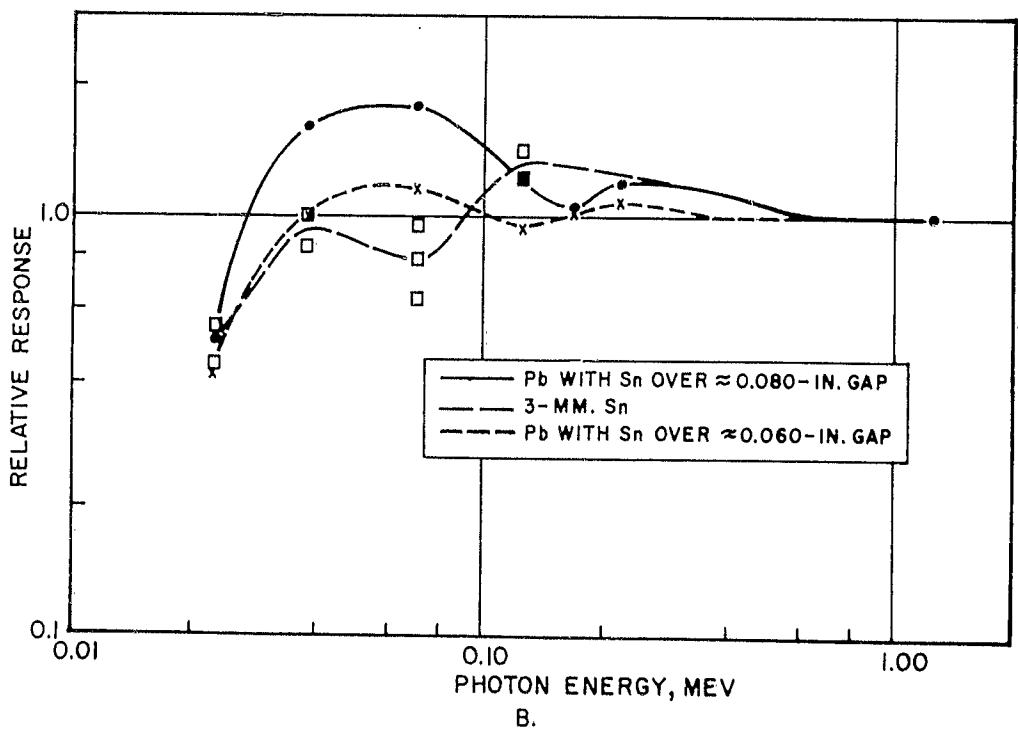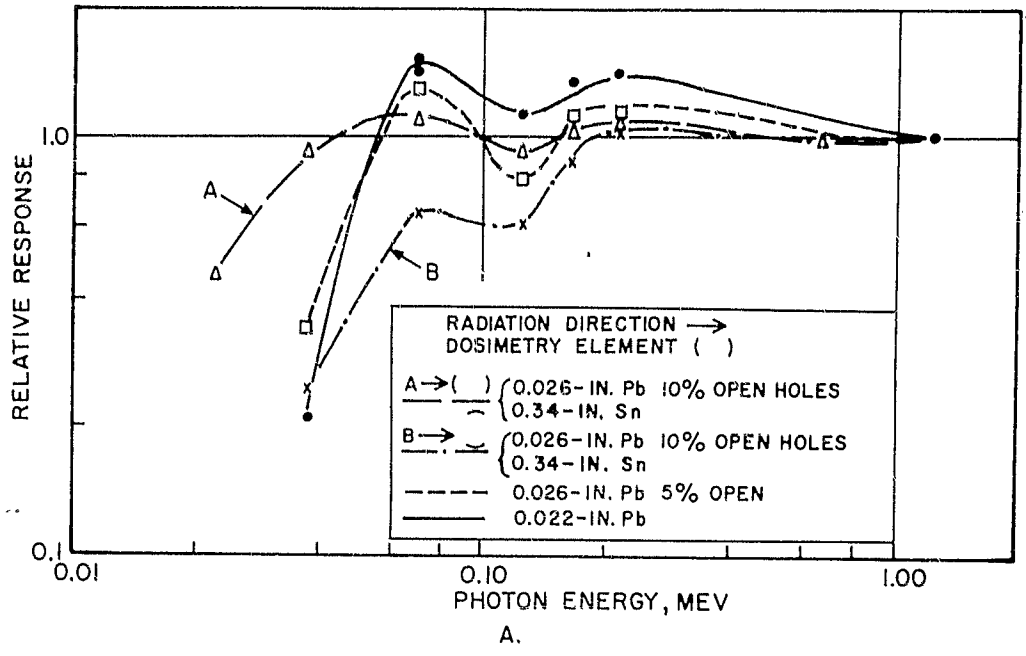
FIGURE 58. RESPONSE OF THERMOLUMINESCENT DOSIMETER FOR SHIELD
STUDIES WITH NICKEL MESH ELEMENT

A series of shields were constructed as listed below and the energy response is shown in Figure 59.

Shield No.	Plastic Case, (in.)	Tin, (in.)	Lead, (in.)	Spacer, (in.)
1	0.057	0.033	0.027	0.080
2	0.047	0.037	0.025	0.100
3	0.057	0.030	0.023	0.080
4	0.057	0.033	0.027	0.045
5	0.057	0.030	0.023	0.045

The results of these experiments indicate a rather severe loss of response between 70 to 150 kev. This is similar to the effect seen in the silver glass shield. Therefore, the tin portion of the shield was extended over the window to decrease the over-response below 70 kev, and in turn the window was opened wider to allow for the extra shielding. Figure 60 shows the response for two shield configurations.

Shield No.	Plastic Case, (in.)	Tin, (in.)	Lead, (in.)	Spacer, (in.)
6	0.057	0.0165	0.023	0.085
7	0.057	0.0095	0.025	0.085

Shield No. 7 seems very satisfactory for this dosimeter. An end cap was also fabricated from 0.025 inch of lead and 0.0095 inch of tin and a rotational response for 165-kev x-rays is shown in Figure 61. The response for a plain unshielded end cap is also shown for a top-to-side incidence. The energy response for an end-on exposure with the shielded
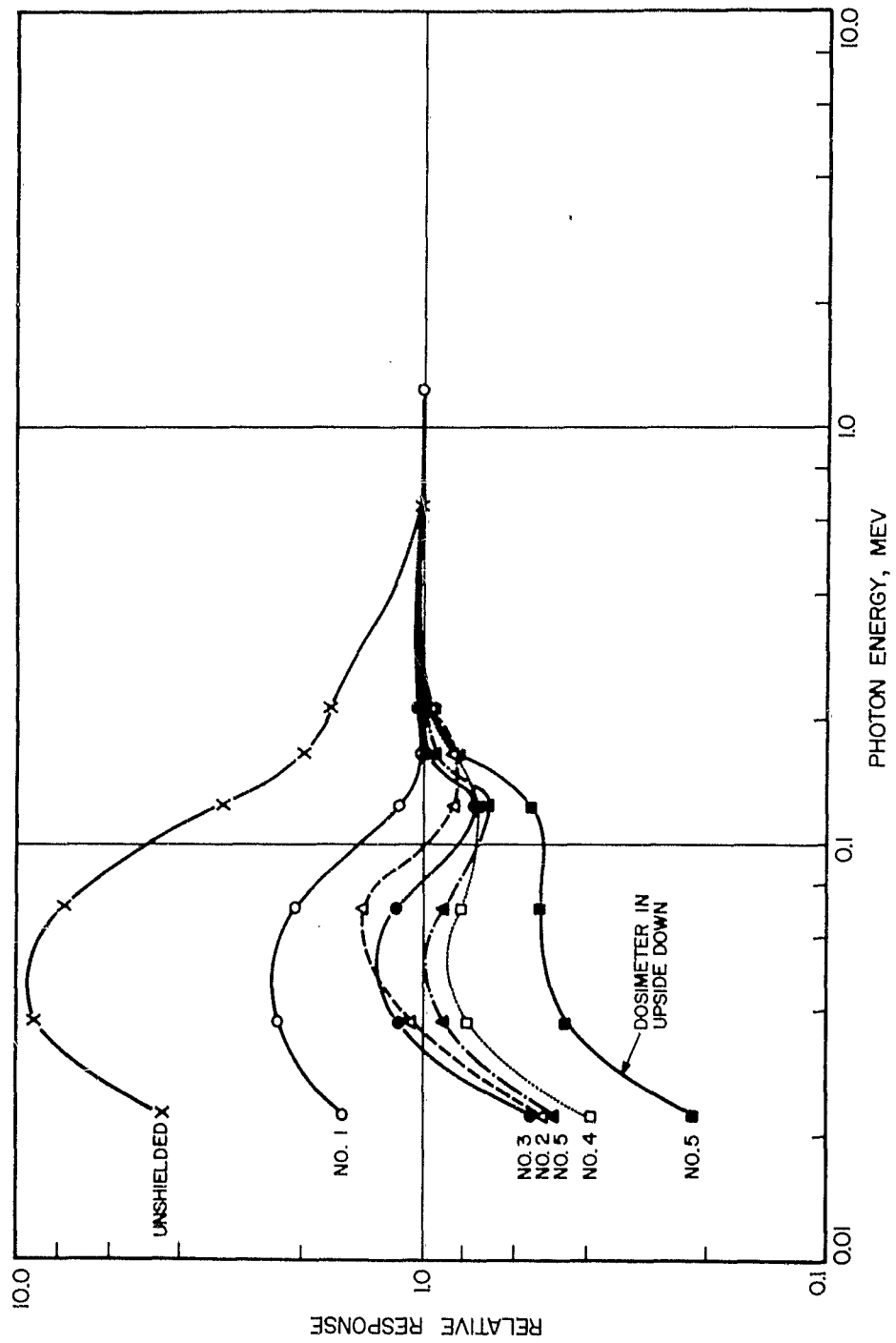
FIGURE 59. SPIRAL ELEMENT THERMOLUMINESCENT DOSIMETER RESPONSE (OPEN WINDOW)

98

FIGURE 60. SPIRAL ELEMENT THERMOLUMINESCENT DOSIMETER RESPONSE (TIN-COVERED WINDOW)

99
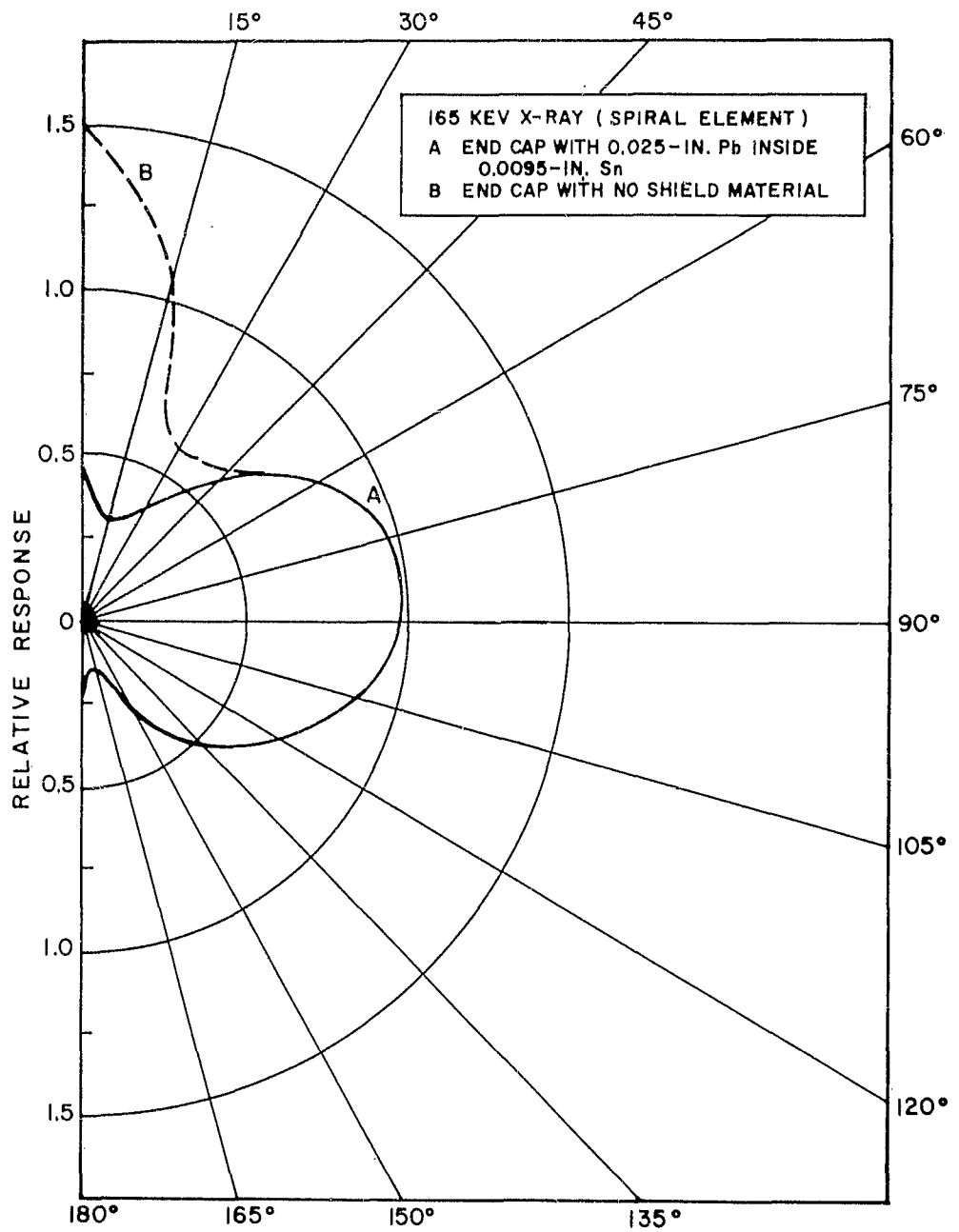
FIGURE 61. THERMOLUMINESCENT DOSIMETER SHIELD
ROTATIONAL RESPONSE

end cap is shown in Figure 62. A hole in the lead portion
of the end cap has been considered for increasing the low-energy
response in this direction.

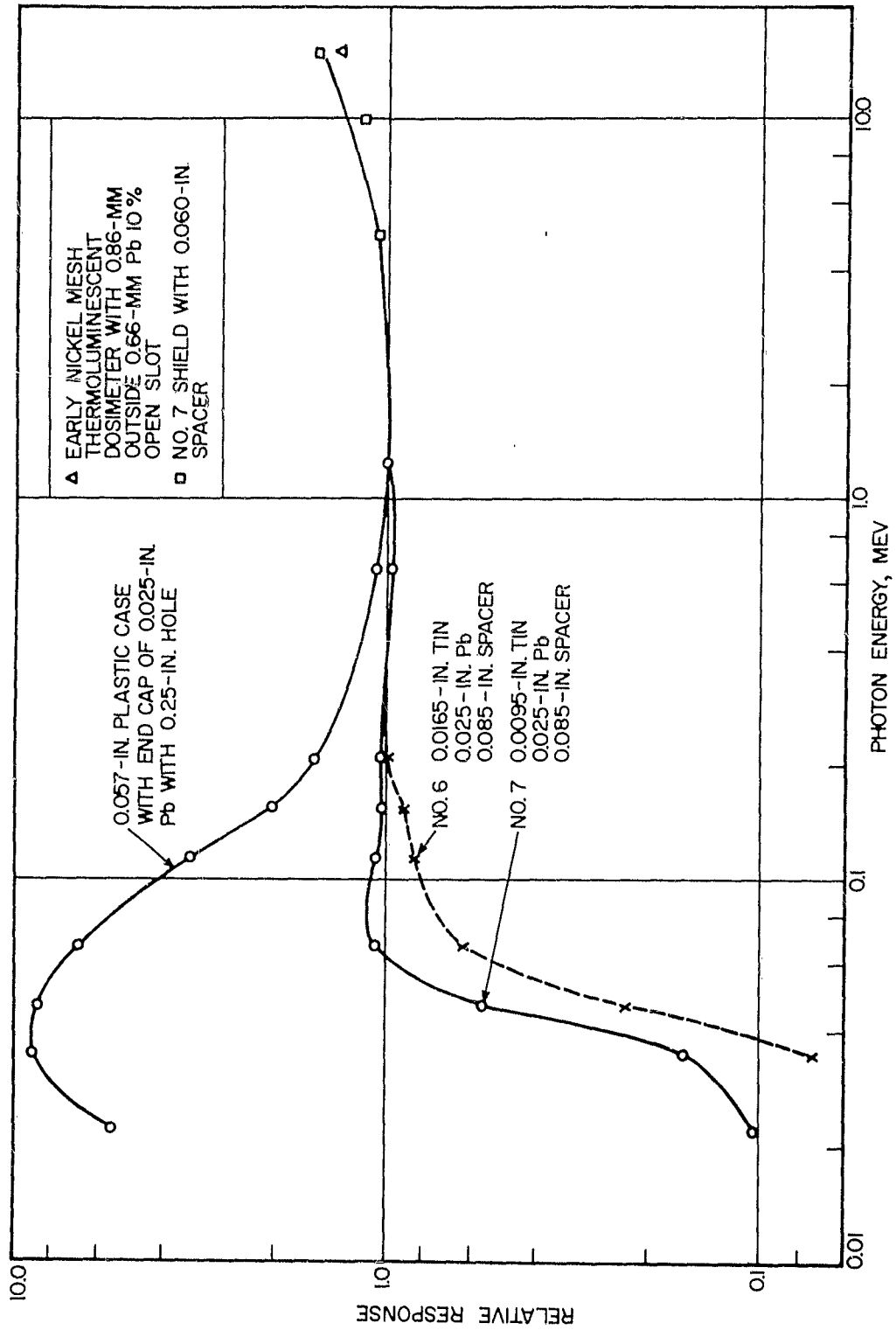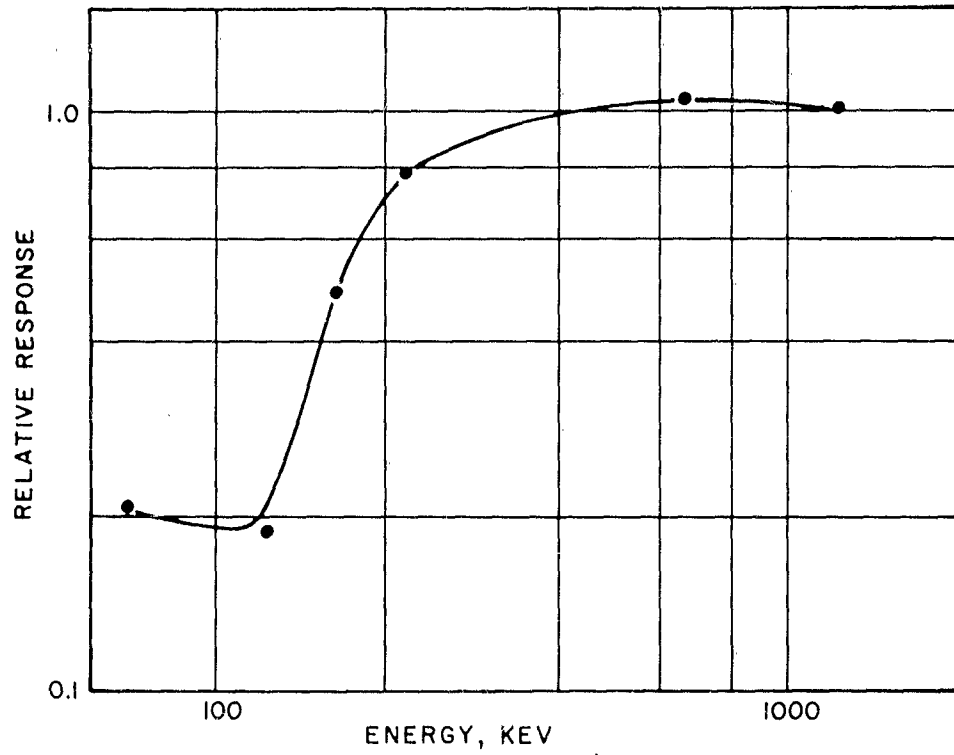FIGURE 62. THERMOLUMINESCENT DOSIMETER END-ON ENERGY DEPENDENCE
(SPIRAL ELEMENT)

G. THERMOLUMINESCENT DOSIMETER NEUTRON RESPONSE

The thermoluminescent dosimeter was exposed at a distance of 10 cm from the Pu-Be fast neutron source for periods of 50 minutes. Exposures were made both in a plastic can containing the energy-discriminating shield and in a plastic can with no shield. Table 5 shows the fast neutron sensitivity for these exposures.

Table 5
Fast Neutron Sensitivity of the Thermoluminescent Dosimeter Using the Pu-Be Neutron Source

	Without Shield	With Shield
Total apparent exposure dose rate, mr/min	0.78	0.90
Measured gamma exposure dose rate, mr/min	0.70	0.70
Net neutron response, mr/min	0.08	0.20
Fast neutron flux, n/cm^2	7.55×10^5	7.55×10^5
Dosimeter response, $r/n/cm^2$	0.11×10^{-9}	0.27×10^{-9}

Similar exposures were made using 14-Mev neutrons. The response of the unshielded dosimeters was 1.47×10^{-9} $r/n/cm^2$ and the shielded response was 1.29×10^{-9} $r/n/cm^2$.

The thermal neutron response was determined at the General Dynamics/General Atomic thermal column. A special lithium-6-enriched LiF shield was made by packing the material in the walls formed by two concentric plastic pill bottles; filling was also provided for the two ends. The attenuation for this shield was determined by gold foils to be 978.

The thermoluminescent dosimeter response was evaluated in a manner analagous to that used with the silver-activated glass rod dosimeter response. The response is 1.41×10^{-10} $r/n/cm^2$.

The Bureau of Ships production dosimeter elements were finally acquired and exposed in the prototype shield (No. 7) previously described. The response of this combination, shown in Figure 63, was not satisfactory; this appears to be due to the small change in the spiral wire coil size. The new dimensions are:

	Latest Prototype	Production Unit
Coil wire size (AWG)	21	20
Coil outside diameter (inch)	0.275	0.202

To regain the proper response for these production elements, the shielding materials have been changed in the following manner:

Shield No.	Plastic Case (in.)	Tin (in.)	Lead (in.)	Spacer (in.)	Hole (in.)
7	0.057	0.0095	0.025	0.085	---
Final Shield	0.057	0.0065	0.018	0.075	0.160

In addition, a hole in the lead portion of the top end cap was devised for better response in this direction.

Figure 63 shows the dosimeter response after these alterations, and a sketch of the final shield is shown in Figure 64.

103
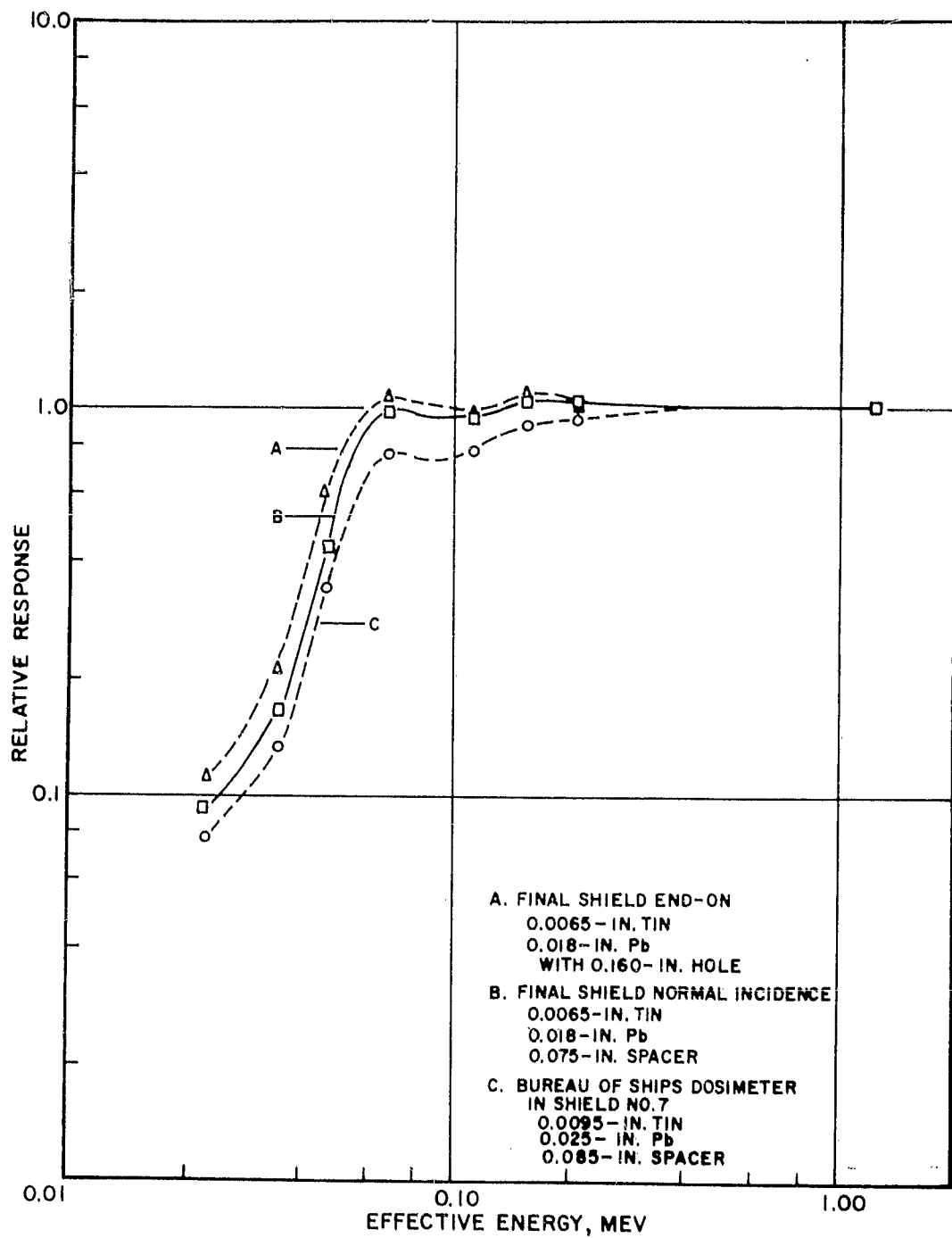
FIGURE 63. PRODUCTION MODEL THERMOLUMINESCENT
DOSIMETER RESPONSE

104
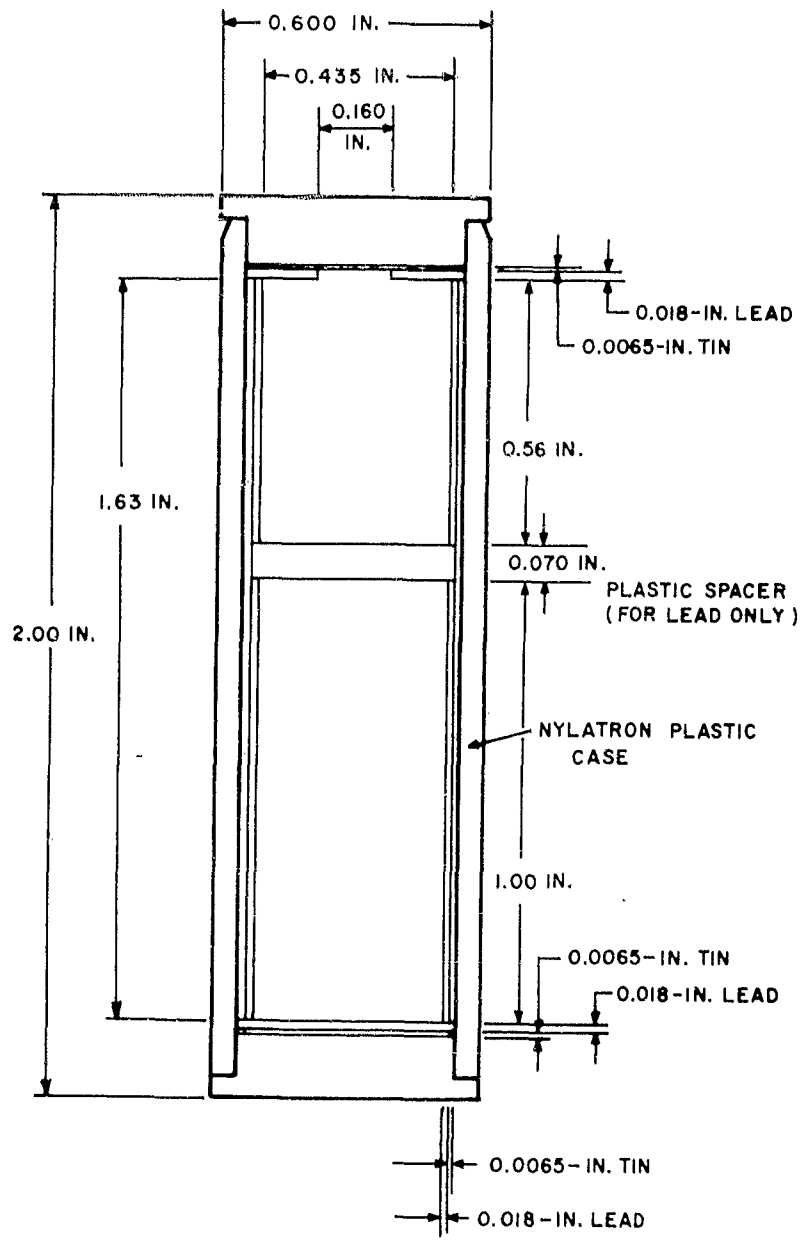
FIGURE 64. THERMOLUMINESCENT DOSIMETER FINAL SHIELD

VIII. PHOTODIODE-FLUOR DETECTOR

A photodiode-fluor detector was fabricated from an FW-114 high-current photodiode and a 1-inch-diameter by 1-inch-long polished NE-102 plastic scintillator.

Provision was made to remove the scintillator and measure the response of the photodiode to the incident beam. The system was tested at 15-Mev bremsstrahlen with and without scintillator, at a potential of 500 volts. The signal was integrated and compared to the response of the monitor. Results of these measurements are shown in Figure 65.

In addition, the energy response for the filtered x-ray energies, Cs-137 and Co-60, were determined for the system. The sensitivity of the detector is 78.6 esu/r at Co-60 energy.

FIGURE 65. ENERGY RESPONSE OF NE-102 PLASTIC FLUOR

The figure includes the following labels:

- I IN. x I IN. CYLINDRICAL FLUOR NORMALIZED TO COBALT-60 RESPONSE
- EFFECTIVE ENERGY, MEV
- RELATIVE RESPONSE

IX THERMAL NEUTRON ATTENUATION SHIELDS

The thermal neutron attenuation shield is intended as a separate shield for use when mixed neutron and gamma radiation environments are encountered. Design aims included keeping the dimensions commensurate with the small size and weight of the dosimeter systems, and making the shield serve also as a container for the dosimeter and its associated gamma ray energy discrimination shield, thus eliminating problems of incomplete shielding associated with the presence of a secondary container at the point of closure.

Lithium-6, with its high thermal neutron cross section and light atomic weight, appears ideal for shielding applications if incorporated in an inert chemical compo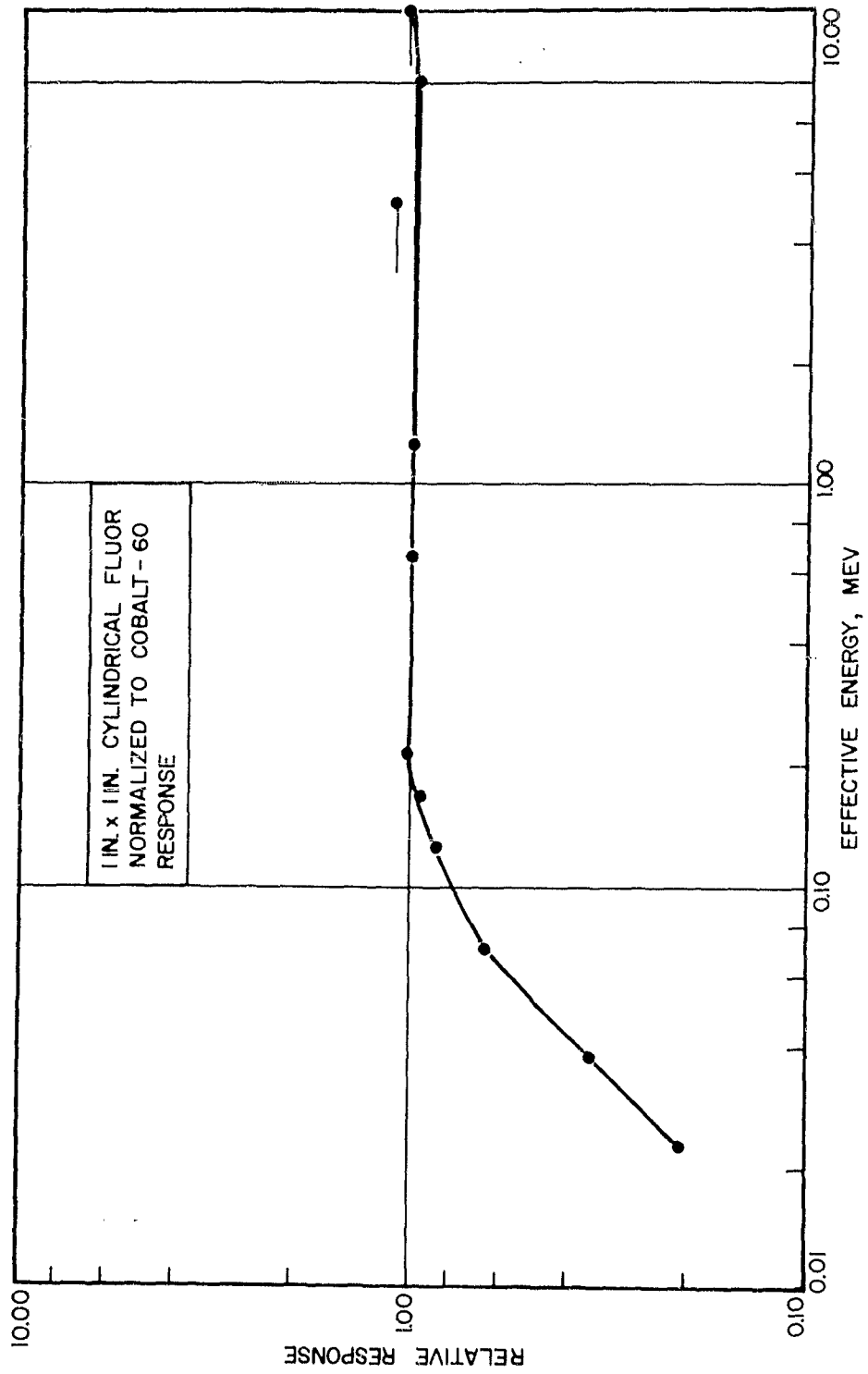und. Such a compound is lithium fluoride. In addition to being chemically inert, this material has a high melting point and permits a high concentration of the lithium isotope.

The gamma ray attenuation properties of lithium fluoride are negligible in this application. Its physical characteristics are similar to those of aluminum, as can be seen from the following tabulation.

	Li^6F (Sintered)	Al
Density (g/cc)	2.5	2.7
Atomic No.	12	13
Atomic Weight (g/mol)	25.06	26.98

Shield fabrication methods considered included the use of a binder with the lithium-6 fluoride powder, but this procedure was rejected in view of possible radiation damage to the binder. Several attempts were then made to melt and cast the powder into a glass. This, however, proved difficult because of the great change in density between the liquid and solid phases of the material.
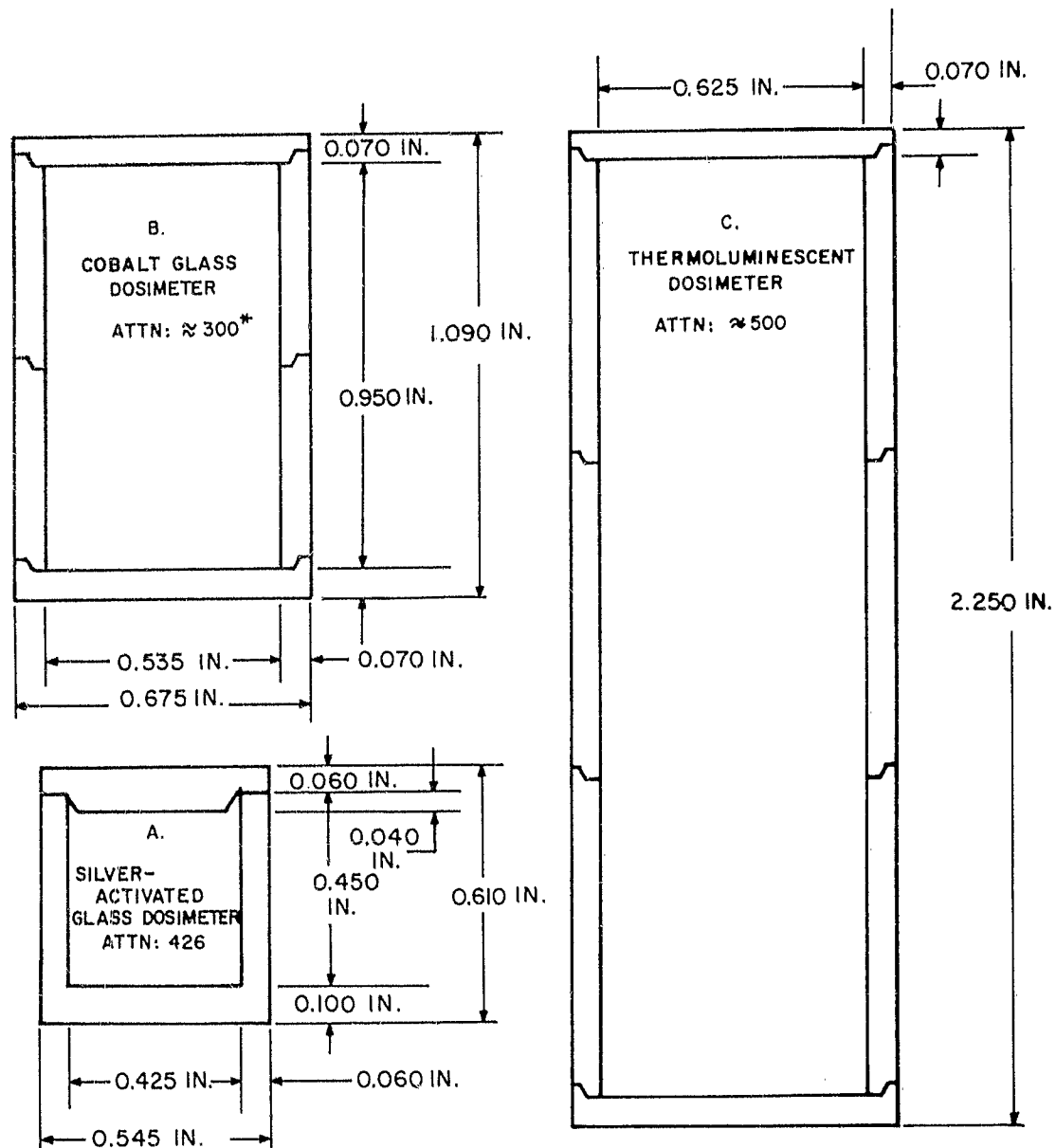
In the process of melting, however, a fortunate accident indicated the possibility of sintering the material. Although

no information on this process could be found, a procedure was developed by the Pacific Sintered Metals Company of Los Angeles, California, to sinter lithium-6 enriched lithium fluoride into the required thermal neutron attenuation shields.

The sintered material is a hard, ceramic-like substance with a density of 2.5 g/cc. Although a limited amount of machining is possible, extensive work results in delamination of the material. To conserve material, the parts will be sintered to size, allowing for a shrinkage of approximately 20 per cent during the sintering process. Allowance must also be made for a certain loss of concentricity of the shield which may occur during the sintering operation; in the case of the thermoluminescent dosimeter shield, this allowance amounted to 30 per cent. Prototype shields were made 0.060 inch thick and large enough to accept the silver-activated glass rod dosimeter system. The attenuation of these shields was determined to be 426. The final shields have been increased in thickness to 0.070 inch, which should give an attenuation of 1000.

Three sizes of shields are being fabricated for each of the dosimeter systems. The individual shields are shown in Figure 66, A, B, and C. The two large shields were made in sections and cemented together with Shell No. 828 epoxy resin. As designed, the stepped sections and covers provide a complete and sufficient shield for thermal neutron attenuation, without the leakage normally encountered in separately contained cup and cap shields. If it should prove that the resin fails under extensive radiation, an alternative method would be to enclose the sections in a thin aluminum shell.

Also under consideration is a fabrication process involving hot pressing the lithium-6 fluoride powder. Samples of hot pressed magnesium fluoride and calcium fluoride suggest that this method might result in a material stronger than the sintered powder and permit more precisely fabricated shields. Further investigation of fabrication methods should be

109

B.
COBALT GLASS
DOSIMETER

ATTN: ≈ 300*

0.070 IN.

1.090 IN.

0.950 IN.

0.070 IN.

0.535 IN.

0.675 IN.

A.
SILVER-
ACTIVATED
GLASS DOSIMETER
ATTN: 426

0.060 IN.

0.040 IN.

0.450 IN.

0.610 IN.

0.100 IN.

0.425 IN.

0.060 IN.

0.545 IN.

C.
THERMOLUMINESCENT
DOSIMETER

ATTN: ≈ 500

0.625 IN.

0.070 IN.

0.070 IN.

2.250 IN.

*LOW VALUE DUE TO IMPROPER SINTERING

FIGURE 66. LITHIUM-6-ENRICHED LITHIUM FLUORIDE THERMAL NEUTRON SHIELD

110

continued in order to develop an ultimate thermal neutron
shield for gamma ray dosimeters used in a mixed neutron and
gamma ray environment.

At present, the effects of neutrons on the lithium-6
shield at energies other than thermal have not been in-
vestigated.

REFERENCES

1. "Protection Against Betatron-Synchrotron Radiations up
    to 100 Mev," National Bureau of Standards Handbook 55,
    pp. 32-33.

2. J. C. Villforth, R. D. Birkhoff, and H. H. Hubbell, Jr.,
    "Comparison of Theoretical and Experimental Filtered
    X-Ray Spectra," ORNL-2529, 1958.

3. "Report of the International Commission on Radiological
    Units and Measurements (ICRU)," National Bureau of
    Standards Handbook 78, 1958.

4. F. R. Shonka, J. E. Rose, and G. Faila, "Conducting
    Plastics Equivalent to Tissue, Air, and Polystyrene,"
    Second U. N. International Conference on the Peaceful
    Uses of Atomic Energy, 1958.

5. G. J. Hine and J. L. Brownell, Editors,"Radiation Dosi-
    metry," Academic Press, N. Y. (1956) pp. 164-175.

6. E. S. Troubetzkoy, M. H. Kalos, H. Lustig, et al.,
    "Fast Neutron Cross Sections of Ni, Ca, S, and Na "
    NDA 2133-4, January 31, 1961.

7. Leona Stewart, "Neutron Spectrum and Absolute Yield
    of a Plutonium-Beryllium Source," Phys. Rev. 98,
    3740-3743 (1955).

8. W. T. Thornton, J. A. Auxier, "Some X-Ray and Fast Neu-
    tron Response Characteristics of Silver Metaphosphate
    Glass Dosimeters," ORNL-2912, 1960.

APPENDIX A
EFFECTIVE X-RAY ENERGIES

The effective energies of the x-ray machine were determined from half-value layer measurements in aluminum and copper. Figure A-1 shows the attenuation of the primary beam for various thickness attenuators. National Bureau of Standards Handbook 583* values of x-ray attenuation were converted to half-value layers and plotted as a function of energy for aluminum (Figure A-2) and copper (Figure A-3). After determining the half-value layer for each peak energy and filter condition, this value was entered on the appropriate plot and an effective energy determined. Calculations were based on a good geometry experiment, and data which considered coherent scattering were used.

During the course of these experiments, both an x-ray tube and two high-voltage windings failed and have been replaced. To determine if any of these replacements had affected the energy spectrum, this half-value layer measurement procedure was repeated. Figure A-4 shows the new set of attenuation curves.

In one instance at 150 kv, collimation was removed, and a poor geometry experiment was performed. In evaluating these data, a curve of half-value layer as a function of energy without coherent scattering must be used, Figure A-3. Also several filter-energy combinations were evaluated to achieve an energy point at about 50 kev. These combinations are shown in Figure A-5. The present effective energies for the various filters and peak operating energies are as follows:

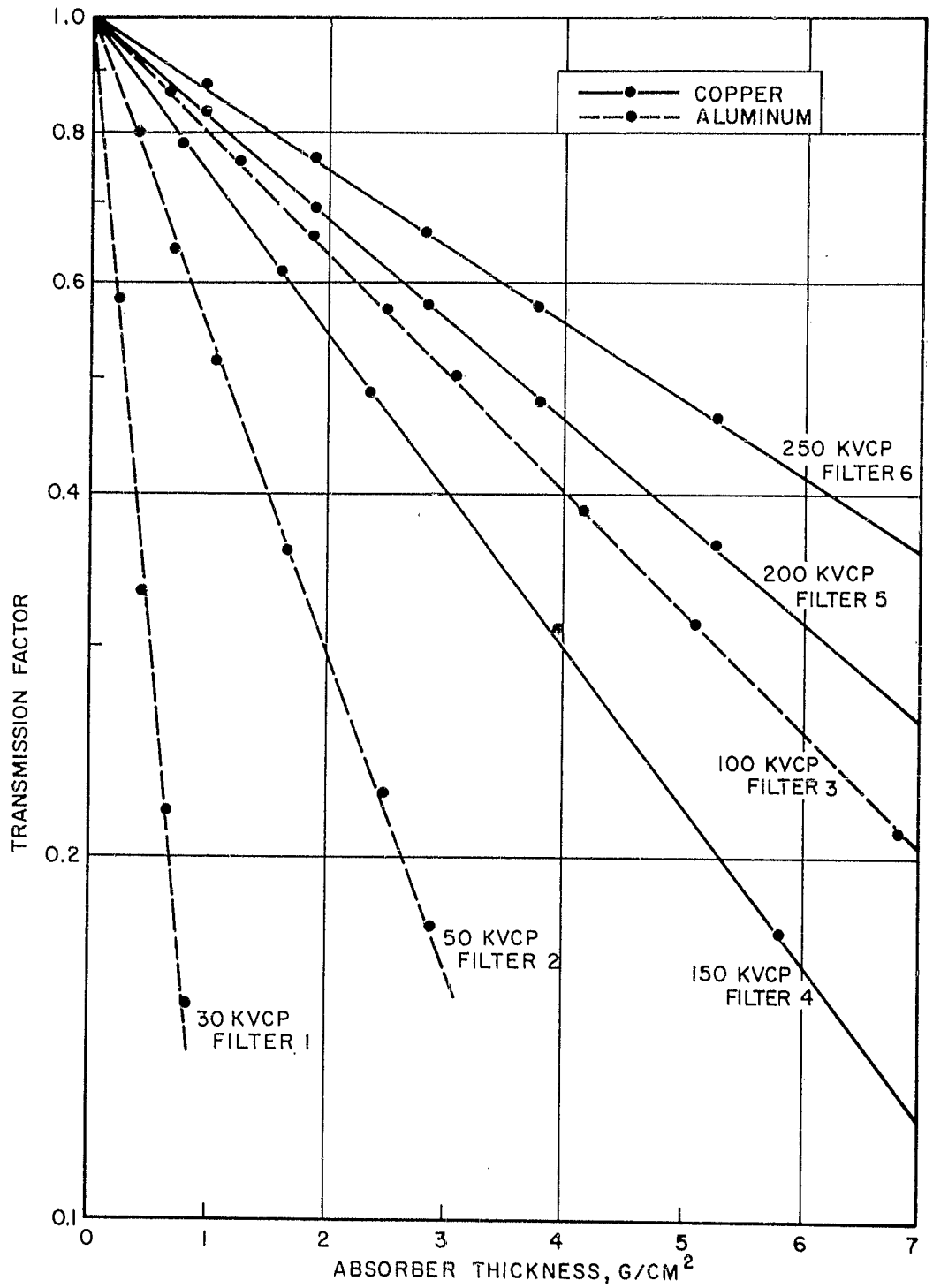*NBS Circular 583, "X-Ray Attenuation Coefficients from 10 kev to 100 Mev," Gladys White Grodstein, April 30, 1957.

112

FIGURE A-I. NARROW BEAM ATTENUATION DATA FOR DETERMINING
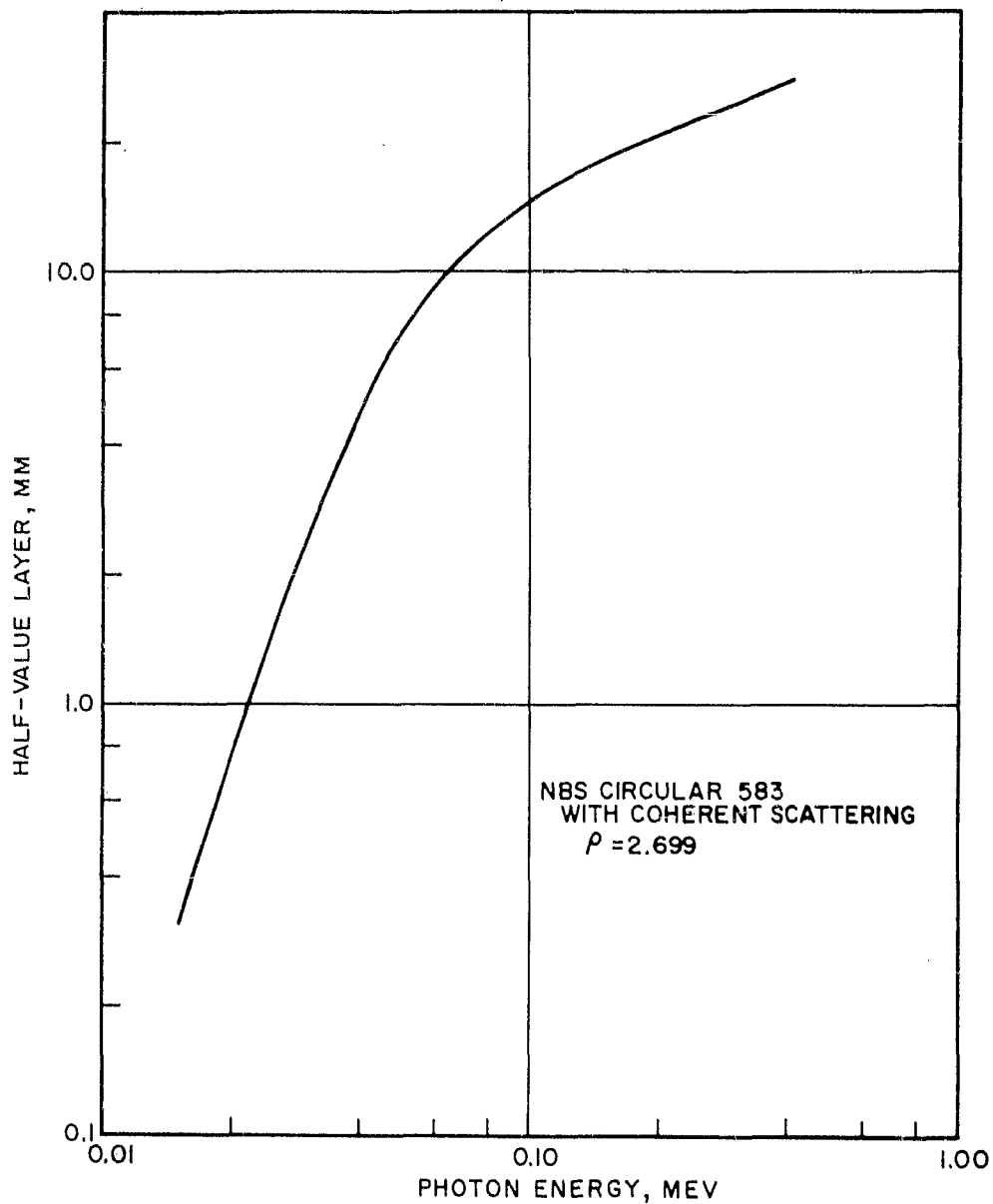EFFECTIVE X-RAY ENERGY

113

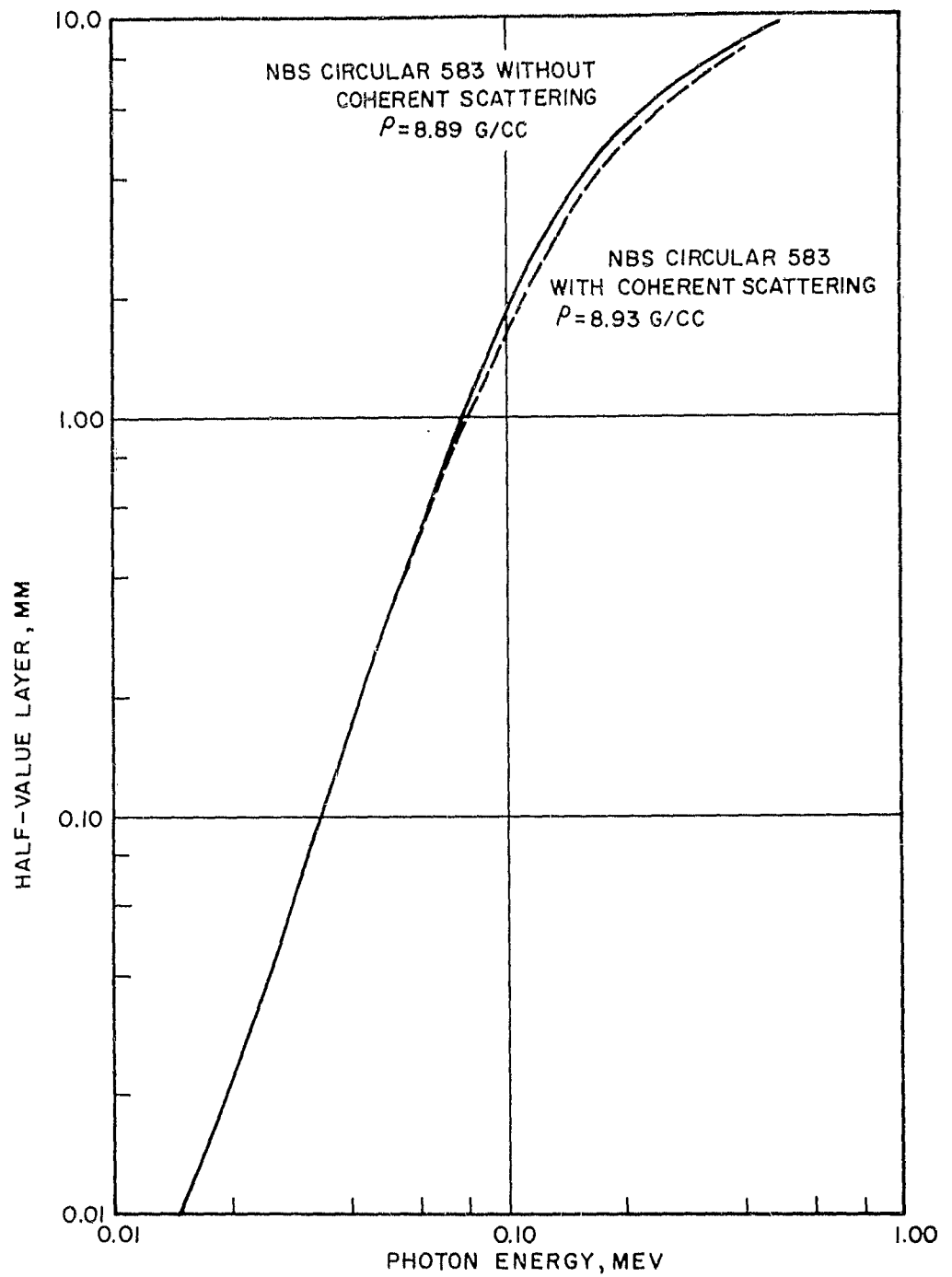FIGURE A-2. ALUMINUM HALF-VALUE LAYER AS A FUNCTION OF ENERGY

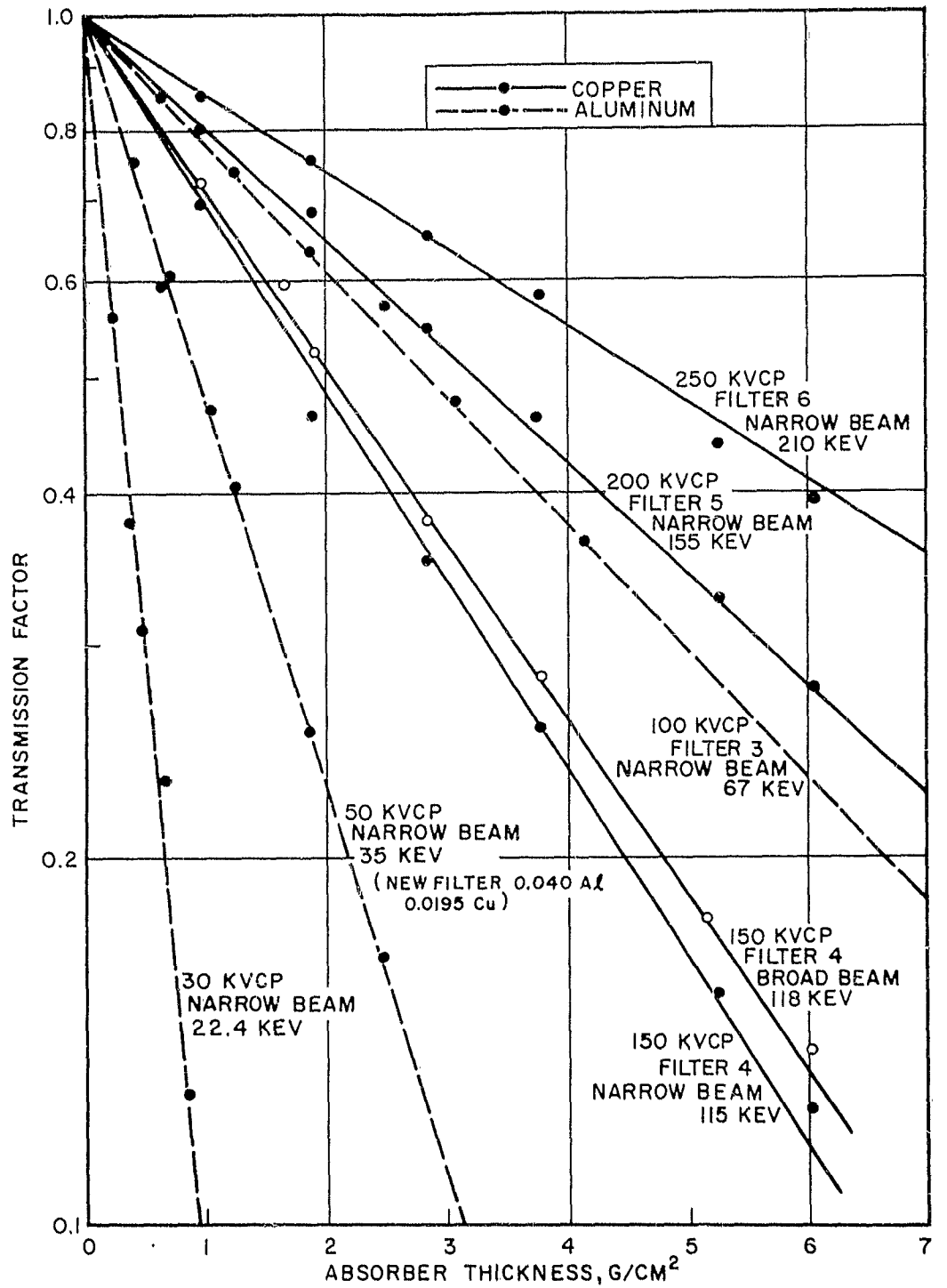FIGURE A-3. COPPER HALF-VALUE LAYER AS A FUNCTION OF ENERGY

FIGURE A-4. NARROW BEAM ATTENUATION DATA FOR DETERMINING
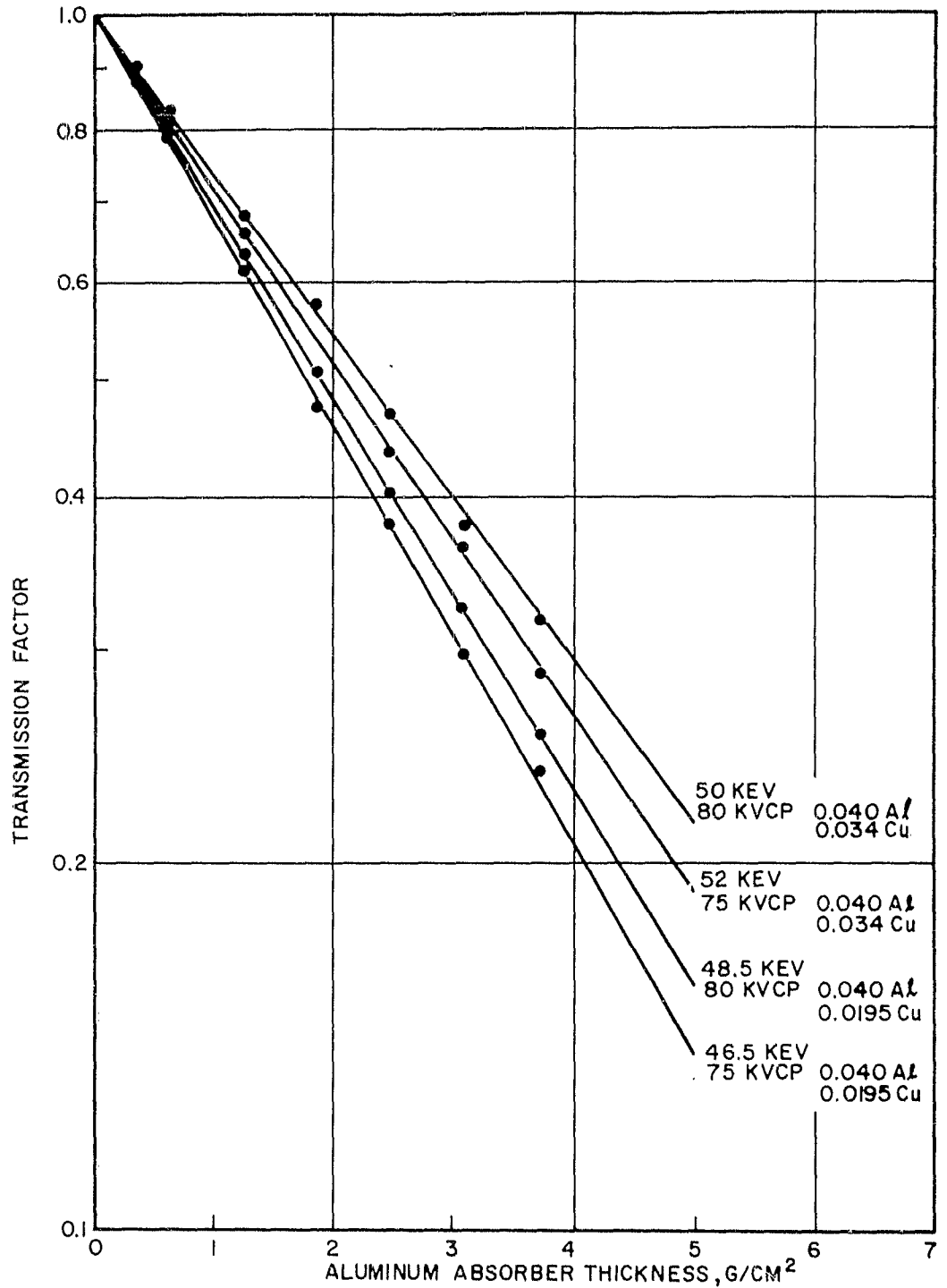EFFECTIVE X-RAY ENERGY REEVALUATION

116

FIGURE A-5. NARROW BEAM ATTENUATION DATA FOR DETERMINING
NOMINAL 50-KEV FILTER

Table 6

Present X-Ray Filters and Effective Energies for 250-kv X-Ray Machine

Peak kv Constant Potential	Filter No.	Filter mg/cm^2				Effective Energy
		Pb	Sn	Cu	Al	
30	1	-	-	-	133	22.4
50	2	-	-	233	133	35.0
75	-	-	-	441	279	46.5
100	3	548	-	-	279	67
150	4	-	913	2790	279	115*
200	5	716	1863	929	279	155
250	6	2363	861	959	279	210

*150 kvcp broad-beam effective energy - 118 kev.

To obtain rate effects at low and moderate dose rates and to effect high doses in the cobalt glass dosimeters, exposures were made on the oil displacement cone and window assembly of the x-ray machine. The abundance of soft x-rays, short distance, and over-response of the dosimeters to low-energy radiation provided an excellent method for dose rate effects on silver-activated glass rods and total dose for the cobalt glass. On the assumption that the mechanism for dosimeter response is independent of energy, only a normalization of the data is required.

Typical dose rates at 1 meter for several energies are:

Energy, kv	Current, ma	Dose Rate, r/min
30	20	1.9
50	20	5.8
100	20	17.9
150	20	34.4
200	20	52.4
220	20	60.8
250	10	38.6

Extrapolation for the 220 kv at 20 ma to the tube window where the target-to-window distance is 5 cm indicates a dose rate of 326 r/sec. Assuming over-response factors of 20 and 2.5 for silver-activated and cobalt glass, the apparent dose rate to each is 6520 r/sec and 800 r/sec, respectively. The 1-cc air-equivalent ionization chamber and aluminum ionization chamber were used later and a plot of this dose rate as a function of distance is shown in Figure A-6.

The effective energy of the 1-Mev General Electric Company x-ray machine was determined from the attenuation of the beam by lead absorbers. Figure A-7 is a plot of these data which indicate that the half value layer for this machine is 3.27 mm. From Figure A-8, which is a plot of the half value layer vs photon energy, the corresponding effective energy is 425 kev.
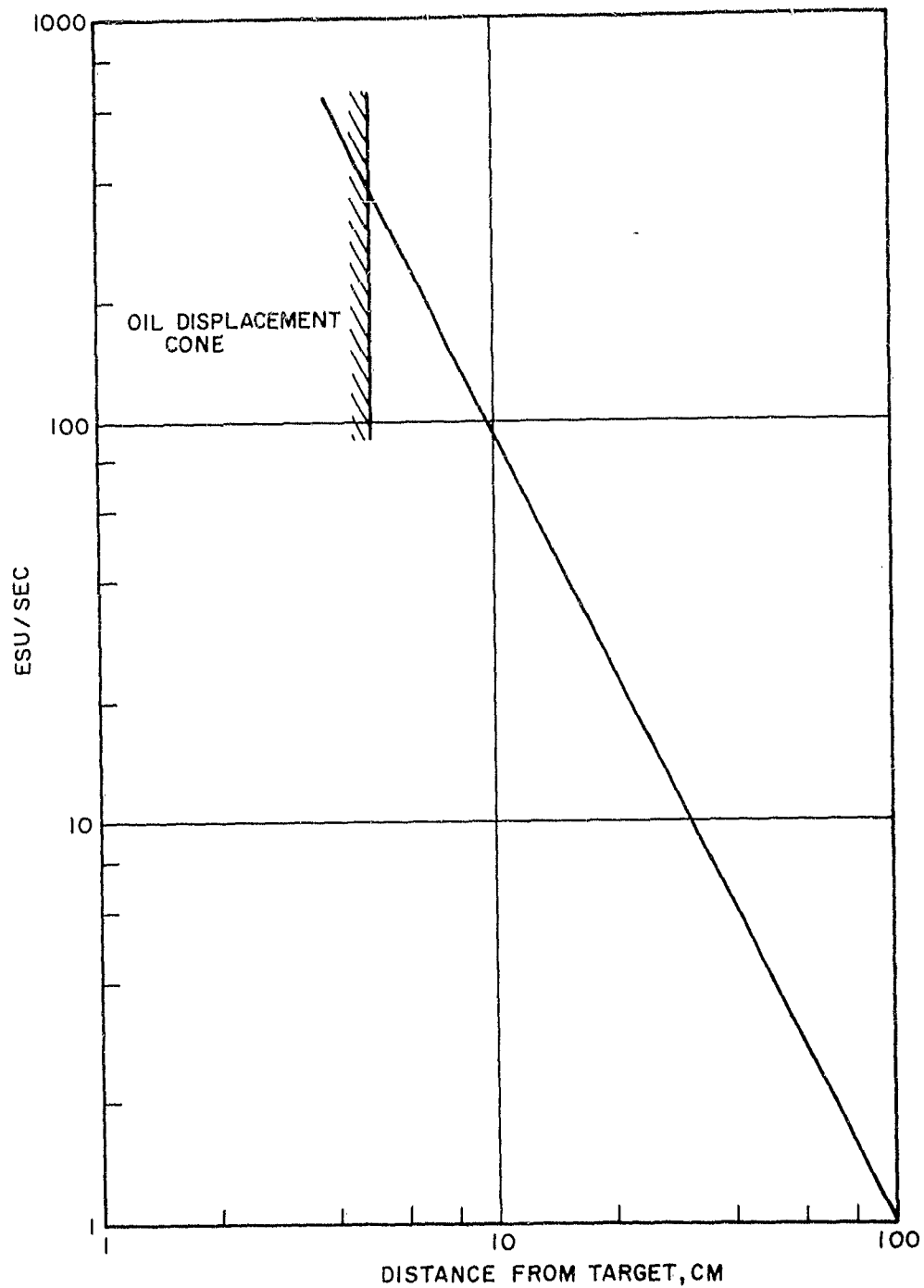
FIGURE A-6. NO-FILTER DOSE RATE AS A FUNCTION OF DISTANCE
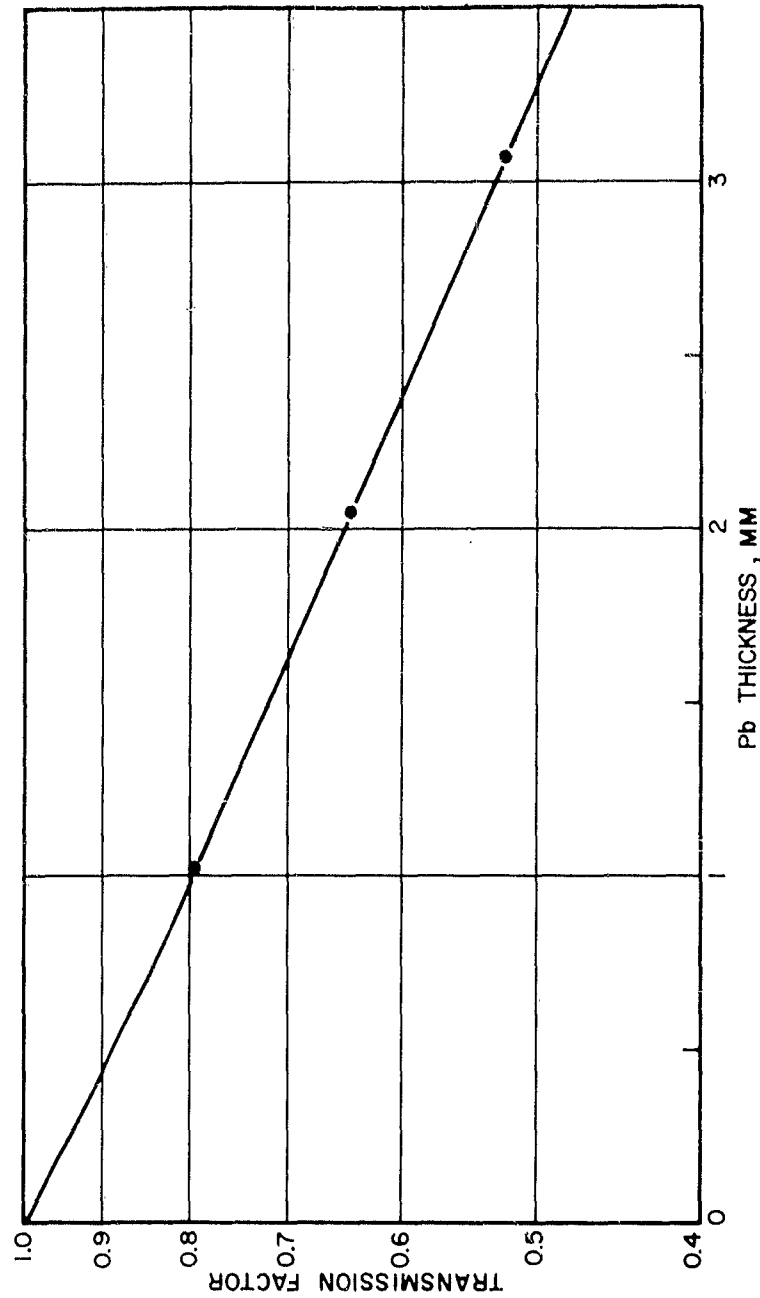FOR 220-KV, 20-MA X-RAY MACHINE OPERATION

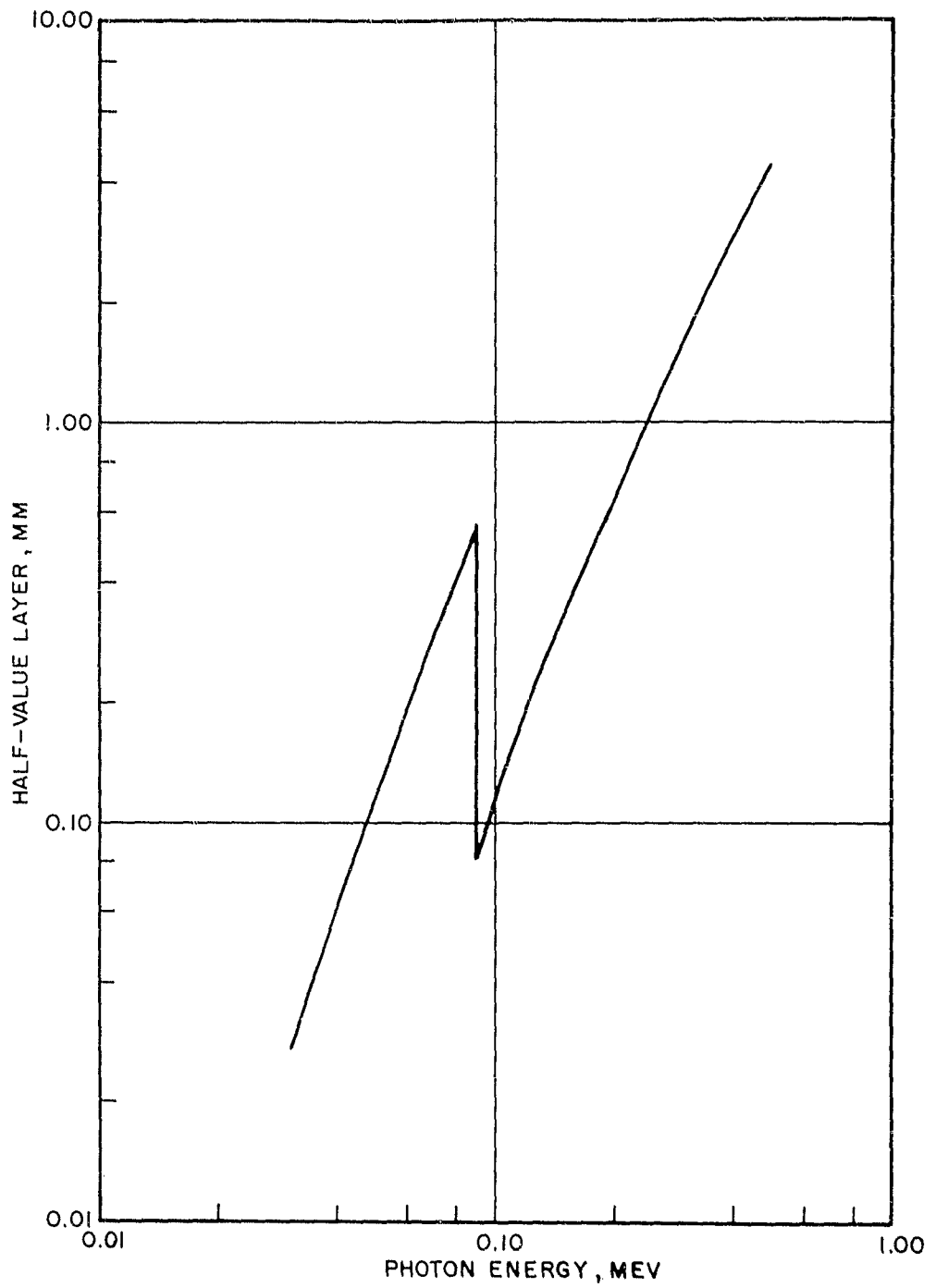FIGURE A-7. 1000-KEV X-RAY HALF-VALUE LAYER DETERMINATION

121

FIGURE A-8. LEAD HALF-VALUE LAYER AS A FUNCTION OF ENERGY

APPENDIX B
BUILDUP STUDIES OF CESIUM AND COBALT SOURCES

The use of radioactive sources always presents a problem of scattering from the source mounting fixture. This scattered radiation, which consists of low-energy gamma rays and energetic electrons, contaminates the useful beam. For the evaluation of dosimeters which have inherently a large over-response to low-energy radiation, this contaminated beam will give erroneous data.

To determine the degree of beam contamination, a buildup study is performed with a thin window ionization chamber. The thin window provides a means of detecting electrons and low-energy gamma rays that would otherwise be stopped in the thick wall chambers ordinarily used. By adding successive layers of plastic film in front of the thin window, the electrons and low-energy gamma rays in the beam are attenuated; in addition, electron equilibrium (buildup) is established by the primary beam and the wall material. A large number of electrons and low-energy gamma rays is indicated by a decrease in ion current with increasing absorber, while a clean, high-energy beam is indicated by an increase in ion current with increasing absorber. This technique was utilized to evaluate the beam contamination and the efficiency with which different collimators suppress the scattered electron and gamma radiation of various cesium and cobalt sources used in this study. Figures B-1 and B-2 show the characteristics of the cesium and cobalt sources at EG&G; Figures B-3 and B-4 show the same data for the Cottage Hospital sources.
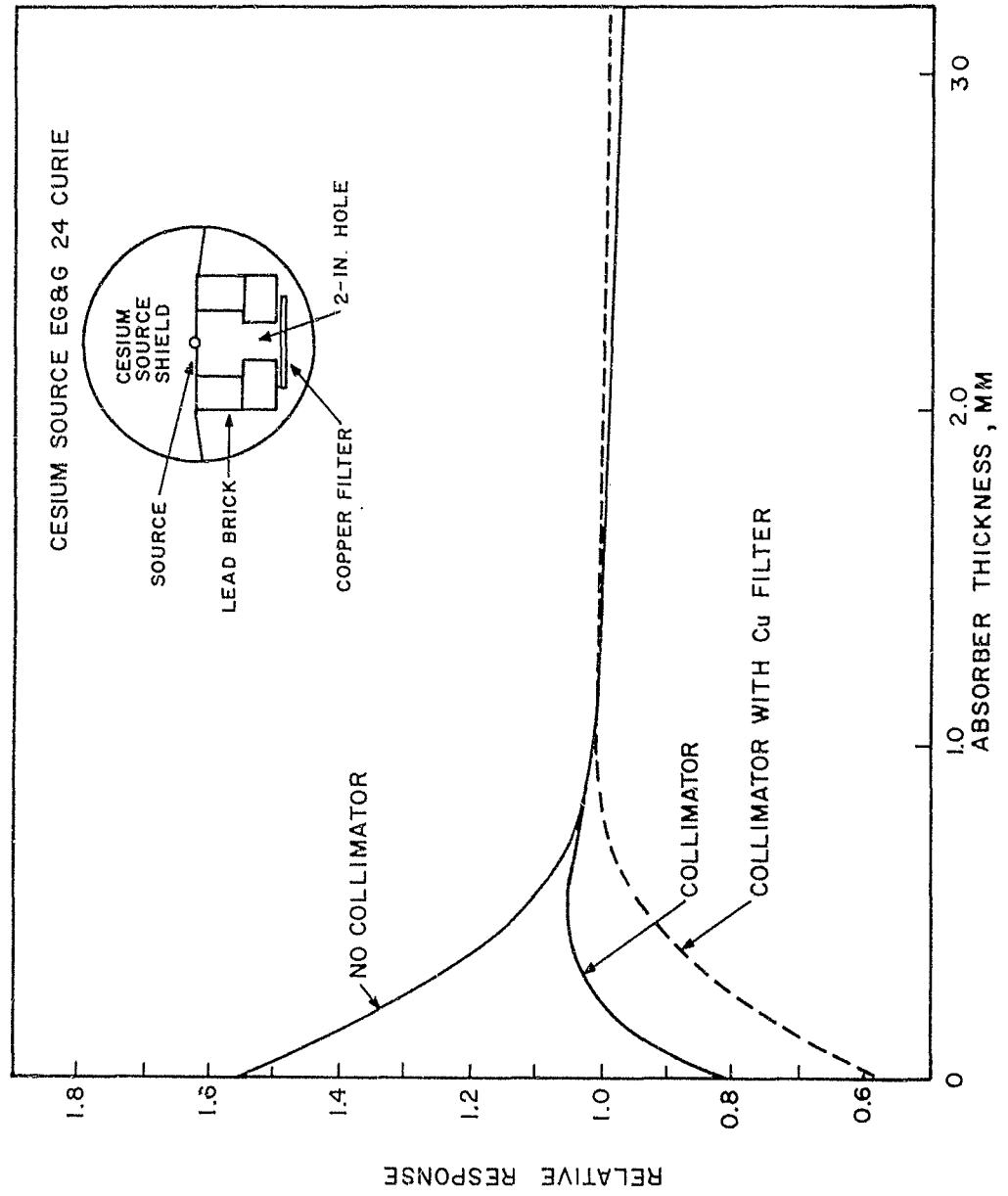
FIGURE B-I. RELATIVE IONIZATION CURRENT AS A FUNCTION OF ABSORBER THICKNESS FOR A 24-CURIE CESIUM SOURCE WITH AND WITHOUT COLLIMATOR
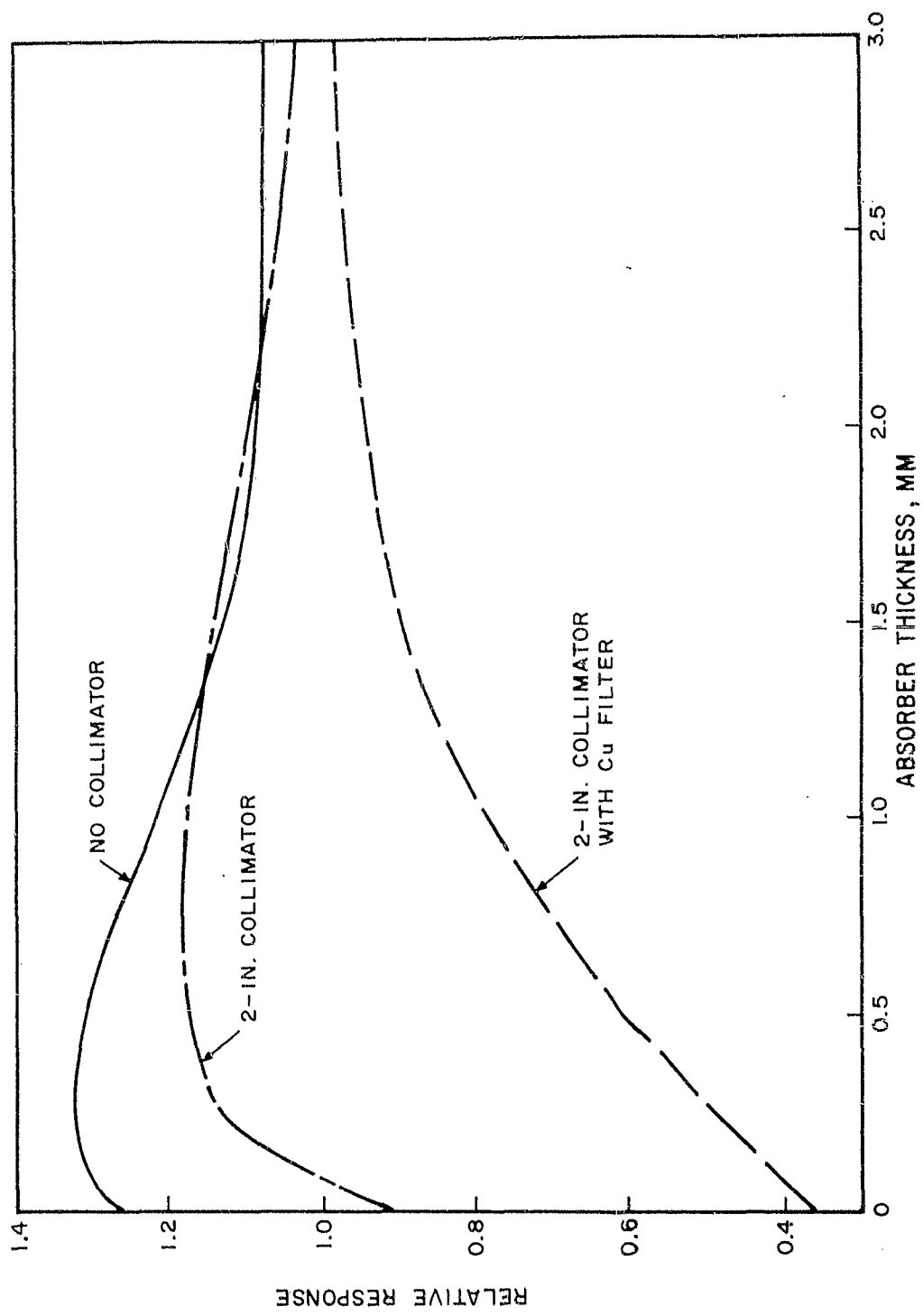
FIGURE B-2. RELATIVE IONIZATION CURRENT AS A FUNCTION OF ABSORBER THICKNESS FOR A 50-CURIE COBALT SOURCE WITH AND WITHOUT COLLIMATOR
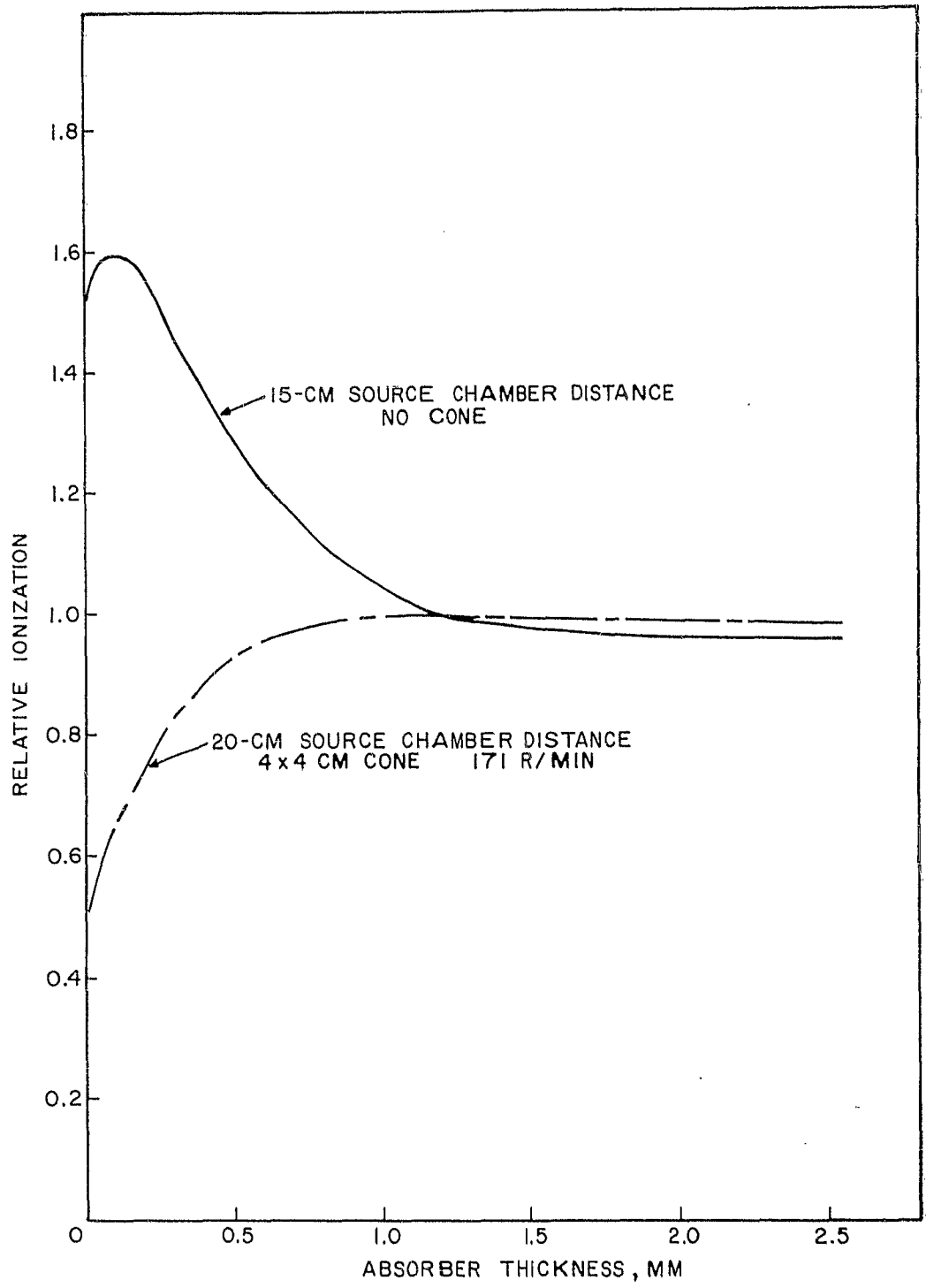
125

FIGURE B-3. IONIZATION AS A FUNCTION OF ABSORBER THICKNESS,
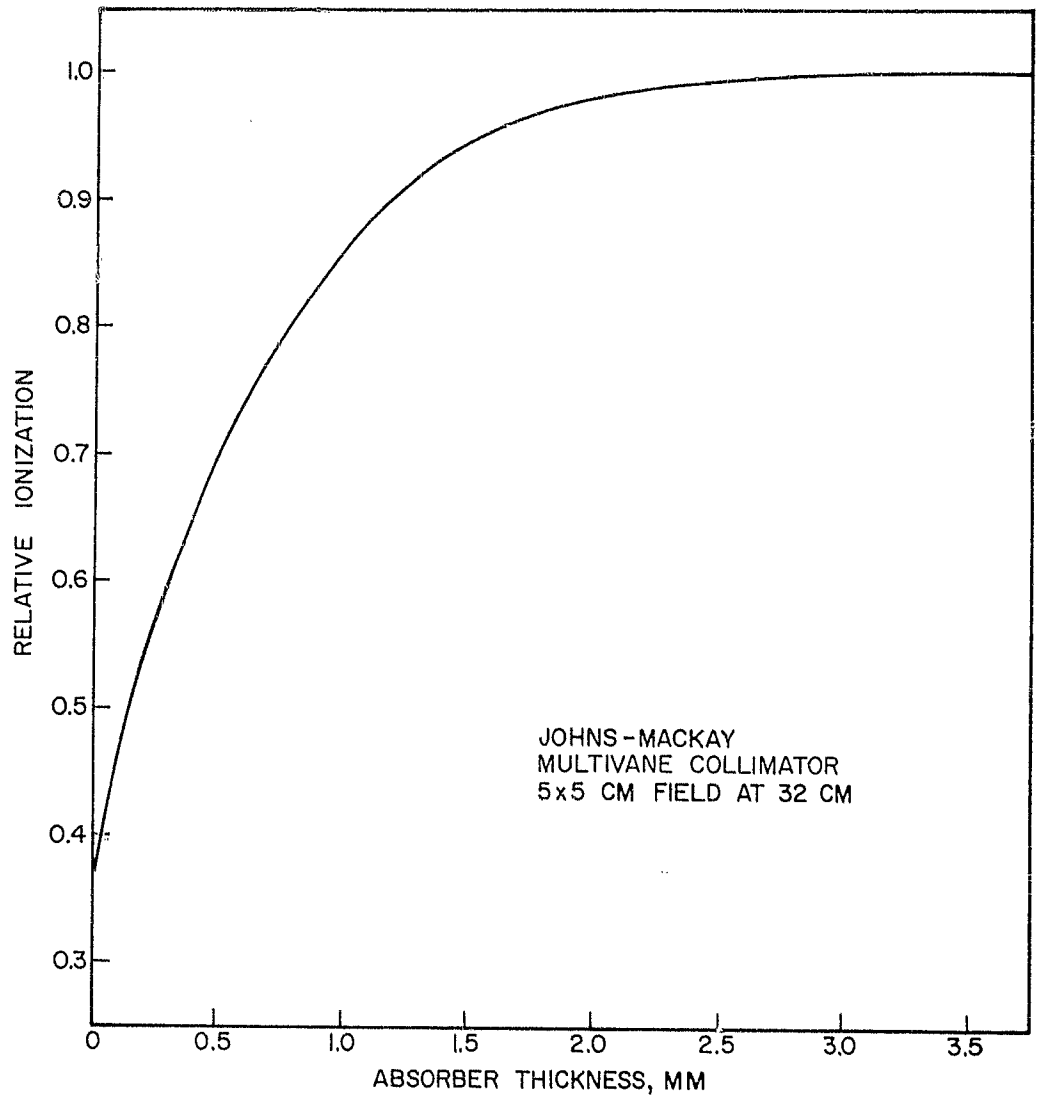PICKER CESIUM SOURCE

FIGURE B-4. IONIZATION AS A FUNCTION OF ABSORBER THICKNESS, PICKER C-1000 COBALT SOURCE

APPENDIX C
ROTATIONAL DEPENDENCE OF SILVER-ACTIVATED GLASS RODS

It was noted early in this study that dose values from a rod being repeatedly cleaned and evaluated varied in a random manner up to 10%. A few attempts to determine if a rotational dependence existed were made without any conclusive results, principally from loss of exact rod position. A stereo microscope was finally mounted so that the top ends of glass rods could be examined while in the Bausch & Lomb reader chuck assembly. By carefully opening and closing the chuck a rod could be made to rotate. A fiducial orientation was determined by certain visual characteristics of the top surface of the glass rod. A fluorescence determination was made and the rod then rotated clockwise to 45° of its previous position. Successive readings and rotation are made until a complete 360° rotation is accomplished. To show reproducibility, several revolutions were made. Figure C-1 shows the results from rods with and without radiation dose.

In turning the rod end-for-end with great care, it was of interest that the same high- and low-intensity points did not exactly coincide. Figure C-2 shows these data. The curves for each rod are drawn so that the rotation vector is reversed for the inverted rod position - i.e., one curve plotted clockwise and the other curve plotted counterclockwise.

To increase the reliability of further reading, two steps were undertaken:

1. Each rod was evaluated at two positions 180° apart because the cyclic fluctuations were assumed to be sinusoidal;

2. Each rod was evaluated on both ends in a manner consistent with the preceding step for variations in end-to-end fluorescence.
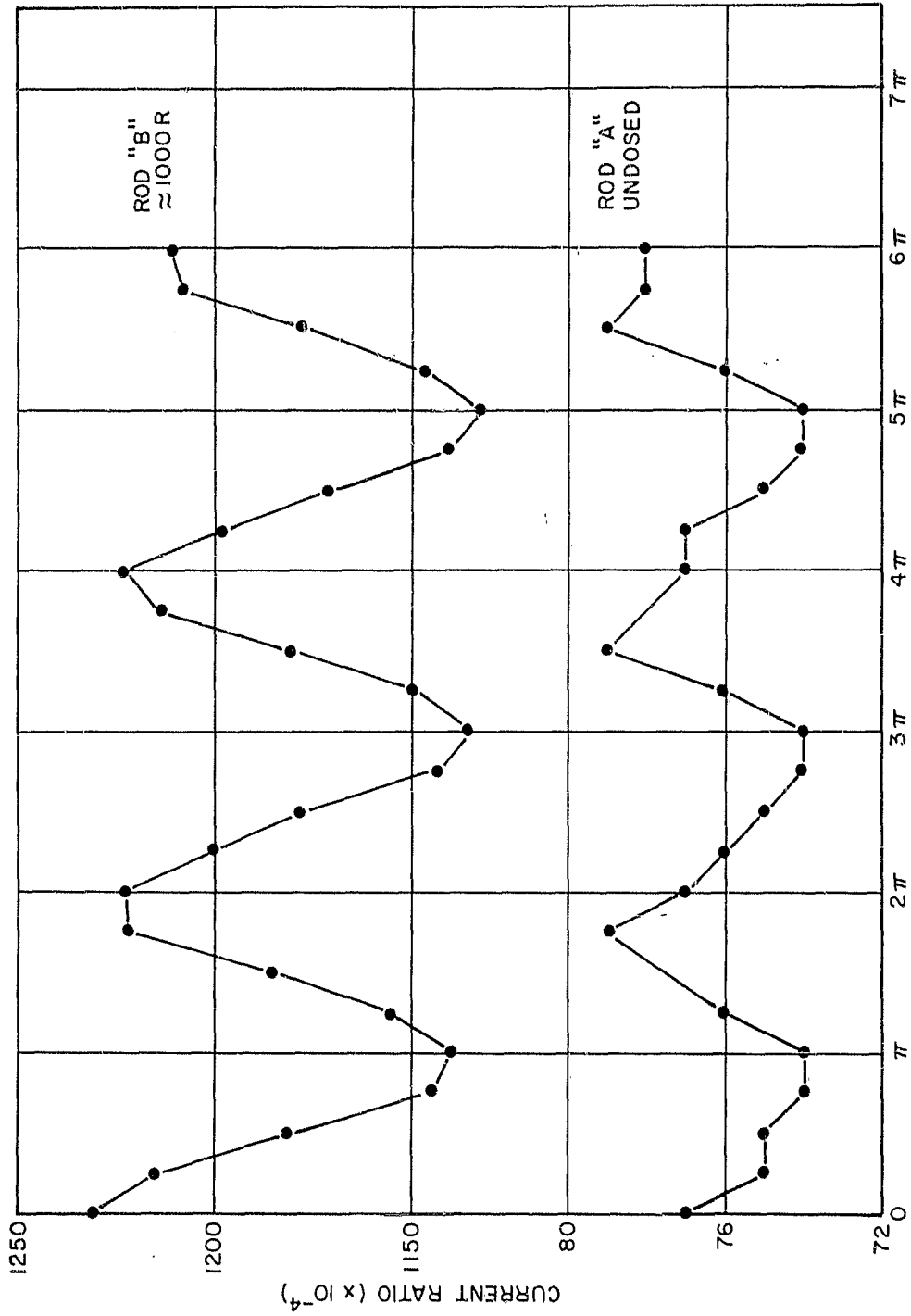
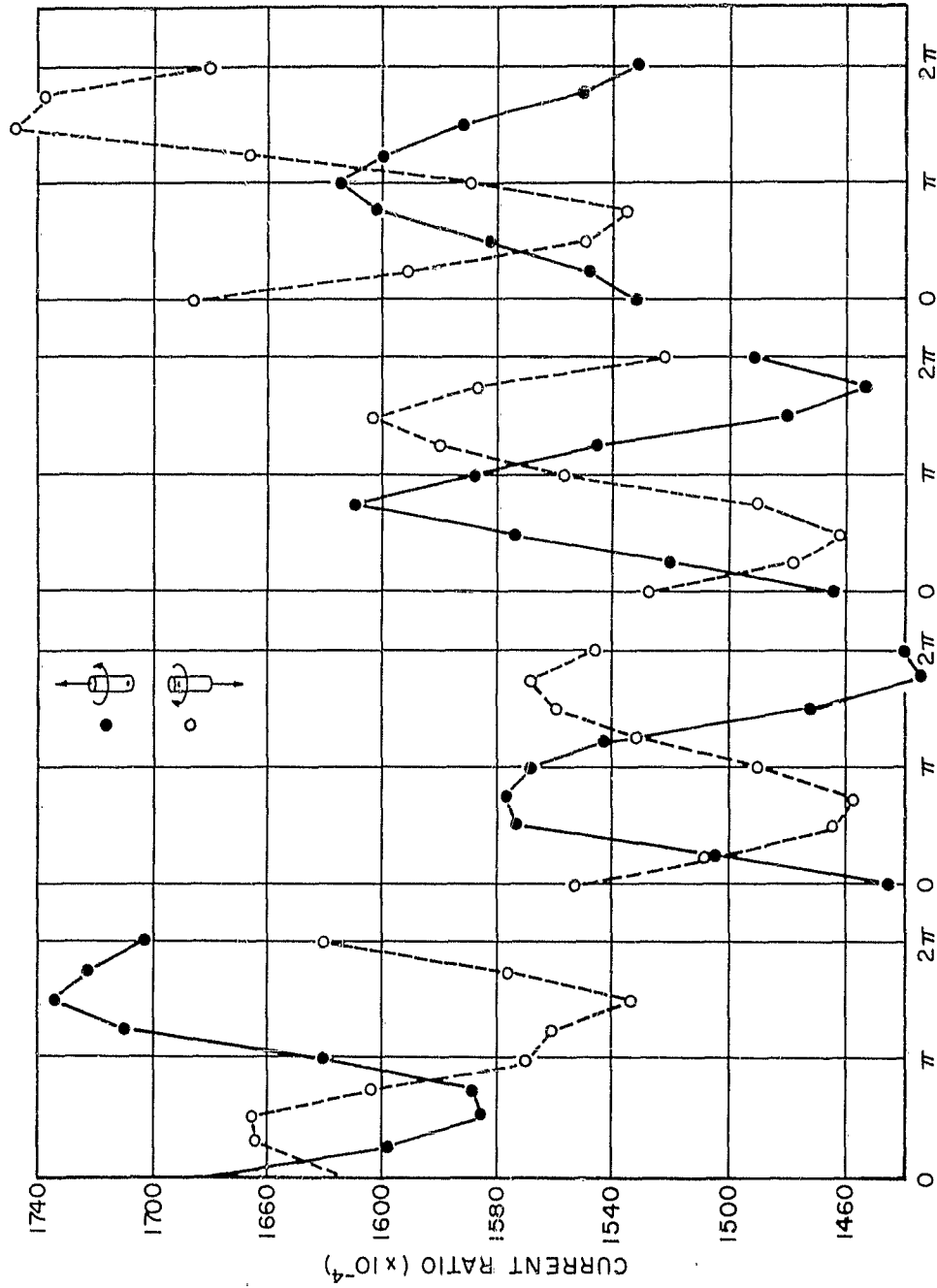FIGURE C-1 FLUORESCENT INTENSITY AS A FUNCTION OF GLASS ROD ROTATION

129

FIGURE C-2. FLUORESCENT INTENSITY AS A FUNCTION OF GLASS ROD ROTATION

130

The four fluorescent intensity readings were then averaged for the final evaluation. No further direct work was pursued on this problem. However, it was noted that the rods are not perfect right cylinders. This is evidenced by placing the rods on end on a flat surface. It was also noted that the 0.8-mm aperture upon which the rods were placed in the Bausch & Lomb Model 1 reader became scored by the chuck and the glass rods. Less rotational dependence seems evident when this iris was replaced with a new one. The non-uniform photocathode sensitivity of the orange fluorescence tube should be considered as a contributing influence when investigating this problem further.

A mechanism for rotating the orange sensitive photomultiplier tube was constructed, but time did not permit further study of the problem.

APPENDIX D
MISCELLANEOUS ATTEMPTS AT SHIELDS
FOR SILVER-ACTIVATED GLASS RODS

In addition to the few composite shields described in the body of this report which are significant to the point of defining the shield problem, a collection of responses for other prototype shields is presented. No attempt has been made to show the evolution because several ideas for shields may be evaluated simultaneously and analyzed together. It is of historic value that certain configurations were considered during this study. Some response curves are represented by only a few measurements and the remainder are constructed from previous examples. This action is based upon the measured responses being too high or low and further data are superfluous. A series of these limited point experiments is tabulated on the following page.

Figures D-1, D-2 and D-3 show the response of silver-activated glass rods to primarily single-metal shields. An insert of plastic was used to attenuate the secondary electrons emitted from the shield material in some shields.

Later studies for investigating a uniform, homogeneous shield resulted in the following multiple-metal shields with plastic inserts. Figure D-4 and D-5 show these data. It is significant to note that a flat response can be obtained only by the sacrifice of low-energy response. The response of the EG&G 5-rod dosimeter shield, Figure D-6, is included to point out this limitation for a commercial shield.

In designing and evaluating shields for the silver-activated glass rods, every effort has been made to achieve the lowest possible low-energy cutoff for the system.

Shield Material Thickness (inch)

Core	First Shield	Second Shield	Response of Dosimeter to Effective Gamma Energy		
			1.25 Mev	210 kev	123 kev
0.040 plastic	0.030 Pb	0.035 Sn	1.00	1.28	0.39
0.040 plastic	0.030 Pb	0.015 Sn	1.00	1.57	0.67
0.040 plastic*	0.015 Sn	0.030 Pb*	1.00	1.54	0.69
0.040 plastic	0.033 Pb	0.0215 Ta	1.00	0.92	0.08
0.150 plastic	0.0215 Ta		1.00	-	0.89
0.150 plastic	0.0215 Ta	0.033 Sn	1.00	-	0.47
0.150 plastic	0.0315 Ta		1.00	-	0.32
0.070 plastic	0.0315 Ta		1.00	1.29	0.25
0.070 plastic	0.042 Sn	0.025 Pb	1.00	1.54	0.42
0.070 plastic	0.033 Sn	0.025 Pb	1.00	1.37	0.51
0.070 plastic	0.033 Sn	0.035 Pb	1.00	1.15	6.295

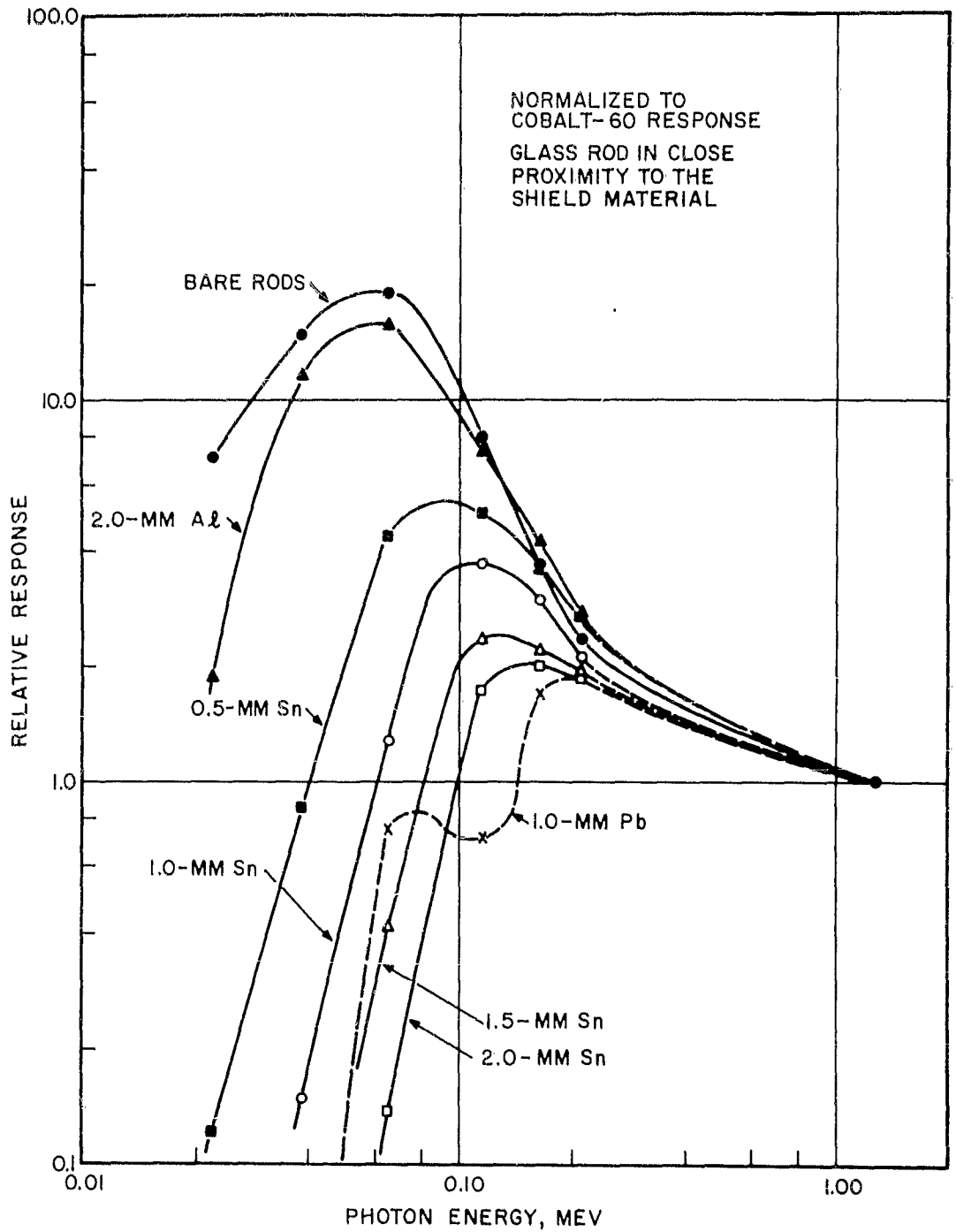*This shield contained a third metallic shell of 0.015 inch Sn.

133

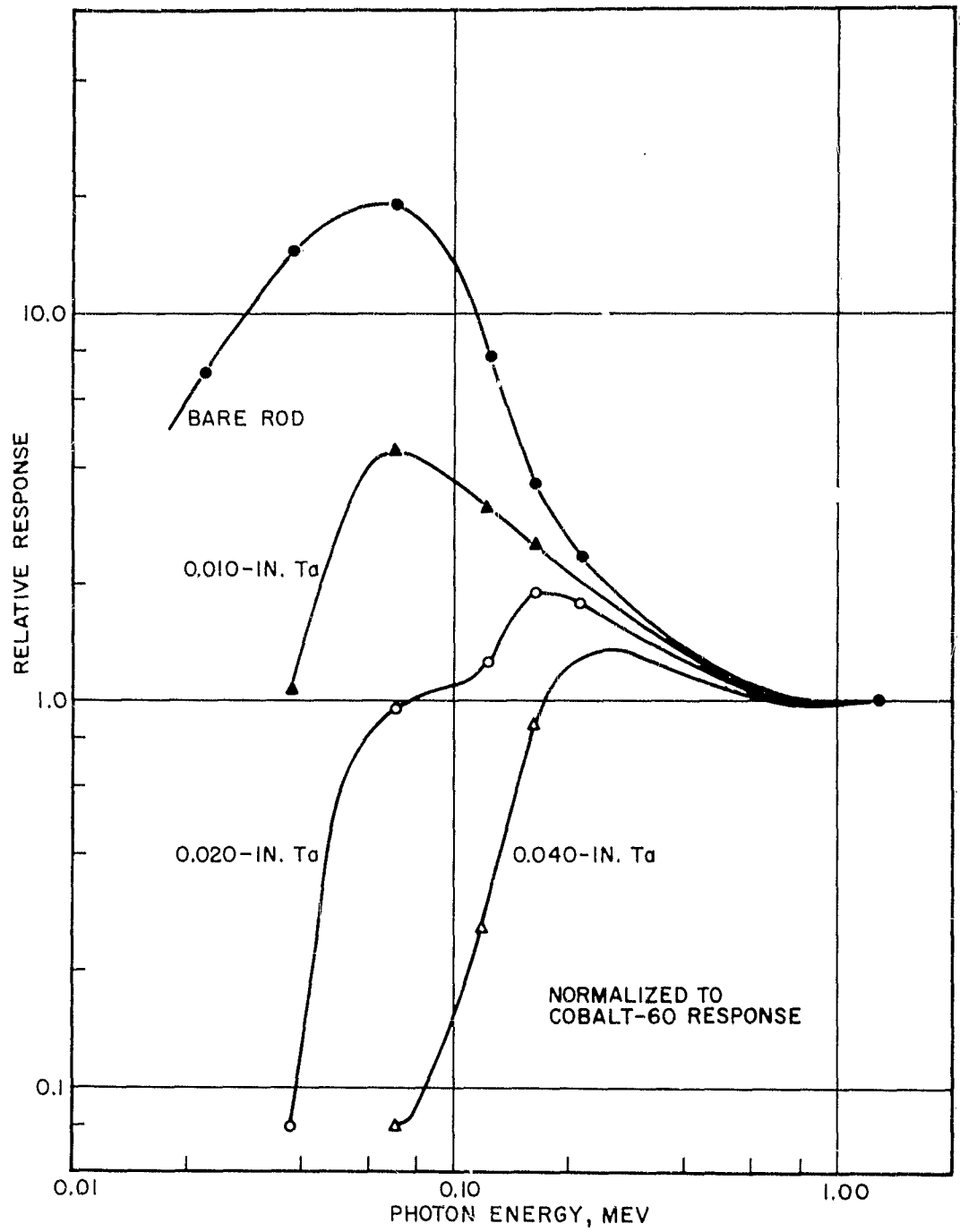FIGURE D-I. SILVER-ACTIVATED GLASS ROD RESPONSE IN ALUMINUM, TIN, AND LEAD SHIELDS.

134

FIGURE D-2. SILVER-ACTIVATED GLASS ROD RESPONSE
IN TANTALUM SHIELDS

135

NORMALIZED TO
COBALT-60 RESPONSE
GLASS RODS IN 2-MM WALL
PLASTIC INSERTS

A. 0.030-IN. Pb
B. 0.040-IN. Pb WITH 0.025-IN.
   DEEP GROOVES, 0.080
   IN. APART
C. 0.030-IN. 50/50 Pb-Sn ALLOY
D. 0.040-IN. 50/50 Pb-Sn ALLOY
   WITH 0.025-IN. DEEP
   GROOVES, 0.040
   IN. APART
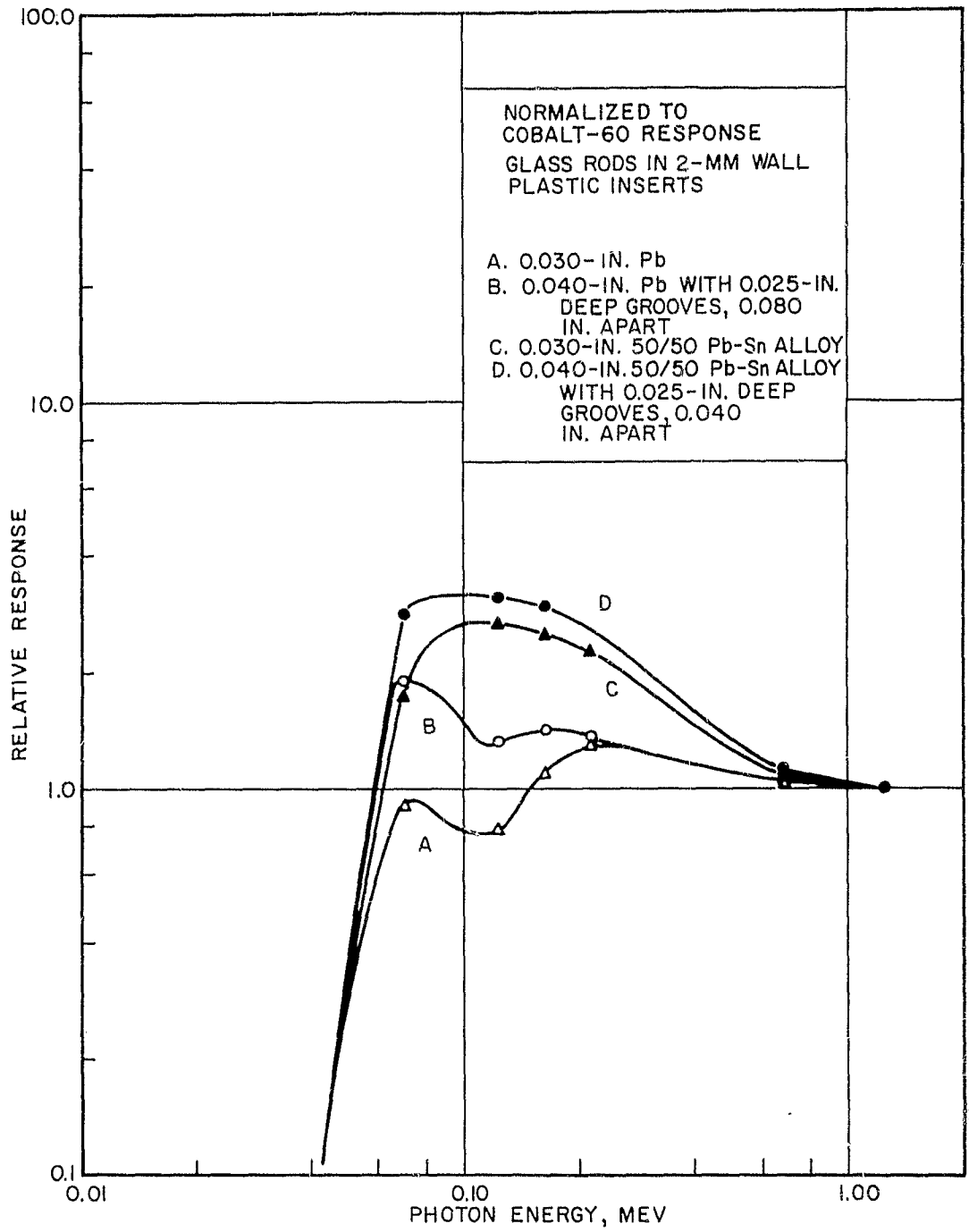
FIGURE D-3. SILVER-ACTIVATED GLASS ROD RESPONSE IN LEAD
AND LEAD-TIN ALLOY SHIELDS

NORMALIZED TO
COBALT-60 RESPONSE

A. 0.020-IN. Ta WITH
    0.040-IN. PLASTIC
B. 0.040-IN. PLASTIC
    IN 0.015-IN. Sn
    IN 0.030-IN. Pb
    IN 0.015-IN. Sn
C. 0.040-IN. PLASTIC
    IN 0.040-IN. Sn
    IN 0.025-IN. Pb
D. 0.070-IN. PLASTIC
    IN 0.033-IN. Sn
    IN 0.035-IN Pb
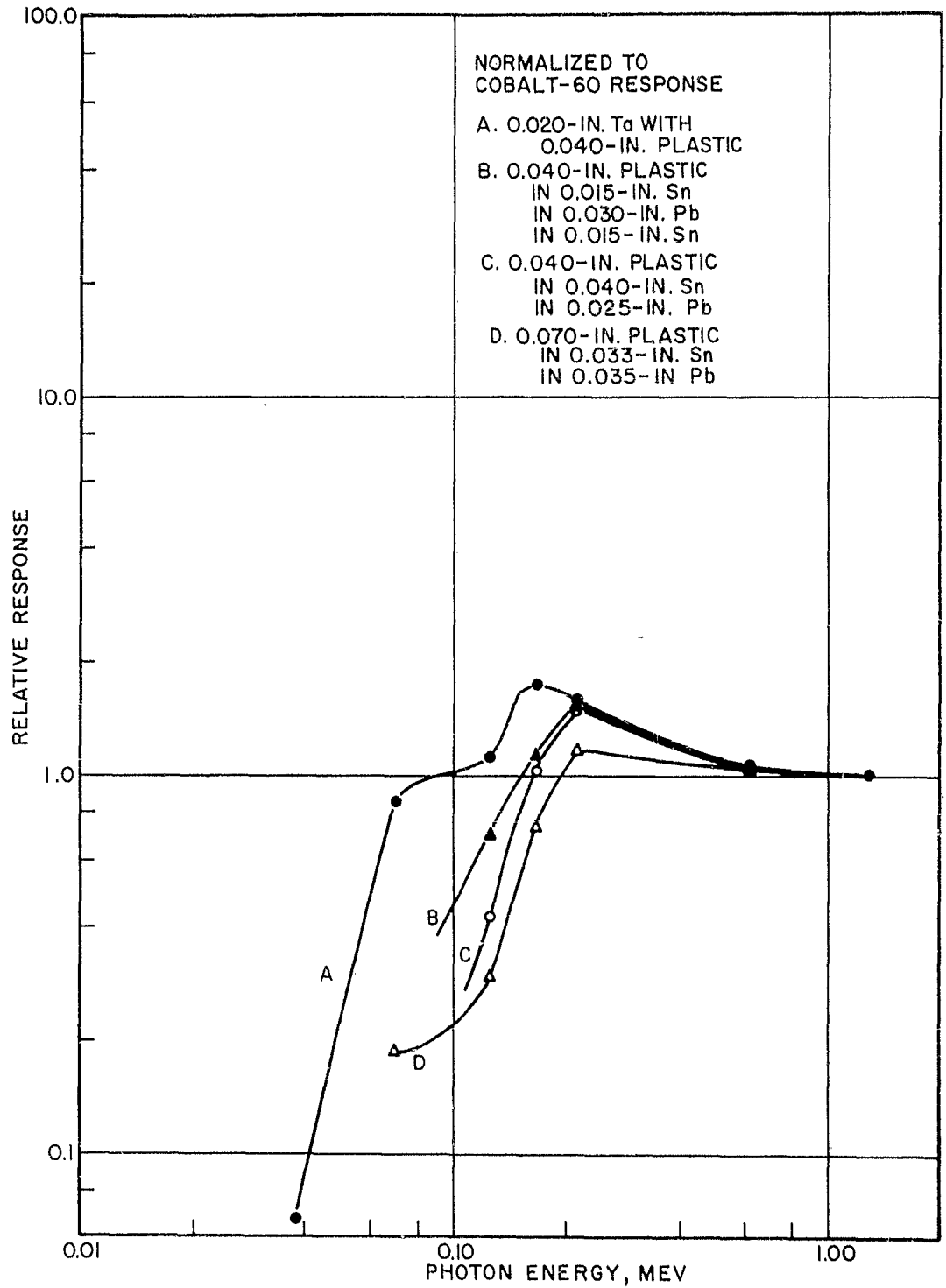
FIGURE D-4. SILVER-ACTIVATED GLASS ROD RESPONSE
IN COMPOSITE SHIELDS

NORMALIZED TO
COBALT-60 RESPONSE

A. 0.040-IN. PLASTIC
IN 0.030-IN. Pb
IN 0.015-IN. Sn

B. 0.040-IN. PLASTIC
IN 0.030-IN. Pb
IN 0.035-IN. Sn

C. 0.040-IN. PLASTIC
IN 0.033-IN. Pb
IN 0.215-IN. Ta
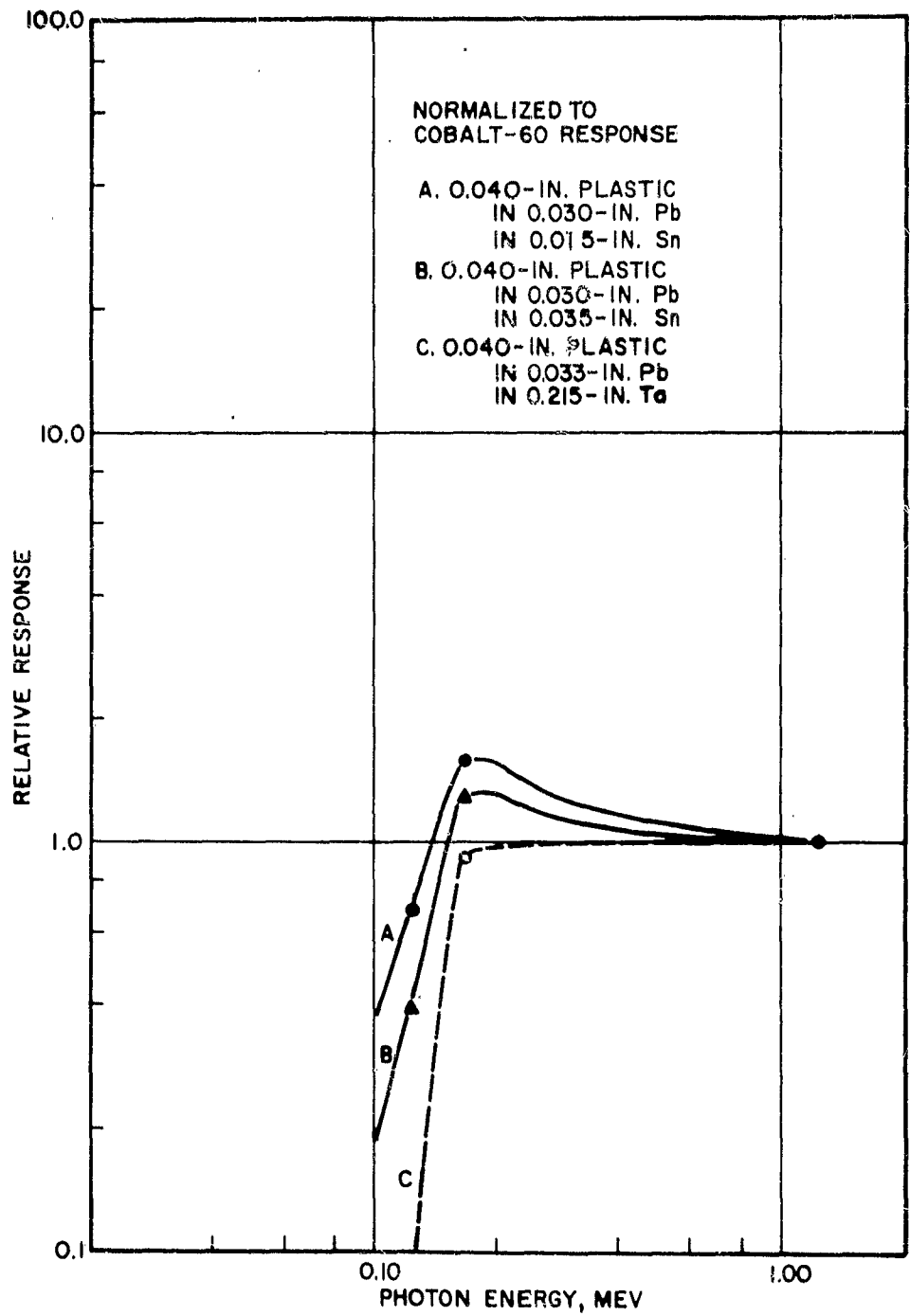
FIGURE D-5. SILVER-ACTIVATED GLASS ROD RESPONSE
IN COMPOSITE SHIELDS

138

100.0

NORMALIZED TO
COBALT-60 RESPONSE

0.045-IN. PLASTIC IN
0.033-IN. TIN IN
0.050-IN. LEAD IN
0.020-IN. ALUMINUM

10.0

RELATIVE RESPONSE
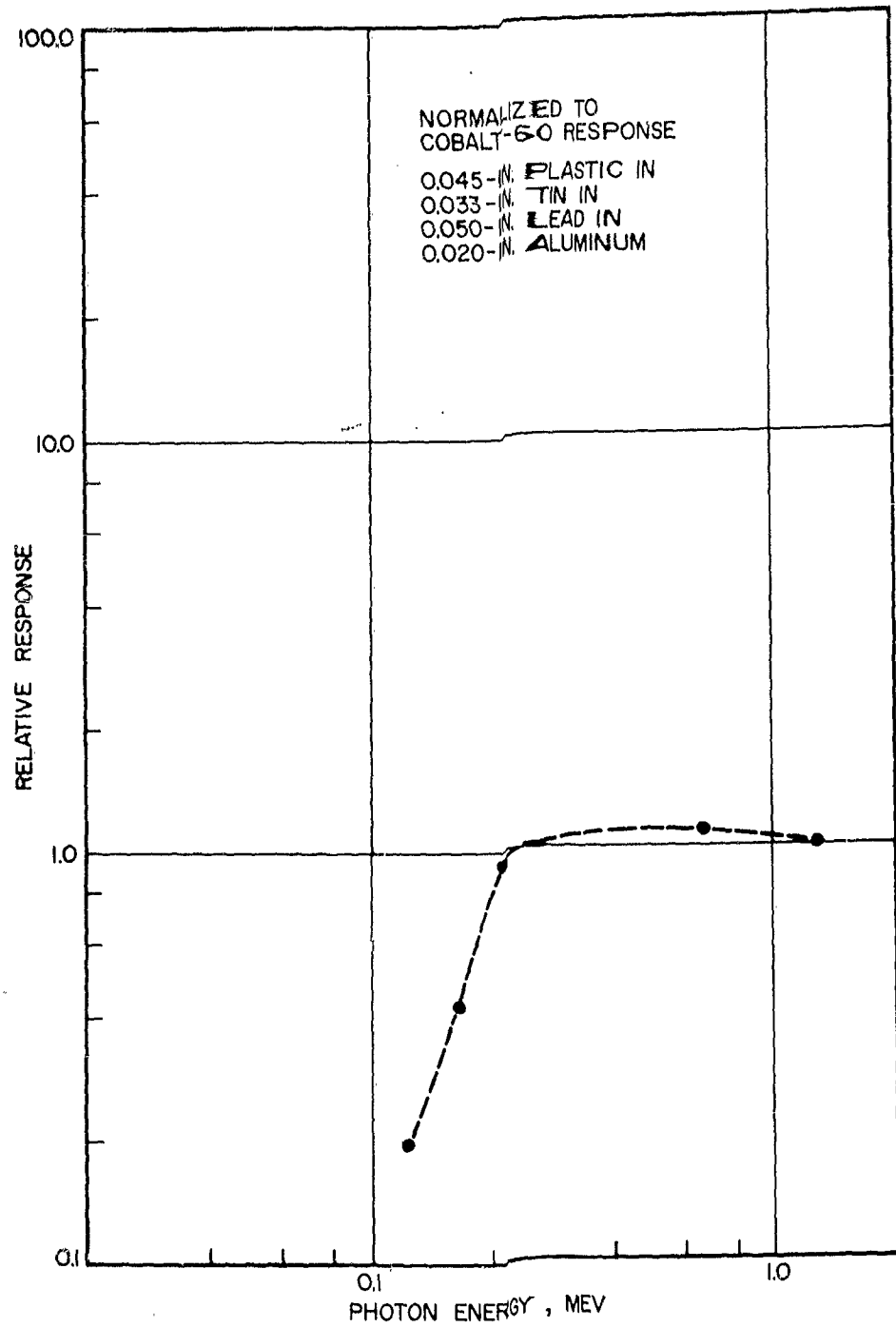
1.0

0.1

0.1   1.0

PHOTON ENERGY , MEV

FIGURE D-6. SILVER-ACTIVATED GLASS ROD RESPONSE IN EG&G SHIELD